NEW FRONTIERS IN CHEMISTRY
New Front. Chem.

(*former Annals of West University of Timişoara – Series of Chemistry*)

(2015) Volume 24, Number (Issue) 1, pp. 1-79

Ordinary Issue

TABLE OF CONTENTS

continuing…

…continued

PUBLISHER:
Universitatea de Vest
din Timişoara

NEW FRONTIERS IN CHEMISTRY: METADATA

New Frontiers in Chemistry (New Front. Chem.) is an open-access fee-free peer-review international academic journal addressing the modern trends and frontiers in fundamental, applicative and multidisciplinary chemistry, paralleling the ever-expanding chemical data, methods, and compounds available and continuously produced, towards cross fertilizing the multidisciplinary ideas as coming from Chemistry combined with Mathematics, the Natural and Applied sciences (Physics, Biology, Medicine, Agriculture, Environmental, Engineering), and beyond.

NEW FRONTIERS IN CHEMISTRY
(NEW FRONT. CHEM.)
is published biannually by

West University of Timişoara
Blvd. V. Parvan 4
Timisoara 300223, ROMANIA
E-mail: newfrontchem@iqstorm.ro
Web: www.newfrontchem.iqstorm.ro

ISSN 2393 – 2171
ISSN-L 2393 – 2171

Subscription Price per Volume
Electronic: open access   Print: on demand by above email address

Additional color graphics is available in the e-version of this Journal

NEW FRONTIERS IN CHEMISTRY: EDITORS

Editorial Board:

Advisory Editors
(from members of Biology-Chemistry Department of West University of Timișoara):

VASILE OSTAFE (Biochemistry, Chromatography, Environmental Chemistry)
IONEL CIUCANU (Instrumental Techniques for Analytical Chemistry)
ADRIANA ISVORAN (Biophysics, Bioinformatics)
MIHAI V. PUTZ (Nanochemistry, Quantum Chemistry)
TITUS VLASE (Thermal Analysis, Chemical Kinetics, Chemistry of Solid State)
GABRIELA VLASE (Inorganic Chemistry, Thermal Analysis)
OTILIA BIZEREA (Inorganic Chemistry)
GABRIELA PREDA (Organic Chemistry, Catalysis)
CONSTANTIN BOLCU (Organic Chemistry, Polymers)
VLAD CHIRIAC (General and Analytical Chemistry, Electrochemistry)
DANA VLASCICI (Analytical Chemistry)
DANIELA DASCALU (Thermodynamics and Chemical Statistics)
CORINA DUDA-SEIMAN (QSAR, Organic Chemistry, Medicinal Chemistry)
LAURA PITULICE (Environmental Chemistry)
HORIA POPOVICI (Colloidal Chemistry, Analytical Chemistry)
BEATRICE VLAD-OROS (Chemical and Enzyme Kinetics)
MARIANA ALBULESCU (Organic Chemistry, Natural Compounds)
DORINA MODRA (Organic Chemistry)
MIRCEA SELEGEAN (Biotechnologies)
NICOLETA IANOVIC (Aerobiology, Plant Physiology)

Honorary Editors
(as Doctor Honoris Causa of WUT/CBG & Formers Editors and Developers of Annals of West University of Timișoara – Series Chem.):

ALEXANDRU BALABAN (Texas A&M University at Galveston, USA, & Romanian Academy, Romania)
HAGEN KLEINERT (Berlin Free University, Germany)
KATLEEN SWALLOW (Merrimack College, USA)
GABOR NÁRÁY-SZABÓ ("Lorand Eőtvős" University Budapest, Hungary)
EUGEN SEGAL (University of Bucharest, Romanian Academy, Romania)
VICTOR EMANUEL SAHINI (Polytechnic Bucharest, Romanian Academy, Romania)
MARIUS ANDRUH (Romanian Academy, Bucharest)
ZENO SIMON (Romanian Academy, Romania)
ADRIAN CHIRIAC (West University of Timisoara, Romania)
MIRCEA MRACEC (West University of Timisoara, Romania)
VASILE OSTAFE (West University of Timisoara, Romania)
NICOLAE BONCIOCAT (†, Babes-Bolyai University, Cluj-Napoca, Romania)
ALAN R. KATRITZKY (†, University of Florida, Gainesville, USA)

NEW FRONT. CHEM. (**2015**)
Volume 24, Number 1, pp. 1-2
ISSN 2393-2171; ISSN-L 2393-2171

Former: Ann. West Univ. Timisoara – Series Chem.
ISSN: 1224-9513

Editorial

FACING NEW FRONTIERS IN CHEMISTRY

Mihai V. Putz $^{(1,2)♣}$

[1] Laboratory of Structural and Computational Physical-Chemistry for Nanosciences and QSAR, Biology-Chemistry Department, West University of Timisoara, Str. Pestalozzi No. 16, 300115 Timisoara, ROMANIA;

[2] Laboratory of Renewable Energies-Photovoltaics, R&D National Institute for Electrochemistry and Condensed Matter, Dr. A. Paunescu Podeanu Str. No. 144, Timisoara, RO-300569, ROMANIA.

At the middy of the second decade of XXI the modern man would like knowing the main concepts, trends and frontiers the science (fundamentals) and technology (applications) are preparing for the rest of the growing century. Roughly the main humankind chapters can be identified as: organisms (living bodies), medicines (health and life prolongation), food (the earth supply), energy (life and environmental fuel), and communication (spiritual needs). Going down to specific disciplines, these items may be defined, modeled, controlled, planned, and functionalized by a systematic research management whose the first 14 challenges, for the first 14 years of XXI may be eventually be learn also as new frontiers in Chemistry:

1. *Personal genome* it is for sale [1]: „Sequencing will be so cheap and so easy to access that everybody could get sequenced if they want. It'll be iPod pricing; the $1,000 genome is within sight, and … that barrier has been smashed."
2. *Global warming and climatic changing* [2]: „To those who say today's warming is natural variation, the natural forcings are actually pushing us in the wrong direction; If you have enough arbitrary parameters, you can make any model work; Unfortunately, the data now show us that we have underestimated the climate crisis."
3. *Building small* the societal economy through the „eyes" of nano-technology [3]: „ The nanotechnology ideas finding their way into construction in a practical way are probably now starting to gain momentum."
4. *The race for sunlight* – the sustainable energy [4]: „There are so many new PV (photovoltaics) and CSP (concentrated solar power) projects being discussed today, I really can't keep up; Future prospects for solar are good, but without state renewable portfolio standards the scale of the plants is likely to come down."
5. *Men-action like the digital element* of life sciences [5]: „Major firms have used acquisitions to expand in lab informatics; A new breed of researchers born in the digital age will influence decisions on how computers and automation evolve in the laboratory."

♣ Author E-Mail: mv_putz@yahoo.com; Tel.: +40-256-592-638; Fax: +40-256-592-620

6. *Chemical weapons* (for mass destruction) – lessons without repetition [6]: „The WWI ends, but research continues… .”
7. *Pollution* – the never ending story [7]: „Where do the chemicals come from? ... Are they ever going to go away? We are lucky to have scientists driven this work for many years!”
8. *The diet in XXI century* – health by plants vs. alimentary suppliers [8]: „The tenet that protein is a cornerstone of a healthy diet, that it helps us feel full and more satisfied, remains constant; Soy is the only common plant protein that contains sufficient quantities of the essential amino acids.”
9. *X- Rays after the first 100 years* of epochal discoveries (viz. penicillin, DNA, tRNA, B-12 vitamin, lisosime, G-protein etc.) [9]: „The most definitive statement we can make about the future of X-ray crystallography is that it has no future in its present form.”
10. *The anti-HIV molecule* – aiming the secrets of the secret antagonist [10]: „small molecules, the smaller they are the cheaper … to make, and the easier .. to formulate.”
11. *Chemistry as a business* – the possible solution of the global crisis by global needs [11]: „with in-house R&D pared down, companies will look for innovation; renewable rebound from hype deficit; above-average demand by cars and energy production.”
12. *Sugar and salt* – from the original sin to the lost paradise of the alimentary consumerism [12]: they „have attributes as well: function, color, texture, preservation, fermentation.”
13. *Fighting cancer* – from nanochemistry to nanotechnology to nanomedicine [13]: „By conjugating camptothecin to a polymer nanoparticle, the drug gets delivered inside tumor cells. It’s right where you want it to be.”
14. *Graphene* – the miraculous multidisciplinary mater of XXI [14]: „graphene products are here today. They’re not five years away; graphene forms a strong conductive circuit that tolerates flexing and bending and stands up well!”

With all these, one can hope only an integrative approach such as the nanochemistry can face the challenges which act on many levels, either on vertical (molecule-man-environment-universe) as well as horizontally (man-communication-economy-long life preservation) directions in human evolution towards an equilibrated present and a sustainable future – to which also the present Journal venture aims to give an international academic contribution.

REFERENCES

1. Arnaud C.H. Your own personal genome. *Chem. Eng. News* **2009**, *12(14)*:13-15; idem. DNA sequencing forges ahead, 16-18.
2. Ritter S.K. Global warming and climate change. *Chem. Eng. News* **2009**, *12 (21)*:11-21.
3. Bethany H. Building small. *Chem. Eng. News* **2011**, *06(13)*:12-17.
4. Johnson J. A new race for solar. *Chem. Eng. News* **2013**, *12(16)*:9-12.
5. Mullin R. The human element. *Chem. Eng. News* **2014**, *10(20)*: 12-15.
6. Everts S. When chemicals became weapons of war. *Chem. Eng. News* **2015**, *02(23)*:10-17; idem. Who was Fritz Haber, 18-19.
7. Ritter S.K. Measuring persistence. *Chem. Eng. News* **2015**, *03(2)*:10-14.
8. Bomgardner M.M. Protein evolution. *Chem. Eng. News* **2015**, *02(9)*:8-13.
9. Petsko G. Crystallography without crystals. *Chem. Eng. News* **2014**, *08(11)*:42-43.
10. Halford B. Aiming for HIV’s weak spot. *Chem. Eng. News* **2014**, *09(1)*:14-21.
11. *** World chemical outlook. *Chem. Eng. News* **2014**, *01(13)*:9-16.
12. Bomgardner M.M. Healthier food - by stealth. *Chem. Eng. News* **2013**, *09(16)*:11-15.
13. Halford B. Tiny tech to treat cancer. *Chem. Eng. News* **2013**, *06(4)*:10-15.
14. Jacoby M. Graphene moves towards applications. *Chem. Eng. News* **2011**, *11(21)*:10-15.

NEW FRONT. CHEM. (**2015**)
Volume 24, Number 1, pp. 3-16
ISSN 2393-2171; ISSN-L 2393-2171

Former: Ann. West Univ. Timisoara – Series Chem.
ISSN: 1224-9513

Review

MACROMOLECULAR CROWDING UPON IN-VIVO-LIKE ENZYME-KINETICS: EFFECT OF ENZYME-OBSTACLE SIZE RATIO

Cristina Balcells*[1]*, Isabel Pastor*[1,2]*, Laura Pitulice*[3]*,
Claudia Hernández*[1]*, Mireia Via*[1]*, Josep Lluís Garcés*[4]*,
Sergio Madurga*[1]*, Eudald Vilaseca*[1]*, Adriana Isvoran*[3]*,
***Marta Cascante*[5]*, and Francesc Mas*[1,♣]
[1] Department of Physical Chemistry and Research Institute of Theoretical and Computational Chemistry (IQTCUB) of Barcelona University, C/ Martí I Franquès, 1, 08028-Barcelona (Spain)
[2] Small Biosystems Lab, Department of Fundamental Physics, University of Barcelona, Barcelona and CIBER-BBN, Carlos III Health Institute, Madrid (Spain)
[3] Department of Biology-Chemistry, West University of Timisoara, Timisoara (Romania)
[4] Department of Chemistry, University of Lleida, Lleida (Spain)
[5] Department of Biochemistry and Molecular Biology and Institute of Biomedicine (IBUB) of Barcelona University, Barcelona (Spain)

ABSTRACT

In the present work, the volume exclusion phenomenon, also known as macromolecular crowding, has been applied to the field of enzyme kinetics. It has been approached by adding polymeric obstacles in the media of different enzymatic reactions. The concentration and size of these obstacles have been changed systematically in order to obtain kinetic information about each reaction. Results indicate that the performance of a certain enzyme always depends on the amount of excluded volume. However, only large, oligomeric proteins display an obstacle size-dependent behavior. Besides, crowding can hinder diffusion to the extent of being capable of shifting reaction control from activation to diffusion.

Keywords: Enzyme kinetics, crowding, Dextran, excluded volume effects, enzymatic reaction control

---

♣ corresponding author: fmas@ub.edu

1. INTRODUCTION

Physicochemical characterization of biomolecules, both theoretically and experimentally, has been traditionally developed in dilute solution conditions. This scenario, even though easy to study and close to ideal condition, does not resemble the real situation inside cells: the cell cytosol contains macromolecules up to 300-400 g/L, and the space in it is highly structured and compartmented [1].

However, studying biomolecules in their natural environment is still impossible for most biological processes at molecular scale, and it can lead to a dead end: having such a great number of variables that the outcome may be impossible to interpret and comprehend. Thus, all the interrelations between the biological system (e.g. a protein and its substrates) and its environment must be studied separately in a model system.

Macromolecular crowding aims to mimic the high levels of excluded volume existing in the cell and tries to discern how this can affect any physicochemical process occurring inside [2,3]. It is achieved by experimentally modelling the cytosol using a wide variety of neutral, relatively inert and random-coil shaped macromolecules, such as Dextrans, Ficolls or Polyethylene glycol (PEG).

Ultimately, an *in-vivo*-like environment is sought, an in vitro environment that truly reconstructs the cell cytosol by all means: obstacles of different sizes all together, confined spaces, filamentous structures similar to the cytoskeleton… Yet, this is still far away since the effect of excluded volume with homogeneously sized, coil-shaped obstacles is yet to be fully understood. Such artificial recreation of the cell environment could be useful in drug and protein therapy development and routine enzyme activity assays. This will allow obtaining activity values which are closer to the physiological ones rather than if tested in dilute solution. Thus, the use of synthetic polymers, allows avoiding the inconveniences and costs of cell cultures or animal manipulation in pre-clinical stages, as well as providing more realistic values for systems biology approaches.

Excluded volume is just one of the effects that a macromolecule can face inside the cell, but it has been shown to be relevant in a wide variety of biological phenomena, in particular when proteins are involved [3], which include macromolecule diffusion [4-6], macromolecular interactions [7-8], protein stability [9], conformational equilibria [10] or enzyme kinetics [10-21].

In the past years, research focus has been set on enzyme kinetics. A decent number of enzymatic reactions have been studied in crowding conditions, but still few trends are understood. In terms of Michaelis-Menten kinetic parameters, in the majority of cases maximum velocity, $v_{\max}$, decreases [13,14, 17-19, 21], but in a few cases the overall enzyme activity has been found to increase [11, 14-16], and the Michaelis constant, K_{m}, that represents the affinity of the enzyme to bind the substrate, can increase [11, 16, 17], decrease [13-15, 18, 19, 21] or remain constant [19].

One trend that has seen some light in the last years is the enzyme/obstacle size ratio. Results suggest that small enzymes reaction rates are influenced by the amount of excluded volume – that is obstacle concentration – and not by obstacle size; while bigger enzymes are affected by both obstacle size and concentration [12, 19-21].

Besides, the effects of macromolecular crowding seem to differ between diffusion-controlled reactions and activation-controlled reactions. In fact, such effect is rather intuitive since it has been proven that macromolecular crowding can alter protein diffusion [4-6] and it can also modify conformational dynamics of the active site [22].

Both issues will be addressed in the present review, which aims to contribute in setting general trends about mechanisms by which excluded volume effects may alter the function of enzymes.

2. METHODS/MODELS

2.1. Theoretical Model

Kinetic behaviour of enzymes under crowded media conditions may be studied using the reaction scheme proposed by Henry in 1902 of a single-substrate, single-enzyme-catalysed reaction, and known as irreversible Michaelis-Menten scheme [23]:

$$E + S \underset{k_{-1}}{\overset{k_1}{\rightleftarrows}} ES \xrightarrow{k_2} E + P \tag{1}$$

which can be solved approximately using the stationary state assumption, SSA (*d[ES]/dt* ≈ 0), which is less restrictive than the reactant stationary assumption, RSA ($[S] \approx [S]_0$), (see the recent review of Schnell for a detailed discussion) [24], to yield the well-known Michaelis-Menten equation:

$$v_0 = \frac{v_{\max}[S]_0}{K_m + [S]_0} \tag{2}$$

where v_0 is the initial velocity, $v_{\max} = k_2[E]_t$ is the maximum velocity and $K_m \equiv (k_2 + k_{-1}) / k_1$ is the Michaelis constant. This assumption holds when $[E]_0 << K_m + [S]_0$ and it can be seen that the reactant stationary assumption, RSA, holds when $[E]_0 \approx [S]_0$ as long as $[E]_0 << K_m$.

Therefore, the reactant stationary assumption, RSA, is a stronger condition than the required for the steady-state assumption, SSA, and it can be seen as a necessary condition for the steady-state assumption [24].

In fact, the Michaelis-Menten equation (2) often fits the behaviour of enzymatic reactions with a known different mechanism than the one depicted in scheme (1), even for bi-substrate reactions in pseudo-first order conditions. Such easy fitting allows us to use it to approach a wide variety of enzymatic reactions, taking the values of the kinetic parameters as apparent values, allow us to generalize the Michaelis-Menten equation (2) as:

$$v_0 = \frac{v_{\max}^{app}[S]_0}{K_m^{app} + [S]_0} \tag{3}$$

where $v_{\max}^{app}$ and K_m^{app} are the apparent maximum velocity and apparent Michaelis constant which can be put in terms of the kinetic parameters of the detailed mechanism involved [23].

In principle, in order to evaluate the effect that crowding may exert to different reaction mechanisms, numerical integration of temporal progression of the different reaction components would be necessary. This issue will be addressed in future steps. However, to evaluate the effect of macromolecular crowding in a given enzymatic reaction, obtaining apparent kinetic parameters and being able to study their fluctuations upon different experimental conditions is significant enough by itself.

2.2. Experimental Methods

Three enzymatic systems were studied in comparable conditions: bovine pancreas alpha-chymotrypsin (E.C. 3.4.21.1), horseradish peroxidase (HRP, E.C. 1.11.1.7) and rabbit muscle L-lactate dehydrogenase (LDH, E.C. 1.1.1.27), used without further purification. The three enzymes as well as all the reagents necessary for the reactions they catalyse – detailed in Table 1 - were purchased from Sigma-Aldrich Chemical (Milwaukee, WI, USA).

Dextrans, with a range of molecular weights from 5 to 410 kDa, were used as crowding agents: D5 (5 kDa), D50 (50 kDa), D150 (150 kDa), D275 (275 kDa) and D410 (410 kDa) were obtained from Fluka (Buchs, Switzerland).

Activity measurements of each enzyme were followed spectroscopically using UV-1603, and UV-1700 Shimadzu spectrophotometers through the absorption of reagents or products at the wavelengths specified in Table 1. All the experimental conditions tested during these studies are shown in Table 1 – regarding enzyme and substrate concentrations – and in Table 2 – regarding crowding agent sizes and concentrations. It is worth mentioning that since crowding agent concentrations are calculated in weight, they are directly related to the amount of excluded volume.

Moreover, all the studied systems present a negligible volume change in the reaction process (that is substrates and products are similar in size and much smaller than the enzymes).

Comprehensive experimental details and complete information about the aforementioned enzymatic reactions are described in previous references, as well as the complete results obtained for each reaction in crowded media [17-19].

Table 1: Enzymes and substrates concentrations, buffer and ionic strength experimental conditions and reaction tracking method.

Enzymes	Substrates		Buffer solution	Reaction tracking
Alpha-chymotrypsin from bovine pancreas type II	N-succinyl-L-phenyl-Ala-p-nitroanilide ($0 - 4.8 \cdot 10^{-4}$ M)		Tris-HCl 0.1 M pH = 8.0 10 mM $CaCl_2$	Monitored by UV–vis spectroscopy at λ =410 nm (25 °C)
Peroxidase from horseradish	ABTS diammonium salt ($0 - 23 \cdot 10^{-4}$ M)	H_2O_2 (33% aq.) ($10 \cdot 10^{-4}$ M)	Phosphate buffer 0.1 M pH = 7.4	Monitored by UV–vis spectroscopy at λ =414 nm (25 °C)
L-Lactate dehydrogenase from rabbit muscle	Sodium pyruvate ($0 - 5.4 \cdot 10^{-4}$ M)	β-NADH ($1.17 \cdot 10^{-4}$ M)	Imidazole-CH_3COOH 30 mM pH = 7.5 60 mM CH_3COOK 30 mM $MgCl_2$	Monitored by UV–vis spectroscopy at λ =320 nm (25 °C)

Table 2: Experimental conditions assayed in crowded media: dextran molecular weight, gyration radius and dextran concentrations used.

	D50	**D150**	**D275**	**D410**
Dextran molecular weight, M_W (kDa)	48.6	150	275	409.8
Dextran gyration radius, R_g (nm)	5.8	11.2	14.7	17
Dextran concentrations used in crowded media experiments (g/L)	25, 50, 100	25, 50, 100	25, 50, 100	25, 50, 100

Data analysis was performed assuming the validity of Michaelis-Menten theory and thus of the steady-state approximation, which is realistic in our experimental conditions and according to previous references [17-19]. Initial velocity values (v_0) were obtained by linear fitting of the initial part of each absorbance-time plot for each single experiment mentioned in Tables 1 and 2, repeating each one for 3 to 5 times with independent samples.

3. RESULTS AND DISCUSSION

3.1. Results

α-Chymotrypsin: 25 kDa

An initial linear raise and a subsequent plateau in the absorbance/time plot upon N-succinyl-L-phenyl-Ala-p-nitroanilide depletion were observed. Following the kinetics of this reaction under all the conditions depicted combining Table 1 and Table 2, one can observe that kinetic parameters of this reaction depend on obstacle concentration – that is excluded volume – but not on obstacle size, as seen in Figure 1A.

Figure 1: Maximum velocity (v_{max}) versus crowding agent size (from 5 to 410 kDa) for three different enzymes: A) α-Chymotrypsin, B) HRP, C) LDH. Each point corresponds to an average value with standard deviation of 3 to 5 single experiments in different conditions: in dilute solution (black squares) and at increasing concentrations of dextran as crowding agents: 25 g/L (red circles), 50 g/L (green up-triangles) and 100 g/L (blue down-triangles).

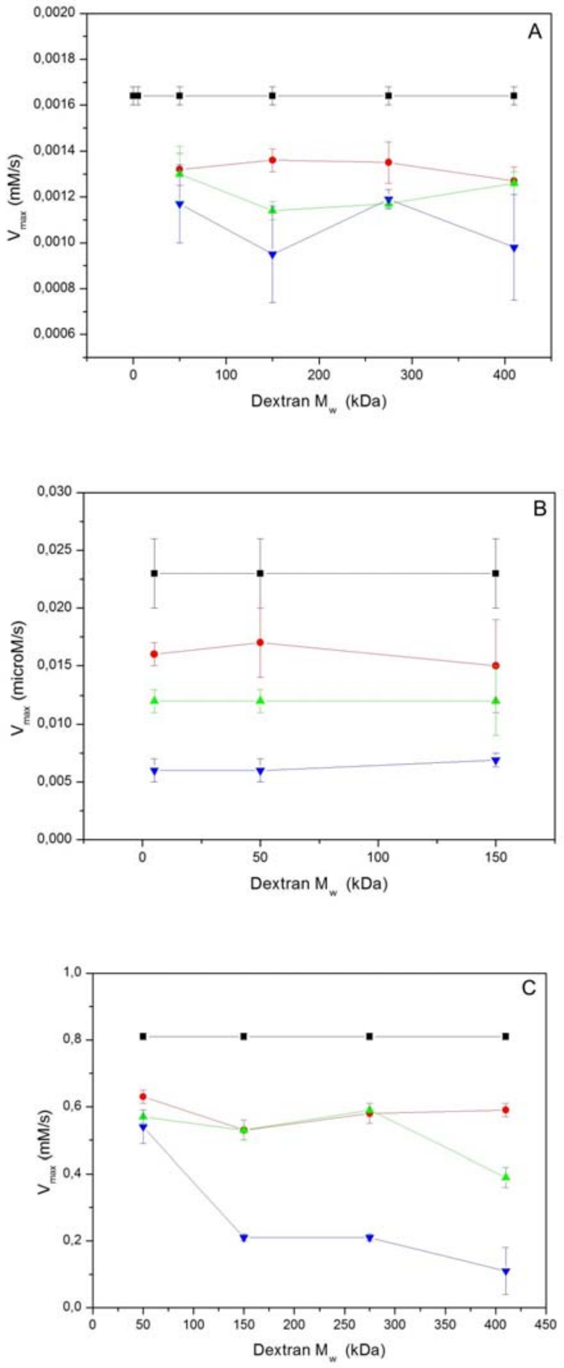

In accordance to these results, a previous study on the diffusion of this enzyme revealed that its diffusion depended strongly on crowding agent concentration and only slightly on crowding agent size, in the same buffer and ionic strength conditions [5].

In particular, it was found that v_max decreased, whereas Km increased when increasing Dextran concentration present in the sample [17], as depicted in Fig. 2A and Fig. 3A.

Figure 2: Relative v_{max} in dextran media for three different enzymes: A) α-chymotrypsin, B) HRP, C) LDH, in dextran concentrations ranging from 25 to 100 g/L (increasing from dark to light tone) of increasing dextran sizes: D50, D150, D275 and D410.

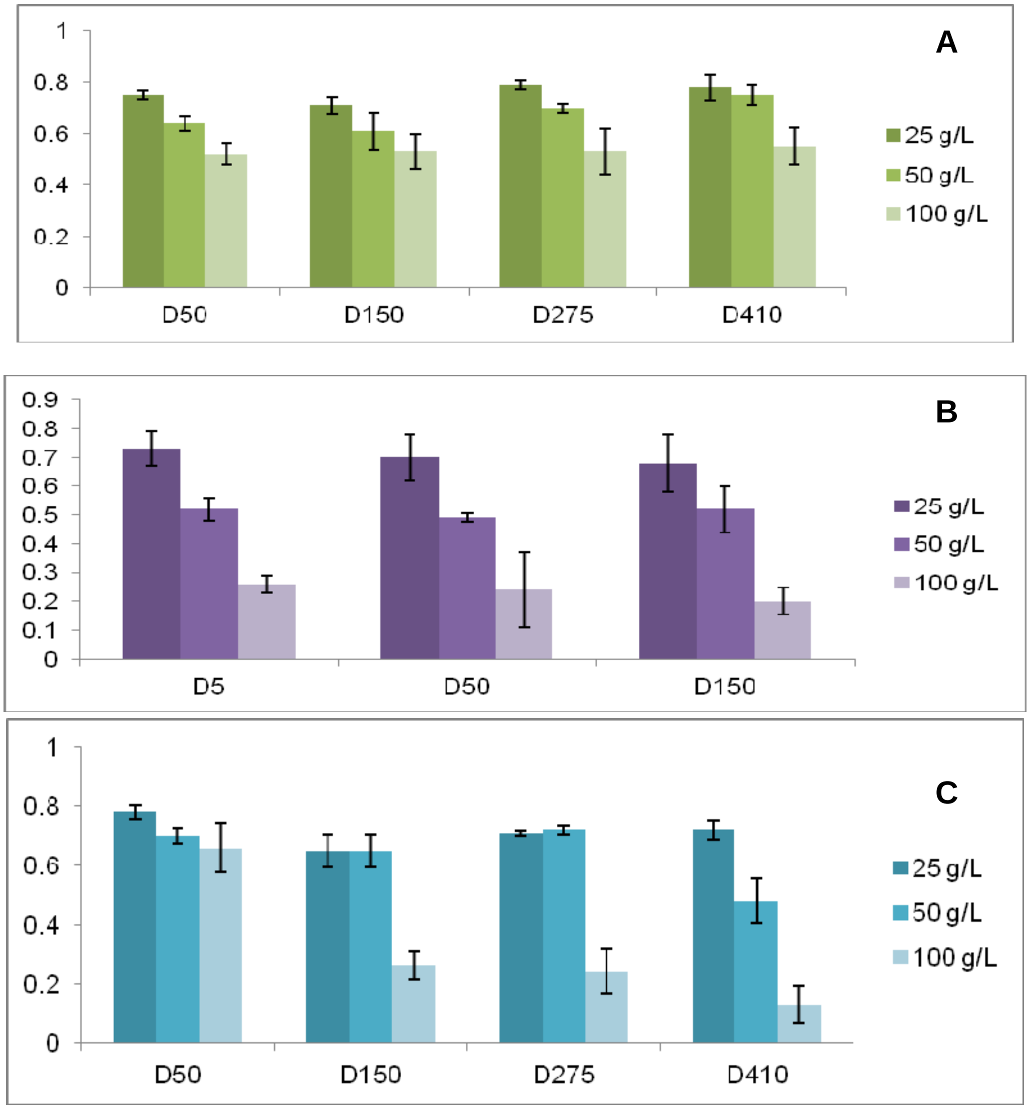

Figure 3: Relative K_m in dextran media for three different enzymes: A) α-chymotrypsin, B) HRP, C) LDH, in dextran concentrations ranging from 25 to 100 g/L (increasing from dark to light tone) of increasing dextran sizes: D50, D150, D275 and D410. Note that in figure 3C, relative K_M axis is shown from 0.6 to 1.

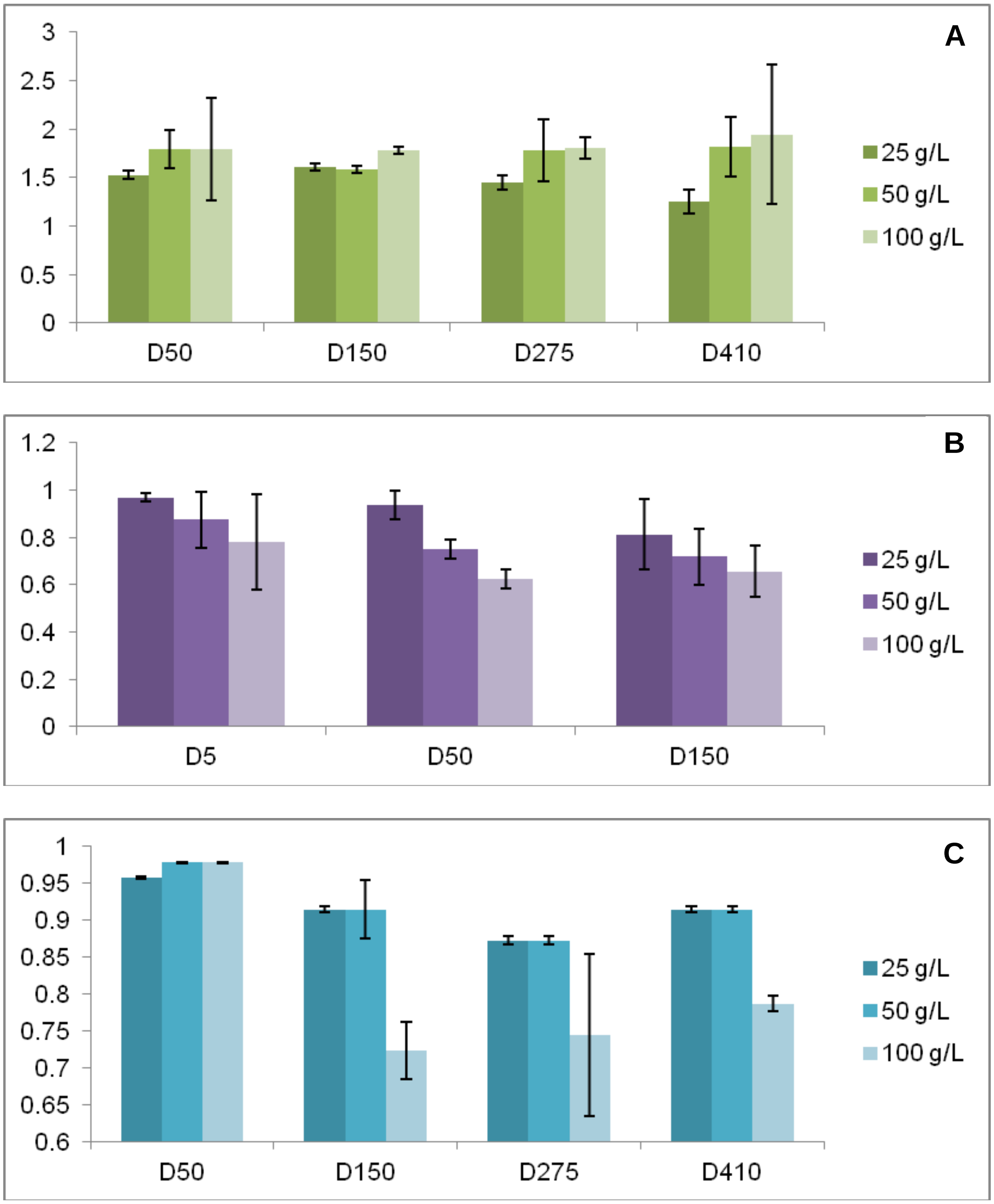

Horseradish peroxidase (HRP): 42 kDa

We studied the effect of macromolecular crowding in the oxidation of 2,2'-azino-bis(3-ethylbenzothiazoline-6-sulfonate (ABTS) by H2O2 catalysed by HRP [18]. With this purpose we used this system under different concentrations and sizes of the crowding agent, as seen in Fig. 1B.

The results show that the total excluded volume by the Dextran brings a greater impact on the velocity of the reaction than the size of the crowding agent. Moreover, the results indicate that both the value of vmax and Km decay as increasing the Dextran concentration in the sample, as depicted in Fig. 2B and Fig. 3B.

In fact, this enzymatic system does not show any significant tendency when increasing the molecular weight of the crowding agent. So, regarding the obstacle size-independence, this kinetic behaviour is also shown in the previous case, α-chymotrypsin.

Lactate dehydrogenase (LDH) from rabbit muscle: 140 kDa

The oxidation of NADH by pyruvate catalyzed by lactate dehydrogenase performed in crowded media conditions reveals that the apparent kinetic parameters, vmax and Km, are dependent on both crowding agent size and concentration, as seen in Fig. 1C.

In particular, it has been found that Km remains unaltered for all dextrans at low concentrations (25 g/L) and, at higher dextran concentrations (50-100 g/L), it shows a slight decrease for low molecular weight dextrans and a substantial decrease for high molecular weight dextrans, as seen in Fig. 2C.

Regarding vmax, it always decreases with respect to diluted solution, but the decrease is significantly larger for large dextrans at high concentrations, and partially compensated for smaller dextrans and low concentrations [19], as seen in Fig. 3C.

3.2. Discussion

A schematic summary of the evidences that one can extract by analysing the crowded media kinetics of an enzyme under the generalized Michaelis-Menten equation (3) in crowded media is detailed in Table 3. Table 4 is devoted to oligomeric proteins acting as enzymes in catalysed reactions, which could yield different behaviour than monomeric proteins [12, 19-21].

The main effect of macromolecular crowding is the excluded volume effect [1] that yields an increasing value of $v_{\max}$ (defined as $k_2[E]_t$) due to an increase of protein effective concentration. In addition, a decrease of the effective volume for the reactants is also experimentally given (Table 3). However, there are different causes that produce changes in the kinetics parameters of the enzymatic reaction. These causes can be classified in two main groups, depending if the size of the obstacle, for the same excluded volume fraction, affects or not the kinetic parameters of the enzymatic reaction.

Table 3: Effect of macromolecular crowding on proteins

K_m	v_{max}	k_1	k_2 or $[E]_t$	v_{max}/K_m	Why?	examples Refs.
↑	↑	↓	$[E]_t$ ↑	?	• Diffusion control • Exclude volume effect	[11, 16]
	↓	↓	k_2 ↓	↓	• Diffusion control • Conformational change or k_2 is affected by changes in the environmental surroundings • Inhibition by product	α-Chymotrypsin [17]
↓	↑	?	k_2, $[E]t$ ↑	?	• Activation control • Increase in chemical activity of E and/or S in crowded media • Exclude volume effect	Refs. [14-15]
	↓	↑	k_2 ↓	↓	• Activation control • More affinity for the encounters S+E • Conformational change or k_2 is affected by changes in the environmental surroundings	HRP [18], LDH [19] and Refs. [13-14, 21]

Table 4: Effect of macromolecular crowding on oligomeric proteins, as LDH. Mc refers to the molar mass of the obstacles and Mp refers to the molar mass of the protein [19].

Particular case	Relative size	K_m	v_{max}	k_1	k_2 or $[E]_t$	v_{max}/K_m	Why?
LDH tetramer 140 kDa	$M_c < M_p$	~	↓	↓	k_2 ↓	↓	• Mixed activation-diffusion control • Conformational change or k_2 is affected by changes in the environmental surroundings
	$M_c > M_p$	↓	↓	↓	k_2 ↓↓	↓	• Mixed activation-diffusion control • Reduction of the encounters S+E for large obstacles

Effect of crowding on the reaction control

Macromolecular crowding can affect both diffusion-controlled and activation-controlled enzymatic reactions through different mechanisms of action. If we try to dissect the overall reaction velocities in the classical Michealis-Menten scheme (1), we can analyse the effect of crowding in individual rate constants and Michaelis-Menten parameters, v_{max} and K_m.

In diffusion-controlled reactions, the reactive step is fast and the complex formation step is diffusion-dependent because a limited and/or anomalous diffusion is translate into less frequent enzyme-substrate encounters, which in turn means a decrease in k_1. Therefore, provided that k_2 is not modified, the Michaelis constant, K_m, should increase (Table 3).

Conversely, in activation-controlled reactions, the enzyme-mediated transformation of the substrate onto the product is the limiting step. Thus, even if the enzyme and the substrates present anomalous diffusion, it will not affect the overall kinetics of the reaction, since diffusion is much faster than the product formation. However, macromolecular crowding will play another role here: when volume exclusion is not negligible, enzyme and substrate effective concentrations are undeniably higher, since the reaction volume is lower than in dilute solution, thereby causing an increase in k_1, due to the increase of the affinity for the substrate-enzyme encounters, and therefore a decrease in K_m (Table 3).

Regarding v_{max}, several mechanisms can affect its value: it has been reported that macromolecular crowding can affect self-association equilibrium, conformational equilibrium and induce conformational changes in enzymes [2, 3, 10, 20, 22]. Subsequently, conformational changes that affect the catalytic capability of the enzyme – via slight modifications of the active site or oxyanion holes – can modify k_2 and thus v_{max} [20].

Nevertheless, the sign of this possible k_2 alteration is not clear, since the crowding-induced conformational changes may favour or hinder the interactions between the side chains of the enzyme amino acids and the substrate. And hence, for now it is not possible to predict whether v_{max} will raise or decay in crowded media [20].

As mentioned previously, another mechanism through which v_{max} (defined as $k_2[E]_t$) may be altered is because of higher enzyme effective concentration. Thus, an increase in enzyme effective concentration should result in higher values of v_{max} in crowded media. However, in the majority of studies, v_{max} is found to decrease and, consequently, volume exclusion must also cause alterations in k_2. This contribution must be predominant over the effective enzyme concentration effect, according to the available experimental results [13, 14, 17-19, 21].

Effect of crowding on different enzyme/obstacle size ratios

As shown in the results section, in some systems with enzymes such as LDH [19], crowded media does not only affect the kinetic behaviour as a result of the amount of excluded volume, but also when increasing the size of the crowding agent.

This behaviour has been only reported for relatively big enzymes, being the malate dehydrogenase the smallest enzyme (MDH, 70 kDa) [21]. Moreover, not only enzyme size may be important in order to present this effect, but also the relative size between the enzyme and the obstacle. Existing data still lacks convergence in this matter: while some results such as ALKP [12] and MDH [21] show that kinetic parameters are most largely affected by obstacles of a similar size as the enzyme, other enzymes such as LDH show that the largest effect occurs when obstacles are bigger than the enzyme at large amounts of excluded volume.

This size-dependence suggests that depletion forces may gain importance inside the cell cytosol, a medium in which large amount of particles of different sizes heterogeneously distributed is present.

4. CONCLUSIONS

Different consequences of high volume occupancy on the field of enzyme kinetics have been addressed: on the one hand, the obstacle size-dependent functioning of oligomeric enzymes and, on the other hand, the effect of volume exclusion upon the reaction control of enzyme-catalysed reactions.
In the first one, small enzymes such as α-chymotrypsin or HRP show an obstacle size-independent relationship, unlike bigger oligomeric enzymes such as ALKP, MDH or LDH.

The later of these, LDH, also shows an interesting behaviour when increasing excluded volume and obstacle size: v_{max} decays slightly and K_m remains constant with small obstacles at moderate concentrations, while both parameters clearly decay with big obstacles at high concentrations. These results may only be explained if the reaction control is considered as being mixed, and provided that it shifts from reaction to diffusion as crowding levels are increased.

Both findings, obtained using synthetic polymers to model volume exclusion levels typically found in the cells, remark the necessity of reconsidering traditional in-vitro enzymology and setting new bases in more biophysically realistic environments.

ACKNOWLEDGEMENTS

For the spanish authors, this work was supported by the Spanish Ministry of Science and Innovation & European Commission-European Regional Development Funds (projects CTM2012-39183 and SAF2011-25726), by the Generalitat de Catalunya (grants 2014SGR1017, 2014SGR1132 and XRQTC) and Icrea Academia Award 2010 (granted to MC). For the romanian authors, LP gratefully acknowledges the financial support of the project POSDRU/89/1.5/S/63663 - Transnational network for integrated management of postdoctoral research in the field of Science Communication and Institutional set up (postdoctoral school) and scholarship program (CommScie).

REFERENCES

1. Zimmerman, S.B.; Trach, S.O. Estimation of macromolecule concentrations and excluded volume effects for the cytoplasm of Escherichia coli. *Journal of Molecular Biology* **1991**, 222, 599 − 620.
2. Zhou, H.X.; Rivas, G.; Minton, A. P. Macromolecular crowding and confinement: biochemical, biophysical, and potential physiological consequences. *Annual Review of Biophysics* **2008**, *37*, 375–397.
3. Kuznetsova, I.M.; Turoverov, K.K.; Uversky, V.N. What Macromolecular Crowding Can Do to a Protein. *International Journal of Molecular Sciences* **2014**, 15, 23090-23140.
4. Dix, J.; Verkman, A.S. Crowding effects on diffusion in solutions and cells. *Annual Review of Biophysics* **2008**, *37*, 247–263.
5. Pastor, I.; Vilaseca, E.; Madurga, S.; Garcés, J.L.; Cascante, M.; Mas, F. Diffusion of alpha-chymotrypsin in solution-crowded media. A fluorescence recovery after photobleaching study. *The Journal of Physical Chemistry B* **2010**, *114*, 4028–4034.
6. Vilaseca, E.; Isvoran, A.; Madurga, S.; Pastor, I.; Garcés, J.L.; Mas, F. New insights into diffusion in 3D crowded media by Monte Carlo simulations: effect of size, mobility and spatial distribution of obstacles. *Physical Chemistry Chemical Physics* **2011**, *13*(16), 7396–7407.
7. Zimmerman S.B. Macromolecular crowding effects on macromolecular interactions: some implications for genome structure and function. *Biochimica et Biophysica Acta* **1993**, 1216(2), 175-185.
8. Schreiber, G.; Haran, G.; Zhou, H.X. Fundamental aspects of protein-protein association kinetics. *Chemical Reviews* **2009**, *109*(3), 839–60.
9. Wang, Y.; Sarkar, M.; Smith, A. E.; Krois, A. S.; Pielak, G. J. Macromolecular crowding and protein stability. *Journal of the American Chemical Society* **2012**, *134*, 16614–16618.
10. Minton, A.P.; Wilf, J. Effect of macromolecular crowding upon the structure and function of an enzyme: glyceraldehyde-3-phosphate dehydrogenase. *Biochemistry* **1981**, *20*(17), 4821–4826.
11. Wenner, J.R.; Bloomfield, V.A. Crowding effects on EcoRV kinetics and binding. *Biophysical Journal* **1999**, *77*(6), 3234–3241.
12. Homchaudhuri, L.; Sarma, N.; Swaminathan, R. Effect of Crowding by Dextrans and Ficolls on the Rate of Alkaline Phosphatase-Catalyzed Hydrolysis: A Size-Dependent Investigation. *Biopolymers* **2006**, *83*, 477–486.
13. Olsen, S. N.; Ramløv, H.; Westh, P. Effects of Osmolytes on Hexokinase Kinetics Combined with Macromolecular Crowding Test of the Osmolyte Compatibility Hypothesis Towards Crowded Systems. *Comparative Biochemistry and Physiology Part A: Molecular & Integrative Physiology* **2007**, 148, 339−345.
14. Jiang, M.; Guo, Z. Effects of macromolecular crowding on the intrinsic catalytic efficiency and structure of enterobactin-specific isochorismate synthase. *Journal of the American Chemical Society* **2007**, *129*(4), 730–731.
15. Morán-Zorzano, M. T.; Viale, A. M.; Muñoz, F. J.; Alonso-Casajús, N.; Eydallín, G. G.; Zugasti, B.; Baroja-Fernández, E; Pozueta-Romero, J. Escherichia coli AspP activity is enhanced by macromolecular crowding and by both glucose-1,6-bisphosphate and nucleotide-sugars. *FEBS Letters* **2007**, *581*(5), 1035–1040.

16. Pozdnyakova, I.; Wittung-Stafshede, P. Non-linear effects of macromolecular crowding on enzymatic activity of multi-copper oxidase. *Biochimica et Biophysica Acta - Proteins and Proteomics* **2010**, *1804*(4), 740–744.
17. Pastor, I.; Vilaseca, E.; Madurga, S.; Garcés, J.L.; Cascante, M; Mas, F.. Effect of crowding by dextrans on the hydrolysis of N-Succinyl-L-phenyl-Ala-p-nitroanilide catalyzed by α-chymotrypsin. *The Journal of Physical Chemistry. B* **2011**, *115*(5), 1115–21.
18. Pitulice, L.; Pastor, I.; Vilaseca, E.; Madurga, S.; Isvoran, A.; Cascante, M.; Mas, F. Influence of Macromolecular Crowding on the Oxidation of ABTS by Hydrogen Peroxide Catalyzed by HRP. *Journal of Biocatalysis & Biotransformation* **2013**. 2, 1-5.
19. Balcells, C.; Pastor, I.; Vilaseca, E.; Madurga, S.; Cascante, M.; Mas, F. Macromolecular crowding effect upon in vitro enzyme kinetics: mixed activation-diffusion control of the oxidation of NADH by pyruvate catalyzed by lactate dehydrogenase . *The Journal of Physical Chemistry. B* **2014**, *118*, 4062–8.
20. Pastor, I.; Pitulice, L.; Balcells, C.; Vilaseca, E.; Madurga, S.; Isvoran, A.; Cascante, M.; Mas, F. Effect of crowding by Dextrans in enzymatic reactions. *Biophysical Chemistry* 2014*, 185,* 8-13.
21. Poggi, C. G.; Slade, K. M. Macromolecular Crowding and the Steady-State Kinetics of Malate Dehydrogenase. *Biochemistry* **2015**, *54*, 260–267.
22. Bismuto, E.; Irace, G. The effect of molecular confinement on the conformational dynamics of the native and partly folded state of apomyoglobin. *FEBS Letters* **2001**, *509*, 476–480.
23. Cornish-Bowden, A. *Fundamentals of Enzyme Kinetics*, 4th Ed. Wiley-VCH, Weinheim, Germany, **2012**.
24. Schnell, S. Validity of the Michaelis-Menten equation – steady-state or reactant stationary assumption: that is the question. *FEBS Journal* 2014*, 281,* 464-472.

NEW FRONT. CHEM. (**2015**)
Volume 24, Number 1, pp. 17-25
ISSN 2393-2171; ISSN-L 2393-2171
© West University of Timişoara

Former: Ann. West Univ. Timisoara – Series Chem.
ISSN: 1224-9513

Article

ARE THE SURFACE WATER SOURCES FROM TIMIŞ COUNTY SAFE FOR CHILDREN AND PREGNANT WOMEN HEALTH?

Teofana Otilia Bizerea (1,2) (♣)**, *Silvana Bîgu*** (3,4)

(1) Children Emergency Hospital ”Louis Ţurcanu”, Iosif Nemoianu Street, 2, Timişoara, 300011, România
(2) University for Medicine and Pharmacy ”Victor Babeş”, P-ţa Eftimie Murgu, 2, Timişoara, 300041, România
(3) West University of Timişoara, Biology-Chemistry Department, Pestalozzi Street, 16, Timişoara, 300115, România
(4) Laboratory of Advanced Researches in Environmental Protection (LCAM), Oituz Street, 4, Timişoara, 300086, România

ABSTRACT

Without claiming to achieve an integrated monitoring or intensive activities for the quality of surface water in the investigated area, this paper aims to assess the quality of water from Bega and Timiş rivers with regard to nitrites, nitrates and chlorides. This is part of a larger study on the quality of water sources in the region, with regard to the anionic and cationic pollutants. The study follows the impact of the drinking water on the human health, especially children and pregnant women. The considered parameters were below the admitted value, therefore no pollution problems were found.

Keywords: surface water, water quality, nitrites, nitrates, chlorides

1. INTRODUCTION

Any solid, liquid, gaseous or vapour that enters into the environment, changes the balance of its components and damage living organisms by bringing pollutants [1].

We define the background pollution as that not directly influencing the environment and show pollution impacts in areas directly affected by the pollution sources.

♣ Correspondent author: Tel: 00729093725; Email: teofanabizerea@yahoo.com

The degradation of water quality may be caused by: low level of network equipment catalyst, manure removed from the breeding complexes and poultry, deposits of silt and garbage made on various surfaces, fertilizers and pesticides incorrectly administered on agricultural land.

Nitrates and nitrites are natural, soil components generated by organic matter mineralization of nitrogen of plant and animal origin. Nitrogen mineralization is primarily due to existing soil microorganisms. In countries with temperate climate, this process takes place with maximum intensity in summer [2].

Naturally, between nitrates and nitrites in the soil, water and plant exists a balance that can be broken by the intensive use of natural organic fertilizers (manure), especially nitrogenous synthetic compounds, in agriculture [2, 5]. Their degradation by-products can accumulate in plants growth to levels harmful to consumers.

Nitrates, as such, have a low toxicity (when used in small doses), and they were usually used as a diuretic.

Nitrate is absorbed very quickly by the small intestine and excreted by the kidneys, saliva and gastric juice [1, 2]. To generate problems, nitrate has to be ingested in large amounts (up to 10g per dose). Generally, symptoms of intoxication may be as follows: nausea, vomiting, cramps, diarrhoea, and sometimes blood [2].

The daily intake of nitrate allowed in humans has been established by FAO / WHO to 5 mg / kg body weight, which is 350 mg / day for a 70 kg person [1].

Nitrates have received much attention especially in connection with the so-called blue baby disease (methemoglobinemia). Concentrations between 10 and 20 mg/L produce illness and even death in children less than 6 months. In this case the blood ability to carry oxygen is impaired. This serious condition is caused by the conversion of nitrate to nitrite at increased pH of the infant’s stomach and intestinal tract.

Numerous ground waters contain small amounts of nitrates, generally ranging between 0.1 and 4.3 mg/L. But there are plenty of situations where the values exceed 100 mg/L. Nitrate is present in both shallow and deep wells as a result of water infiltration through soils containing nitrate minerals. Improper use of agricultural fertilizers can be another source of nitrates occurring in excess in the water for consumption. Nitrates are also one of the decomposition compounds of animal or human waste. Therefore, the nitrate in water supplies indicates a possible pollution.

During decomposition, slurry undergoes chemical transformation. Where normally groundwater does not contain natural nitrates, their expanding concentrations, is also an indicator of pollution.

Nitrites are more toxic than nitrates. They are found in small quantities in food as a natural compound. But their concentrations can increase to dangerous levels by reducing the action of microorganisms on nitrates.

Lethal doses of nitrite are in the range of several grams per adult and 0.2 to 0.5 g for children whose blood pigments are more sensitive to oxidation, because they are the higher proportion of foetal type [1]. Therefore, nitrite, daily intake was set at 0.2 mg / kg body weight, respectively 14 mg / day for a 70 kg person.

The oxidant effect is manifested on all cytochromes and redox systems of the body. The effect manifests in terms of oxidant deficiency of vitamin E and vitamin A [2].

A major risk that is borne by nitrates and nitrites presence in food and water is the possibility of forming nitrosamines, substances with mutagenic malignant potential [4].

Methemoglobinemia has been long considered the main condition caused by exposure to nitrates and nitrites from drinking water, especially in infants under 4 months. A big portion of the children's hemoglobin is in the form of fetal hemoglobin which is much easier oxidized to methemoglobin than that of the adults. Therefore, children, especially premature children, are particularly sensitive. Infants were identified as the most sensitive subpopulation because their gastrointestinal pH is more acid, favoring the growth of bacteria that convert nitrate to nitrite (nitrate-reducing bacteria), which in turn binds to hemoglobin to form methemoglobin Instead, the stomach of adults is typically too acidic to allow significant bacterial growth and the resulting conversion of nitrate to nitrite. On the other hand, the amount and activity of the enzyme which reduces methemoglobin is deficient in infants up to 6 months.

At birth, NADH-dependent methemoglobin reductase (also called cytochrome-b5 reductase), the main enzyme responsible for reducing methemoglobin back to normal hemoglobin, presents only half of the activity that adults have and does not reach the level of an adult at least till 4 months of age. Pregnant women and their fetuses are another high-risk group. Pregnancy, with its oxygen demand and increased levels of oxidative stress can overwhelm the body's ability to reconvert methemoglobin back to hemoglobin, leading to increasing levels of methemoglobin [9, 10].

However, recent studies have shown that the effects on thyroid function cannot be neglected. In this respect, effects have been observed in school age children but no study has considered infants, although it would be expected that they are the most vulnerable. Infants remain the most sensitive population because the half-life and storage time of their thyroid hormones are much shorter. In addition, exposure to nitrate during pregnancy can affect the production of thyroid hormones, which could have an impact on fetal development. Therefore, pregnant women at or near the 30 week of pregnancy and their fetuses may be more susceptible to the toxicity of nitrites and nitrates [9, 10].

Also, current research suggests an association between cancer and exposure to nitrates and nitrites from drinking water due to the formation of nitrosamines in the human body.

In water, chlorine reacts to form hypochlorous acid and hypochlorites. All three species exist in equilibrium with each other, the relative amounts varying with the pH. In dilute solutions and at pH levels above 4.0, very little molecular chlorine exists in solution. The concentrations of hypochlorous acid and the hypochlorite ion are approximately equal at pH 7.5 and 25 °C. Chlorine can react with ammonia or amines in water to form chloramines [7, 8].

Chlorine is present in most disinfected drinking-waters at concentrations of 0.2-1.0 mg/L [6]. Calcium hypochlorite has an oral LD50 in the rat of 850 mg/kg of body weight [5].

This paper aims to present some important aspects of quality of surface water resources in the area of Bega and Timiş rivers by monitoring parameters indicating their degree of pollution such as: nitrates, nitrites and chlorides. As part of a larger study on the quality of water sources in the region, the present research tries to identify some anionic and cationic pollutants, which may have an impact on human health. Especially children and pregnant women are sensitive population groups that are prone to be affected when using an improper drinking water. The results of the present study may be of great importance in interpreting the correlation between water quality and various health issues.

The main methods of identifying the nitrite and nitrate anions in water are presented in Table 1.

Table 1: The main methods of identifying NO_2^- and NO_3^- anions from water

ANIONS / **REAGENTS**	NO_2^-	NO_3^-
H_2SO_4 concentrated	$NO + NO_2$ - brown gas	$NO + NO_2$ - brown gas
$AgNO_3$	-	-
$FeSO_4$	$Fe^{2+} \rightarrow Fe^{3+}$ - yellow brown solution	$Fe^{2+} \rightarrow Fe^{3+}$ - yellow brown solution
Zn(metal) in presence of NaOH	Blackened paper impregnated with $Hg_2(NO_3)_2$	Blackened paper impregnated with $Hg_2(NO_3)_2$
Diphenyl-amine	Blue coloration	Blue coloration
Antipyrine - solution 5%	Carmine red coloration, nitro-antipyrine	Green coloration, nitroso-antipyrine
Naphthylamine + acid sulphanilic	-	Azocolorant red

2. MATERIALS AND METHODS

Sampling and Conservation

Samples must be representative and must not introduce changes in the composition and water quality due to poor sampling techniques or improper storage conditions of the samples.

Sampling site should be chosen to ensure a representative characterization of the water source.

The volume of the collected samples depends on the number and type of analyses performed, aiming at collecting water samples to ensure at least three determinations of the same type for each analysed parameter.

Sampling frequency, in general, and frequency variations exceed maximum parameters to follow or overlap with it.

For surface waters, the analysis is performed 2-4 times a year, the most critical periods of pollution being the minimum flows in winter (lowest temperatures) and in summer (highest temperatures) and spring peak flows and / or fall (as rain or melting snow).

The water samples were collected in sealed polyethylene containers for physical-chemical analysis. Recipients were previously washed with hydrochloric acid and detergent, then rinsed with tap water, distilled water and then with the sample to remove any organic or other impurities that may distort the composition of the sample.

To minimize sample changes during sampling, their transport was performed in the shortest possible time, and until their analysis was done they were stored in dark and temperature of approx. 4° C.

There were two water samples taken from each set, given in Table 2.

Table 2: Place of sampling

Samples	Place	GPS coordinates
S1	Lugojel village – Timiş River	45.666858, 21.973176
S2	Coştei village – Timiş River	45.734432, 21.856143
S3	Jabar village – Timiş River	45.731905, 21.818478
S4	Babsa village – Timiş-Bega Channel	45.773397, 21.770354
S5	Bazoş village – Timiş River	45.725161, 21.497938
S6	Şag village – Timiş River	45.63886, 21.187129
S7	Remetea Mare – Bega River Bridge	45.777711, 21.376048
S8	South Recaş – Bega-Timiş Channel	45.77545, 21.513878
S9	Ghiroda village – Bega River	45.762725, 21.304406
S10	Utvin village – Bega River	45.706469, 21.089912

In general, the following analyses have to be made in a short time interval after sampling, within 24 hours.

Measurements

All the reaction agents used in this study were of analytical quality.

The solutions, of different concentrations, were obtained by dissolving the adequate quantity of salt (KNO_3, KNO_2, NaCl), weighed by analytic balance with an accuracy of ± 0.0001 mg, in bidistilled water, in a volumetric flask.

The operations were carried out at room temperature (25 ± 1ºC), without adjusting the pH of the working solutions.

The concentration of the nitrate and chloride (NO_3^-, Cl^-) in the samples was potentiometrically determined using a nitrite-sensitive and chloride-sensitive electrode, ELIT 8227 – NICO 2000 and ELIT 8444 – NICO 2000 respectively. Also, a double junction reference electrode ELIT 003N – NICO 2000 was used.

Potentiometer anion-selective sensors based on liquid membrane / polymer is a method increasingly used to control water quality, due to capacity fast and accurate determination of these parameters.

The measurement process was performed with the help of a customizable Virtual Instrumentation [11, 12]. This solution was preferred mainly because of the possibility to adapt the application to the different calculus requirements involved with the experimental part. Automation of sensor calibration and the flexibility with which one can exploit the calculus power of the PC are two important advantages which the authors considered.

The hardware component consisted of the NI USB 9215A data acquisition device, produced by National Instruments. This device is capable of performing ADC on 16 bits, it provides 4 analog input channels and accepts a max. of ±10 V_{pp} for the input signal. Signal conditioning was implemented using the MCP 601 Single Supply Amplifier. This was necessary since noise reduction/removal is an important issue in data acquisition systems. Visual inspection of acquired data (with and without amplification) showed that fluctuations due to noise presence can be limited if the useful signal is amplified by a factor of 10.

The hardware device was controlled by a dedicated software application programmed in National Instruments' LabVIEW development environment. For running the software components, the authors used a notebook computer with Dual Core – 1.8 GHz CPU, 2 GB DDR3 and Internet Connection. Interaction between the software component and the NI USB 9215A is performed by the NI-DAQmx driver. The measurement procedure was divided into three main parts: acquisition, analysis, and presentation of data. The features include data logging, statistical calculations and graphical presentation of recorded data. Each measurement lasts 130 s and the established sampling period is 1 s. So automated calculations are performed over records of 130 samples and the following parameters are presented: sensor output voltage, sensor output average voltage (over the last 10 samples), calculated concentration, adsorption capacity and process return.

Concentration of nitrite (NO_2^-) in water samples was determined by spectrophotometer. Measurements were performed using a spectrophotometer type T90, measuring range 190-900 nm.

Wavelength at which measurements were made was $\lambda = 650$ nm.

3. RESULTS AND DISCUSSIONS

The results presented in 2013 by the Romanian National Administration of Water [13] suggest that the quality objective of good environmental status was not reached by 4 water bodies, representing 13.33% of the total natural water bodies - rivers from Bega-Timis-Caras basins, and 86.45 km respectively, representing 7.82% km river - natural bodies for which the ecological status was determined.

Considering the biological elements (phytobenthos, phytoplankton, benthic macroinvertebrates and ichtyofauna) the 30 water bodies monitored and evaluated on a length of 1105.60 kilometers were considered of very good condition (16 water bodies) good (13 water bodies) and moderate condition (1 water body) the decisive elements being the benthic macroinvertebrates and ichtyofauna.

Thirty water bodies were generally monitored and evaluated taking into account also the physico-chemical properties. The results are as following: 21 bodies (70.00%) were classified in good condition and 9 bodies (30.00%) were classified in moderate condition, the decisive elements being the oxygenation conditions and the nutrients.

Potentiometric results obtained for the water samples listed in Table 1 are found in Table 5 for nitrates and Table 6 for chlorides, respectively.

It should be noted that because the Mohr method ($AgNO_3$ and $K_2Cr_2O_7$) is a standard one, chlorides were determined also by volumetric method but the values are so small, that fall within the method error.

The spectrophotometric results of nitrite for the water samples listed in Table 1 are given in Table 7.

Table 5: Nitrate content of surface water samples

Sample	**NO_3^- - spectrophotometric**		**NO_3^- - potentiometric**		**Differences between the two methods (%)**
	mg/L (ppm)	**moles/L**	**mg/L (ppm)**	**moles/L**	
S1	4.10	$0.66\cdot10^{-4}$	4.17	$0,67\cdot10^{-4}$	1.68
S2	3.80	$0.613\cdot10^{-4}$	3.98	$0,64\cdot10^{-4}$	4.52
S3	6.60	$1.06\cdot10^{-4}$	6.29	$1.01\cdot10^{-4}$	4.70
S4	8.10	$1.31\cdot10^{-4}$	8.48	$1.37\cdot10^{-4}$	4.48
S5	6.60	$1.06\cdot10^{-4}$	6.94	$1.12\cdot10^{-4}$	4.90
S6	12.90	$2.08\cdot10^{-4}$	12.93	$2.08\cdot10^{-4}$	0.23
S7	18.00	$2.90\cdot10^{-4}$	18.24	$2.94\cdot10^{-4}$	1.32
S8	12.40	$2.00\cdot10^{-4}$	12.70	$2.05\cdot10^{-4}$	2.36
S9	5.40	$0.87\cdot10^{-4}$	5.73	$0.92\cdot10^{-4}$	5.76
S10	11.50	$1.85\cdot10^{-4}$	11.58	$1.87\cdot10^{-4}$	0.70
			LD = 0.3	LD = $0.05\cdot10^{-4}$	
Values range (Law 458/ 08.07. 2002)	**50**	**$8.06\cdot10^{-4}$**	**50**	**$8.06\cdot10^{-4}$**	

Table 6: Chloride content of surface water samples

Sample	**Cl^- - potentiometric**		**Observations**
	mg/L (ppm)	**moles/L**	
S1	4.8920	$1.3800\cdot10^{-4}$	Chlorides were determined by volumetric and Mohr ($AgNO_3$ and $K_2Cr_2O_7$) methods, but the values are so small, that fall into the method error.
S2	5.4660	$1.5418\cdot10^{-4}$	
S3	5.8203	$1.6417\cdot10^{-4}$	
S4	5.7163	$1.6124\cdot10^{-4}$	
S5	6.8262	$1.9254\cdot10^{-4}$	
S6	9.1605	$2.5838\cdot10^{-4}$	
S7	6.9842	$1.9700\cdot10^{-4}$	
S8	6.4816	$1.8282\cdot10^{-4}$	
S9	8.4008	$2.3696\cdot10^{-4}$	
S10	27.318	$7.7054\cdot10^{-4}$	
	LD = 1.000	LD = $0.3\cdot10^{-4}$	
Values range (Law 458/ 08.07. 2002)	**50**	**$8.06\cdot10^{-4}$**	

Table 7: Nitrite content of surface water samples

Sample	**NO_2^- - spectrophotometrically**		**Observations**
	mg/L (ppm)	**moles/L**	
S1	0.12	$0.026\cdot10^{-4}$	All values are well below the allowed limit
S2	0.14	$0.030\cdot10^{-4}$	
S3	0.15	$0.033\cdot10^{-4}$	
S4	0.15	$0.033\cdot10^{-4}$	
S5	0.16	$0.035\cdot10^{-4}$	
S6	0.16	$0.035\cdot10^{-4}$	
S7	0.17	$0.037\cdot10^{-4}$	
S8	0.15	$0.033\cdot10^{-4}$	
S9	0.15	$0.033\cdot10^{-4}$	
S10	0.20	$0.044\cdot10^{-4}$	
Values range (Law 458/08.07. 2002)	**0.5**	**$0.109\cdot10^{-4}$**	

In Tables 5, 6 and 7, we see that the values of nitrate, nitrite and chloride in all analysed samples are below the maximum concentration allowed by law.

4. CONCLUSION

Taking into account the analysed parameters (nitrites, nitrates and chlorides), both Timiş and Bega rivers are within the limits stipulated by the concerning laws (Law 458/08.07.2002 for potable water).

Given that a high concentration of any of these parameters, especially nitrate, is an indicator of pollution, their low concentrations indicate no serious problems of pollution.

On the other hand, we can see that the difference between measurements obtained by spectrophotometric and potentiometric method, respectively, is below 5%, which indicates that potentiometry can be used to serial determinations of nitrate and chloride. This is very useful taking into account that the potentiometric method is less laborious than the spectrophotometric one.

Given the importance of the objective sought within this research, it is imperative to continue to monitor the surface water sources over a long period of time also considering other quality parameters.

ACKNOWLEDGEMENT

The first author acknowledges the financial support of the project *Parteneriat strategic pentru creşterea calităţii cercetării ştiinţifice din universităţile medicale prin acordarea de burse doctorale şi postdoctorale – DocMed.Net_2.0*, POSDRU/159/1.5/S/136893.

REFERENCES

1. Banu, C. *Aditivi şi ingredienţi pentru industria alimentară*. Ed. Tehnică, Bucureşti, România, **2000**;
2. Fan, A.M. Nitrate and Nitrite in Drinking Water: A Toxicological Review. *Encyclopedia of Environmental Health* **2011**, 137-145.
3. Banu, C. *Tratat de chimia alimentară*. Ed. AGIR, Bucureşti, România, 2002.
4. Berlitz, H.D.; Grosch, W.; Schieberle, P. *Food Chemistry - 4th revised and Extended Edition*, Springer-Verlag Berlin Heidelberg, **2009**.
5. Gibbs, M.S.; Morgan, N.; Maier, H.R.; Dandy, G.C.; Nixon, J.B.; Holmes, M. Investigation into the relationship between chlorine decay and water distribution parameters using data driven methods. *Mathematical and Computer Modelling* **2006**, *44*, 485-498.
6. Ben, W.; Anna, H.; Cynthia, J.; Robert, K. A new method for calculation of the chlorine demand of natural and treated waters. *Water Research* **2006**, *40*, 2877-2884.
7. Benoit, B.; Raymond, D.; Chandra, M.; Michele, P. Impacts of water quality on chlorine and chlorine dioxide efficacy in natural waters. *Water Research* **2005**, *39*, 2024-2033.
8. Wen, L.; Laurent, K.; Yves, L. Chlorine demand of biofilms in water distribution systems. *Water Research* **2000**, *33(3)*, 827-835.
9. *** *Nitrate and Nitrite in Drinking Water - Document for Public Comment*, Health Canada, Federal-Provincial-Territorial Committee on Drinking Water **2013**; pp. 2-3, 93-94.
10. *** *Case Studies in Environmental Medicine - Nitrate/Nitrite Toxicity*. US Department of Health and Human Services, Agency for Toxic Substances and Disease Registry **2013**, pp. 32-36.
11. Clark, C.L. *LabVIEW. Digital Signal Processing and Digital Communications*, McGraw-Hill, **2005**.
12. Smiesko, V.; Kovac, K. Virtual Instrumentation and distributed measurement systems, *J Electr Eng* **2004**, *55(1-2)*, 50-56.
13. Moldovan, C.; Soare, F.; Dumitrache, F.; Iliescu, Ş.; Gheorghiu, I.; Rotaru, N.; Costea, F.; Nistor, C. *Sinteza calității apelor din România în anul 2013*. Administraţia Naţională Apele Române, Bucureşti **2014**, pp.69-71.

NEW FRONT. CHEM. (**2015**)
Volume 24, Number 1, pp. 27-36
ISSN 2393-2171; ISSN-L 2393-2171
© West University of Timișoara

Former: Ann. West Univ. Timisoara – Series Chem.
ISSN: 1224-9513

Article

SOME SYSTEMATICS AND SURPRISES IN THE ENERGETICS AND STRUCTURAL PREFERENCES OF "FEW-BORON SPECIES" AND RELATED COMPOUNDS WITH CARBON AND NITROGEN

Maja Ponikvar-Svet (1) ***and Joel. F Liebman*** (2, ♣)
[1] Department of Inorganic Chemistry and Technology, Jožef Stefan Institute, Jamova 39, SI–1000 Ljubljana, Slovenia
[2] Department of Chemistry and Biochemistry, University of Maryland, Baltimore County, Baltimore, MD 21250, US

ABSTRACT

This paper discusses the energetics and structural preferences of "some few-boron species", BH_3, B_2H_6, $[B_3H_8]^-$ and B_3H_9, B_4H_{10} and B_4H_{12} and the corresponding isoelectronic hydrocarbons CH_2, C_2H_4, C_3H_6, C_4H_6 and C_4H_8. Nitrogen hydrides are also briefly discussed as are substituted derivatives. Both systematics and surprises are found.

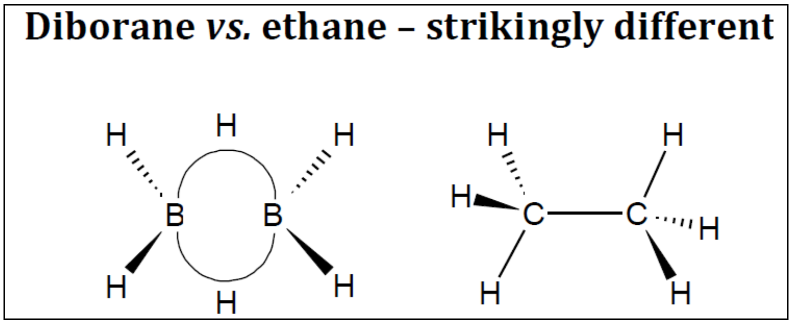

Keywords: boranes, hydrocarbons, nitrogen hydrides, isomer stabilities and preferences

---

♣ Correspondent author: Tel:-1-410-455-2549, Fax -1-410-455-2608:, E-mail: jliebman@umbc.edu

1. INTRODUCTION

Boron forms a large variety of binary species containing hydrogen. These substances are now generally called boranes, occasionally still called boron hydrides, and historically through the decades, almost never named hydroborons. By simply counting the number of SciFinder citations given for each compound of interest [1], we find the most thoroughly studied species so described are the neutral diborane(6) and decaborane(14), B_2H_6 and $B_{10}H_{14}$ with ca. 9000 and 2000 reference citations respectively (very often with the total hydrogen count, 6 and 14, ignored in the name), and the anionic borohydride (most often $[BH_4]^-$ but also quite commonly $[B_3H_8]^-$, $[B_{10}H_{10}]^{2-}$ and $[B_{12}H_{12}]^{2-}$) with ca. 45000 reference citations respectively. The list of species containing only boron and hydrogen is extensive, although admittedly much shorter than that of binary species of carbon with hydrogen.

2. THE TWO BORON SPECIES, B_2H_6, THE RELATED HYDROCARBON C_2H_4, AND THEIR ONE-BORON AND ONE-CARBON MONOMERS

Isoelectronic with B_2H_6 is ethylene, C_2H_4, which is among the simplest of all the hydrocarbons, and indeed, we are reminded of the early description of diborane(6) as having "a protonated double bond" [2]. Both diborane(6) and ethylene are highly stable as written and isolable as bulk, macroscopic samples, while neither species is isolable in the form of its corresponding isoelectronic one-carbon and one-boron monomer, CH_2 and BH_3 respectively, [3-6]. We note an immediate difference between CH_2 and BH_3: they are respectively a ground state triplet and singlet. Among the earliest electron diffraction studies ever reported was an investigation of B_2H_6 [7] which incorrectly suggested a structure like that of ethane, C_2H_6. For a discussion of the differing structures of diborane(6) and ethane within the molecular orbital framework, see [8-10] respectively. However, nearly two decades before the expressions "the STYX rules" and "3-center bonds" entered the chemist's vocabulary [11] and just before the aforementioned electron diffraction study [7], there was a molecular orbital based discussion of B_2H_6 in which this species was assumed to have the ethane-like structure [12].

3. THE CORRESPONDING BH_3 AND CH_2 TRIMERS, TRIBORANE(9), CYCLOPROPANE, AND ALSO $[B_3H_8]^-$

The corresponding BH_3 and CH_2 trimers, B_3H_9 and C_3H_6 are recognized as cyclopropane and triborane(9) respectively. Indeed, long predating the conceptually useful alternative (but nowhere recommended) name of ethylene as "cycloethane" [13,14], in the late 19th and early 20th centuries cyclopropane and its derivatives were not uncommonly named "trimethylenes". Indeed, occasionally the words "cyclopropanes" and "trimethylenes" were both used in the same article [e.g.15]. However, there is a profound distinction between C_3H_6 and B_3H_9. While cyclopropane and numerous derivatives are isolable, see the monographs [16,17], the latter species triborane(9) is but a transient intermediate associated with processes such as the gas phase reaction of diborane(6) with BH_3 [18], the protonation of $[B_3H_8]^-$ salts [19-21] and diborane(6) pyrolysis [22,23]. These studies suggest that 3-membered all-carbon rings are stable but 3-membered all-boron rings are not (by saying all-boron rings we neglect any bridging H's in the ring atom count). Ethylene and its substituted counterparts generally do not equilibrate or otherwise interconvert with the corresponding cyclopropanes.

The thermolysis reaction of the formally simplest case of cyclopropane

$$2C_3H_6 \rightarrow 3C_2H_4 \tag{1}$$

is endothermic [24], entropically favored (two molecules forming three), and unobserved in either direction. (At STP, this reaction may be readily calculated to have fortuitously close to a zero free energy change, and not surprisingly shows a significant temperature variation [25].) Corresponding reactions are also generally not seen for substituted derivatives of cyclopropane and ethylene. Among the few recorded cases [26,27] of thermolysis of a cyclopropane to form the corresponding ethylene is that of the perfluorinated hexafluorocyclopropane, a species known to be highly strained as discussed in [28-31]. (We exclude from our discussion of ethylene/cyclopropane and dimer/trimer interconversions, the extrusion of a carbene from a cyclopropane and the more common reverse addition reaction.)

Computational chemistry affirms the exothermicity of the transformation of triborane(9) into diborane [21,32-35].

$$2B_3H_9 \rightarrow 3B_2H_6 \tag{2}$$

We now remind the reader that B_3H_9 was taken as the hydrogen bridged 3-membered ring species $[BH_2(\mu\text{-}H)]_3$ much as B_2H_6 is the hydrogen bridged $[BH_2(\mu\text{-}H)]_2$. After all, there is another isomer of B_3H_9, $H_2B(\mu\text{-}H)_2BH\text{–}BH_2(H_2)$ which is calculationally found [34,35] to be even less stable than the aforementioned species and has ignored in most discussions of the chemistry of boranes.. Additionally, solution-phase protonation of the well-known $[B_3H_8]^-$ anion results in complexes of B_3H_7 [20] and of BH_3 [19]. As found in numerous salts, it is well-established crystallographically that $[B_3H_8]^-$ has the 3-membered ring structure $[(BH_2)_2(\mu\text{-}H)_2BH_2]^-$ accompanied in the solid by diverse cations: $[(H_3N)_2BH_2]^+$ [36]; $[C_6H_5CH_2N(CH_3)_3]^+$, [37]; Cs^+ [38]; $[(C_6H_5)_4P]^+$ [39]; $[NH_4]^+$, [40]; Na^+ [41]. The $[B_3H_8]^-$ isomer with the structure $[H_2B(\mu\text{-}H)_2BH\text{–}BH_3]^-$ remains experimentally unknown, and calculationally is found to be less stable than $[(BH_2)_2(\mu\text{-}H)_2BH_2]^-$ [34,35].

By contrast, propene, simply describable as CH_2CHCH_3 (as well as speaking of it as a simply substituted derivative of ethylene), is 33 kJ mol^{-1} more stable than the likewise isolable cyclopropane [24]. Comparable differences of enthalpies of formation differences are found for the four methylpropenes (isomeric butenes) and methylcyclopropane [24], and for the vinylpropenes (isomeric methylbutadienes and pentadienes) and vinylcyclopropane [42,43]. Relatedly using the enthalpy of formation data in [24], the isomeric cyanopropenes, whether the species chosen is the (*E*)-1-, (*Z*)-1-, and 3-derivative, are some 30–50 kJ mol^{-1} more stable than cyanocyclopropane. (There are seemingly no experimental thermochemical data on the 2-derivative, a species more commonly known as methacrylonitrile.) This difference is more than doubled to 110 kJ mol^{-1} for the formally related species with two vinyl and cyclopropane moieties apiece as found in 1,3-butadiene, $CH_2\text{=}CH\text{–}CH\text{=}CH_2$, and bicyclobutane, $CH_2(CH)_2CH_2$, and almost doubled for the species with one double bond and one cyclopropane, namely methylenecyclopropane [24].

4. TETRABORANE(10) AND BICYCLOBUTANE, THEIR ISOMERS, DERIVATIVES AND SUBSTITUENT EFFECTS

We have earlier said that B_3 rings are unstable compared to 2-boron species as found in the comparison of B_2H_6 and B_3H_9, but more stable as found for the two isomers of the 3-boron $[B_3H_8]^-$ e.g. [32,34]. So, what is the case for B_4H_{10}? The 4-boron tetraborane(10) has been experimentally shown by electron diffraction and microwave spectroscopy [44,45] to have a structure related to that of bicyclobutane, cf. $BH_2(\mu\text{-}H)_2(BH)_2(\mu\text{-}H)_2BH_2$ and $CH_2(CH)_2CH_2$. Calculational theory [46-49] shows $BH_2(\mu\text{-}H)_2BH\text{–}BH(\mu\text{-}H)_2BH_2$ to be slightly less stable than $BH_2(\mu\text{-}H)_2(BH)_2(\mu\text{-}H)_2BH_2$, where we remember the former had been earlier suggested for B_4H_{10} [2]. (Still earlier electron diffraction measurements suggested a $BH_3\text{–}BH_2\text{–}BH_2\text{–}BH_3$ butane-like structure [50, cf. 7].) In other words, C_4H_6 prefers the 1,3-butadiene structure with two ethylenes and not two 3-membered rings, i.e., $CH_2\text{=}CH\text{–}CH\text{=}CH_2$ and not bicyclobutane, $CH_2(CH)_2CH_2$ while B_4H_{10} prefers the structure $BH_2(\mu\text{-}H)_2B_2(\mu\text{-}H)_2BH_2$ with two 3-membered rings and not $BH_2(\mu\text{-}H)_2BH\text{–}BH(\mu\text{-}H)_2BH_2$.

Substituents have been shown to significantly affect the strain energies of the derivatives of ethylene (cf. the aforementioned cycloethane), cyclopropane and bicyclobutane [14]. In that the last cited paper dealt with substituent effects and strain energies, we accordingly wonder what will be found for the related derivatives of B_2H_6, $[B_3H_8]^-$ and B_4H_{10}? How will the energies and enthalpies of formation of substituted diborane(6) derivatives, B_2H_5X, both $H_2B(\mu\text{-}H)(\mu\text{-}X)BH_2$ and $H_2B(\mu\text{-}H)_2BHX$, compare with those of the ethylene-based vinyl derivatives, CH_2CHX? The last decade has seen a renaissance in thermochemical studies of vinyl derivatives. Along with many examples [24] for vinyl species, e.g. X = H and diverse alkyl, phenyl and other hydrocarbon substituents, we now have enthalpies of formation for the vinyl species: X = Cl [51], Br [52], I [51], CHO [53], COOH [54], CN [55]. This is not the case for the monosubstituted diboranes. Reliable structures have been reported, but these studies are without corresponding energetics data whether it be as enthalpies of formation. We have “merely” relative isomer stabilities from which it is assumed that the observed isomer is the more stable. Examples include X = CH_3 [56], NH_2 [57], SCH_3 [58], Cl [59], Br [60].

How does the enthalpy of formation difference of $(BH_2(\mu\text{-}H))_2BHX$ and its isomer with bridging X depend on the group X? What about the isomeric substituted tetraboranes wherein the substituent may be on boron 1, boron 2 (both endo- and exo-) or replace one of the bridging hydrogens? Almost nothing is known from either experiment or calculational theory: thermodynamic and kinetic data are almost totally absent as to the role of substitutents in their diverse positions on the stability of boranes. Among the few relevant observations include methyldiborane is known from experiment [61] to methylate tetraborane, but from the results of quantum chemical calculations [14] we may deduce the related trans-methylation reaction of propene and bicyclobutane to form ethylene and (either 1- or 2-(exo))methylbicyclobutane is significantly endothermic. Monomeric trimethylboron exchanges hydrogen and methyl groups with diborane to form methyldiboranes [62] – does this tell us that methylation stabilizes a plausible triborane(9) intermediate.

5. TETRABORANE(12) AND CYCLOBUTANE

We close with a brief discussion of the experimentally still unknown B_4 species, tetraborane(12) for which the structure $[BH_2(\mu\text{-}H)]_4$ is plausible [22,63]. This species is a formal dimer of diborane(6). However, the reaction

$$2[BH_2(\mu\text{-}H)]_2 \rightarrow [BH_2(\mu\text{-}H)]_4 \qquad (3)$$

has not been observed experimentally although B_2H_6 and its isotopomers shuffle borons and hydrogens [64,65]. Indeed, the dimerization of diborane is seriously endothermic [33,35] according to calculational theory, and is clearly entropically disfavored as well. (We now acknowledge that the original experimentalists suggested the exchange reaction proceeds through the intermediacy of BH_3.)

We recognize $[BH_2(\mu\text{-}H)]_4$ as analogous to cyclobutane (what other structures could we have [66,67]. None of this is surprising. Ethylene and olefins in general are much more common than cyclobutane and its corresponding substituted derivatives [68]. The dimerization reaction

$$2(CH_2{=}CH_2) \rightarrow (CH_2)_4 \qquad (4)$$

for the parent hydrocarbons is not observed, and for substituted counterparts the reaction is rarely observed without catalysts or photochemical excitation. However, this last reaction of two ethylenes is enthalpically favorable. This nonreaction is unquestionably fortuitous – had the double bonds in so many biomaterials, such as the nucleobases uracil and thymine, unsaturated fatty acids and related triglycerides, the steroidal cholesterol, progesterone, testosterone and the multiple forms of vitamin D, vitamin A and the carotenoids, chosen to dimerize, life would be unrecognizable if not unrealized.

6. STILL OTHER FEW-BORON CONTAINING SPECIES

There are yet other few-boron containing species. These include the nominally homologous series B_2H_2, B_3H_3 and B_4H_4. Are they truly homologous and so reminiscent of the per-aza-cycloalkanes N_xH_x diimide, triaziridine, tetrazetidine and their acyclic counterparts [69]. The first species B_2H_2 has been observed [70] in a cryogenic matrix to be the linear triplet H–B=B–H with a pair of degenerate singly occupied π orbitals. What about the still unknown isomer H_2B–B? We are reminded of diimide amd its substituted counterparts, azo compounds, and their fragile and much less stable isomers H_2N–N and aminonitrenes [71]?

The existence of B_3H_3 has been inferred from the presence of its parent ion via mass spectrometry [72]. As such, it remains experimentally unknown whether neutral B_3H_3 is either of the 3-membered ring species, the B–B or B(H) bridged $(BH)_3$ and $[B(H)]_3$ respectively, or perchance a BH_2 derivative of B_2H_2, H–B=B–BH_2. Triaziridines and triazenes, cyclo-$(NR)_3$ and R–N=N–NR_2 respectively, are both established classes of compounds) although their enthalpy of formation difference remains unavailable [73]. From experiment, we know of the enthalpy of formation of few triazenes (e.g. diphenyltriazene [24]) and no triaziridine at all. The inherent complexity of B_4H_4 is demonstrated by highly colored tetraamino derivatives, the blue and yellow diisopropylamino and tetramethylpiperidino species with their nonplanar central rings [74] and the tetrahedral mixed halo and tetra-tert-butyl species [75]. So, what about N_4H_4 and its derivatives? The enthalpy of formation of some tetrazenes is available from experimental measurements but no tetrahedral assemblage of nitrogens including N_4 is known for comparison. So, what about yet another B_4H_4 isomer, BH_2–B=B–BH_2? There are seemingly few related species, much less relevant data. Indeed, only its 1,4-dioxo derivative B_4O_2 [76]and its radical anion come to mind. Barring meaningful comparisons, discussion of all of these species in this concluding section of the current article will thus be deferred.

ACKNOWLEDGEMENT

One of the authors (MPS) gratefully acknowledges the Slovenian Research Agency (ARRS Grant P1-0045, Inorganic Chemistry and Technology) for financial support.

REFERENCES

1. Scifinder® (American Chemical Society, accessed 17 May 2015).
2. Pitzer, K.S. Electron-deficient molecules. I. The principles of hydroboron structures. *Journal of the American Chemical Society* **1945**, *67*, 1126–1132.
3. Kodama, G.; Parry, R.W. Reaction between phosphorus trifluoride borane and ammonia, synthesis of triamidophosphorus borane, $(NH_2)_3PBH_3$. *Journal of Inorganic & Nuclear Chemistry* **1961**, *17*, 125–129.
4. Bent, H.A. Isoelectronic systems. *Journal of Chemical Education* **1966**, *43*, 170-186.
5. Yao, Y.; Hoffmann, R. BH_3 under pressure: Leaving the molecular diborane motif. *Journal of the American Chemical Society* **2011**, *133*, 21002–21009.
6. Vegas, A.; Notario, R.; Chamorro, E.; Perez, P.; Liebman, J.F. Isoelectronic and isolobal O, CH_2, CH_3^+ and BH_3 as electron pairs; similarities between molecular and solid-state chemistry. *Acta Crystallographica Section B: Structural Science* **2013**, *69*, 163–175.
7. Bauer, S.H. The structure of diborane. *Journal of the American Chemical Society* **1937**, *59*, 1096–1103.
8. Mulliken, R.S. The structure of diborane and related molecules. *Chemical Reviews* **1947**, *41*, 207–217.
9. Buenker, R.J.; Peyerimhoff, S.D.; Allen, L.C.; Whitten, J.L. Geometry of molecules. II. Diborane and ethane. *Journal of Chemical Physics* **1966**, *45*, 2835–2848.
10. Gimarc, B.M. Qualitative molecular orbital study of ethane and diborane. *Journal of the American Chemical Society* **1973**, *95*, 1417–1421.
11. The valence structure of the boron hydrides, Eberhardt, W.H.; Crawford, B. Jr.; Lipscomb, W.N. *Journal of Chemical Physics* **1954**, *22*, 989–1001.
12. Mulliken, R.S. Electronic structures of molecules XIII. Diborane and related molecules. Journal of Chemical Physics 1935, 3, 635–645.
13. Liebman, J.F.; Greenberg, A. A survey of strained organic molecules. *Chemical Reviews* **1976**, *76*, 311–365.
14. Dill, J.D.; Greenberg, A.; Liebman, J.F. Substituent effects on strain energies. *Journal of the American Chemical Society* **1979**, *101*, 6814–6826.

15. Kohler, E.P.; Conant, J.B. Cyclopropane series. *Journal of the American Chemical Society* **1917**, *39*, 1404–1420.
16. The Chemistry of the Cyclopropyl Functional Group (ed. Z. Rappoport), Wiley, Chichester, (1987).
17. The Chemistry of the Cyclopropyl Group, Vol. 2, (ed. Z. Rappoport), Wiley, Chichester, (1995).
18. Fridmann, S.A.; Fehlner, T.P., Reactions of borane (BH_3). V. Mass spectrometric observation of the products of addition to diborane(6) and pentaborane(9). *Inorganic Chemistry* **1972**, *11*, 936–940.
19. Dolan, P.J.; Kindsvater, J.H., Peters, D.G. Electrochemical oxidation and protonation of octahydrotriborate anion. *Inorganic Chemistry* **1976**, *15*, 2170–2173.
20. Jolly W.L., Reed, J.W., Wang, F.T. Hydrolysis of octahydrotriborate in cold acidic methanol-water solutions. Preparation of $B_3H_7OH_2$ and $B_3H_7OH^-$. *Inorganic Chemistry* **1979**, *18*, 377–380.
21. Serrar, C.; Es-Sofi, A.; Boutalib, A.; Ouassas, A.; Jarid, A. Ab initio study of the formation of B_3H_7 derivative from $B_3H_8^-$ anion protonation. *Journal of Molecular Structure-Theochem* **1999**, *491*, 161–169.
22. Pepperberg, I.M.; Halgren, T.A.; Lipscomb, W.N. Extended topological rules for boron hydrides. 1. Structures and relative energies for the transient boron hydrides diborane(4), triborane(7), triborane(9), tetraborane(8), and tetraborane(12). *Inorganic Chemistry* **1977**, *16*, 363–367.
23. Sun, B; McKee, M. L. Computational Study of the Initial Stage of Diborane Pyrolysis. *Inorganic Chemistry* **2013**, *52*, 5962–5969.
24. Pedley, J.B., Thermochemical Data and Structures of Organic Compounds, Vol. 1, TRC Data Texas Series: College Station, Texas, 1994.
25. Stull, D.R.; Westrum, E.F.; Sinke, G.C. The Chemical Thermodynamics of Organic Compounds, a largely reprinted version published by Krieger R.E., Publishing Co., (Malabar) 1987 of the 1969 book published by Wiley (New York).
26. Atkinson, B.; McKeagan, D.J. The thermal decomposition of perfluorocyclopropane. *Chemical Communications* **1966**, 189–190.
27. Cobos, C.J.; Sölter, L.; Tellbach, E.; Troe, J. Shock wave study of the thermal dissociations of C_3F_6 and c-C_3F_6. II. Dissociation of hexafluorocyclopropane and dimerization of CF_2. *Journal of Physical Chemistry A* **2014**, *118*, 4873–4879.
28. Liebman, J.F.; Dolbier, W.R., Jr.; Greenberg, A. Hexafluorocyclopropane and octafluorocyclobutane: a study of the strain energies. *Journal of Physical Chemistry* **1986**, *90*, 394–397.
29. Zeiger, D.N.; Liebman, J.F. The strain energy of fluorinated cyclopropanes: quantum chemical realization of homodesmotic, diagonal and ultradiagonal approaches. *Journal of Molecular Structure* **2000**, *556*, 83–94.
30. Vila, A.; Mosquera, R.A. On the electronic origin of strain energy: QTAIM Study of Perfluorocycloalkanes. *Journal of Physical Chemistry A* **2006**, *110*, 11752–11759.
31. De Lio, A.M.; Durfey, B.L.; Gille, A.L.; Gilbert, T.M. A semi-homodesmotic approach for estimating ring strain energies (RSEs) of highly substituted cyclopropanes that minimizes use of acyclic references and cancels steric

interactions: RSEs for c-C_3R_6 that make sense. *Journal of Physical Chemistry A* **2014**, *118*, 6050–6059.

32. Stanton, J.F.; Lipscomb, W.N.; Bartlett, R.J.; McKee, M.L. Electron correlation effects on the ground-state structure and stability of triborane(9). *Inorganic Chemistry* **1989**, *28*, 109–111.
33. McKee, M.L. Estimation of heats of formation of boron hydrides from ab initio energies. *Journal of Physical Chemistry* **1990**, *94*, 435–40.
34. Korkin A.A.; Schleyer, P.v.R.; McKee, M.L. Theoretical ab Initio study of neutral and charged B_3H_n (n = 3-9) Species. Importance of Aromaticity in Determining the Structural Preferences. *Inorganic Chemistry* **1995**, *34*, 961–977.
35. Cheng, M.F.; Ho, H.O., Lam, C.S.; Li, W.K. Heats of formation for the boron hydrides: a Gaussian-3 study. *Chemical Physics Letters* **2002**, *356*, 109–119.
36. Peters, C.R.; Nordman, C.E. The structure of the $B_3H_8^-$ ion. *Journal of the American Chemical Society* **1960**, *82*, 5758–5758.
37. Mitchell, G.F.; Welch, A.J. Extended Hueckel molecular orbital study of the effects of edge-bridging hydrogen atoms on the lengths of boron-boron and metal-metal bonds in cluster compounds and the crystal structure of benzyltrimethylammonium octahydrotriborate(1-). *Journal of the Chemical Society-Dalton Transactions* **1987**, 1017–1025.
38. Deiseroth, H.J.; Sommer, O.; Binder, H.; Wolfer, K.; Frei, B. Cesium octahydrotriborate (1-): crystal structure and upgrading of the synthesis. *Zeitschrift für Anorganische und Allgemeine Chemie* **1989**, *571*, 21–28.
39. Beckett, M.A.; Horton, P.N.; Hursthouse, M.B.; Pszolla, C. Tetraphenylphosphonium octahydrotriborate. *Acta Crystallographica Section E* **2010**, *66*, o833.
40. Huang, Z.; Chen, X; Yisgedu, T; Meyers, E.A.; Shore, S.G.; Zhao, J.C. Ammonium octahydrotriborate ($NH_4B_3H_8$): New Synthesis, Structure, and Hydrolytic Hydrogen Release. *Inorganic Chemistry* **2011**, *50*, 3738–3742.
41. Dunbar, A.C.; Macor, J.A.; Girolami, G.S. Synthesis and Single Crystal Structure of Sodium Octahydrotriborate, NaB_3H_8. *Inorganic Chemistry* **2014**, *53*, 822–826.
42. Lebedeva, N.D.; Gutner, N.M.; Nazarova, L.F. Enthalpies of burning and the formation of some substituted derivatives of cyclopropane, *Termodinamika Organischeskikh Soedinenii* **1977**, 26-29.
43. Roth, W.R.; Adamczak, O.; Breuckmann, R.; Lennartz, H.W.; Boese, R. The calculation of resonance energies: The MM2ERW-force field. *Chemische Berichte* **1991**, *124*, 2499–2521.
44. Dain, C.J.; Downs, A.J.; Laurenson, G.S.; Rankin, D.W.H. The molecular structure of tetraborane (10) in the gas phase as determined by a joint analysis of electron diffraction and microwave data, *Journal of the Chemical Society-Dalton Transactions* **1981**, 472–477.
45. Brain, P.T.; Morrison, C.A.; Parsons, S.; Rankin, D.W. H. Tetraborane(10), B_4H_{10}: structures in gaseous and crystalline phases. *Journal of the Chemical Society-Dalton Transactions* **1996**, 4589-4596.
46. McKee, M.L.; Lipscomb, W.N. Electron correlation effects in tetraborane(10) structures. *Inorganic Chemistry* **1981**, *20*, 4452–4453.

47. Morris-Sherwood, B.J.; Hall, M.B. Theoretical study of the structure of tetraborane(10). *Chemical Physics Letters* **1981**, *84*, 194–196.
48. Ramakrishna, V.; Duke, B.J. Can the bis(diboranyl) structure of B_4H_{10} be observed? The story continues. *Inorganic Chemistry* **2004**, *43*, 8176–8184.
49. Tian, S. X. Ab initio and electron propagator theory study of boron hydrides. *Journal of Physical Chemistry A* **2005**, *109*, 5471–5480.
50. Bauer, S.H. The structure of the hydrides of boron. V. Tetraborane B_4H_{10} and the pentaborane B_5H_{11}. *Journal of the American Chemical Society* **1938**, *60*, 805–812.
51. Shuman, N.S.; Ochieng, M.A.; Sztaray, B.; Baer, T. TPEPICO Spectroscopy of vinyl vhloride and vinyl iodide: Neutral and ionic heats of formation and bond energies. *Journal of Physical Chemistry A* **2008**, *112*, 5647–5652.
52. Lago, A.F.; Baer, T. A photoelectron photoion coincidence study of the vinyl bromide and tribromoethane ion dissociation dynamics: Heats of formation of $C_2H_3^+$, C_2H_3Br, $C_2H_3Br^+$, $C_2H_3Br_2^+$, and $C_2H_3Br_3$. *Journal of Physical Chemistry A* **2006**, *110*, 3036–3041, errata: Lago, A.F.; Baer, T. *Journal of Physical Chemistry A* **2008**, *112*, 5024.
53. Lewars, E.; Liebman, J.F. What are the enthalpy of formation and the stabilization energy of acrolein? *Structural Chemistry* **2013**, *24*, 741–744.
54. Notario, R.; Roux, M.V.; Bors, D.A.; Liebman, J.F. What is the enthalpy of formation of acrylic acid? *Structural Chemistry* **2007**, *18*, 395–398.
55. Notario, R.; Roux, M.V.; Liebman, J.F. What is the enthalpy of formation of acrylonitrile? *Structural Chemistry* **2010**, *21*, 481–484.
56. Penn, R.E.; Buxton, L.W. Microwave spectrum of methyldiborane. *Journal of Chemical Physics* **1977**, *67*, 831–835.
57. Lau, K.K.; Burg, A.B.; Beaudet, R.A., Microwave spectrum, structure, and dipole moment of aminodiborane. *Inorganic Chemistry* **1974**, *13*, 2787–2791.
58. Muetterties, E.L.; Miller, N.E.; Packer, K.J.; Miller, H.C. Chemistry of boranes. XII. Structure of alkylthioboranes. *Inorganic Chemistry* **1964**, *3*, 870–872.
59. Sugie, M.; Takeo, H.; Matsumura, C. Microwave spectrum of chlorodiborane, B_2H_5Cl. *Journal of Molecular Structure* **1985**, *131*, 225–231.
60. Ferguson, A.C.; Cornwell, C D. Microwave spectrum, molecular structure, and bromine nuclear quadrupole coupling tensor of bromodiborane. *Journal of Chemical Physics* **1970**, *53*, 1851–1859.
61. Lutz, C.A.; Ritter, D.M. observations on alkylboranes. *Canadian Journal of Chemistry* **1963**, *41*, 1344–1358.
62. Seely, G.R.; Oliver, J.P.; Ritter, D.M. Gas liquid chromatographic analysis of mixtures containing methyldiboranes. *Analytical Chemistry* **1959**, *31*, 1993–1995.
63. Shen, M.; Liang, C.; Schaefer, H.F. The tetramer of borane and its heavier valence-isoelectronic analogs: M_4H_{12} with M = B, Al, and Ga, III. *Chemical Physics* **1993**, *171*, 325–345.
64. Maybury, P.C.; Koski, W.S. Kinetics of two exchange reactions involving diborane. *Journal of Chemical Physics* **1953**, *21*, 742–747.
65. Shapiro, L; Keilin, B. Self-exchange of boron in boron hydrides. *Journal of the American Chemical Society* **1955**, *77*, 2663.

66. Bock, C.W.; Roberts, C.; O'Malley, K.; Trachtman, M.; Mains, G.J. An ab initio molecular orbital study of the structures, stabilities, and spectra of tris[tetrahydroborato(1-)boron, tris[tetrahydroborato(1-)]aluminum, and tris[tetrahydroaluminato(1-)]aluminum. *Journal of Physical Chemistry* **1992**, *96*, 4859–4864.
67. Balakrishnarajan, M.M.; Hoffmann, R. Electron-deficient bonding in rhomboid rings. *Journal of the American Chemical Society* **2004**, *126*, 13119–13121.
68. The Chemistry of Cyclobutanes (ed, Rappoport, Z., Liebman, J. F.) Wiley, Chichester (2005).
69. Zhao, M.; Gimarc, B.M. Strain energies of $(NH)_n$ rings, n = 3-8. *Journal of Physical Chemistry*, **1994**, *98*, 7497–7503.
70. Knignt, L.B.Jr.; Kerr, K.; Miller, P.K.; Arrington, C.A. ESR investigation of the HBBH ($X^3\Sigma$) radical in neon and argon matrixes at 4 K. Comparison with ab Initio n SCF and CI Calculations. *Journal of Physical Chemistry* **1995**, *99*, 16842–16848.
71. Schultz, P.G.; Dervan, P.B. Photochemistry of 1,1-diazenes. Direct and sensitized photolyses of N-(2,2,5,5-tetramethylpyrrolidyl)nitrene, dl-N-(2,5-diethyl-2,5-dimethylpyrrolidyl)nitrene, and N-(2,2,6,6-tetramethylpiperidyl)nitrene. *Journal of the American Chemical Society* **1982**, *104*, 6660–6668.
72. Sato, K.; Kanda, N.; Ogata, T.; Kumashiro, Y., Structures of the main precursors and initial decomposition products of diborane chemical vapor deposition: an experimental and ab initio molecular orbital study. *Chemical Physics Letters* **2000**, *325*, 453–456.
73. Magers, D.H.; Salter, E.A.; Bartlett, R.J.; Salter, C., Hess, B.A. Jr.; Schaad, L.J. Do stable isomers of N_3H_3 exist? *Journal of the American Chemical Society*, **1988**, *110*, 3435–3446.
74. Maier, C.J.; Pritzkow, H.; Siebert, W. Blue tetrakis(diisopropylamino)-cyclo-tetraborane and yellow tetrakis(tetramethylpiperidino)tetrabora-tetrahedrane, *Angewandte Chemie International Edition*. **1999**, *38*, 1666–1668.
75. Davan, T.; Morrison, J.A. Tetrakis(tert-butyl)tetraborane(4). $(Me_3C)_4B_4$; Synthesis of the first peralkyl derivative of a 2N framework electron count deltahedral borane. *Journal of the Chemical Society Chemical Communications* **1981**, 250–251.
76. Li, S.D.; Zhai, H.J.; Wang, L.S. $B_2(BO)_2^{2-}$ - Diboronyl Diborene: A Linear Molecule with a Triple Boron-Boron Bond. *Journal of the American Chemical Society* **2008**, *130*, 2573-2579.

NEW FRONT. CHEM. (**2015**)
Volume 24, Number 1, pp. 37-45
ISSN 2393-2171; ISSN-L 2393-2171

Former: Ann. West Univ. Timisoara – Series Chem.
ISSN: 1224-9513

Article

RDX AND HMX FORMATIONS FROM HEXAMINE – A DFT BASED POSTULATE

Lemi Türker[♣]

Middle East Technical University, Department of Chemistry, 06800, Ankara, TURKEY

ABSTRACT

Hexamethylene tetramine (HMTA) is used as the starting material for the synthesis of well known explosives RDX and HMX. The present study postulates series of reactions to rationalize the formation of these explosives from HMTA, based on density functional theory calculations at the level of B3LYP/6-31G(d,p).

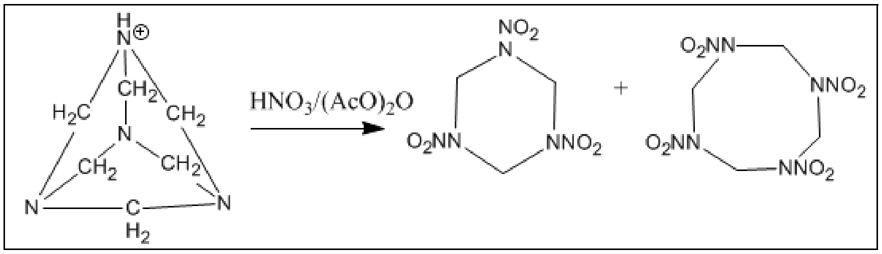

Keywords: Hexamine, hexaminedinitrate, RDX, HMX, DFT calculations.

1. INTRODUCTION

Cyclotrimethylene trinitramine or 1,3,5-trinitrohexahydro-*sym*-triazine (RDX) and cyclotetramethylene tetranitramine or 1,3,5,7-tetranitro-1,3,5,7-tetraazacyclooctane (HMX, Her Majesties' explosive) [1] are important explosives which have been in use for long. RDX is mainly obtained in the industry by direct nitrolysis process (Woolwich) in which hexamethylene tetramine is directly treated with a large excess of strong HNO_3 at a temperature of 20-25 °C [1-4]. On the other hand, in the Bachman (Combination Process) process, which is also an industrial process for RDX, the reaction mixture contains HNO_3, NH_4NO_3, acetic anhydride and acetic acid in addition to hexamine [1,2,4]. The product, RDX,

---

[♣] Tel:+90 312 2103244, Fax:+90 312 2103200, E-mail: lturker@metu.edu.tr

of the Bachman process is higher in yield compared to the previous one, produces RDX (B) which contains 10 % HMX.

HMX/octogen is a superior explosive than RDX/cyclonite because of its higher chemical stability, higher density, higher velocity of detonation and higher ignition temperature, however its cost and sensitivity are higher than RDX [1,2].

Hexamine (hexamethylene tetramine, HMTA) is a heterocyclic organic compound having highly symmetrical cage-like structure. It is prepared from ammonia and formaldehyde [5]. Although it is feebly basic, protonates in strongly acidic media, to form salts. The reaction of hexamine with nitric acid has prime importance because of energetic properties of nitramine type products such as RDX and HMX.

Hexamethylene dinitrate (HDN) can be used as a precursor for manufacturing of RDX and its industrial method of preparation is described in the literature [6]. HDN shows weak explosive character, heating or ignition causes violet deflagration. Its hygroscopic nature prevents its usage in explosive formulations.

Besides the experimental studies on RDX, there are some computational studies on its reaction mechanism [7], conformations and bond dissociation energies [8, 9] and gas-phase structure [10]. RDX formation mechanism has been studied either experimentally [11] or computationally [12].

The present study considers series of reactions to rationalize the formation of RDX and HMX from HMTA, based on density functional theory calculations.

2. METHOD

The initial geometry optimizations of all the structures leading to energy minima were achieved by using MM2 (molecular mechanics) method which are followed by semi-empirical PM3 self-consistent fields molecular orbital (SCF MO) method [13, 14] at the restricted level [15]. Then, geometry optimizations were achieved by using various restricted Hartree-Fock (RHF) methods successively and finally optimizing within the framework of density functional theory (DFT, B3LYP) [16,17] at the level of 6-31G(d,p). Note that the exchange term of B3LYP consists of hybrid Hartree–Fock and local spin density (LSD) exchange functions with Becke's gradient correlation to LSD exchange [17,18]. The correlation term of B3LYP consists of the Vosko, Wilk, Nusair (VWN3) local correlation functional [19] and Lee, Yang, Parr (LYP) correlation correction functional [20].

For each set of calculations, vibrational analyses were done (using the same basis set employed in the corresponding geometry optimization). The normal mode analysis for each structure yielded no imaginary frequencies for the $3N-6$ vibrational degrees of freedom, where N is the number of atoms in the system. This indicates that the structure of each molecule corresponds to at least one local minimum on the potential energy surface. All these computations were performed by using the Spartan 06 [21] package program.

3. RESULTS AND DISCUSSIONS

Experimental studies on RDX and related compounds go back to 1950s [22-24]. Those studies mainly consider the effect of certain component of the synthetic procedures on the product rates etc.

In strong acid HMTA is protonated. The first protonation should be easy but the second and third protonation cannot be so favorable because of the repulsive interactions developed between the protonated centers, thus more forcing conditions are needed. In strongly acidic medium, doubly charged cation of HMTA may have some existence (in the form of hexamine dinitrate (HDN) salt, hexamethylene tetramine dinitrate **1**) which may be in equilibrium with the mono-cation (**2**) (Scheme **1**) especially in solution.

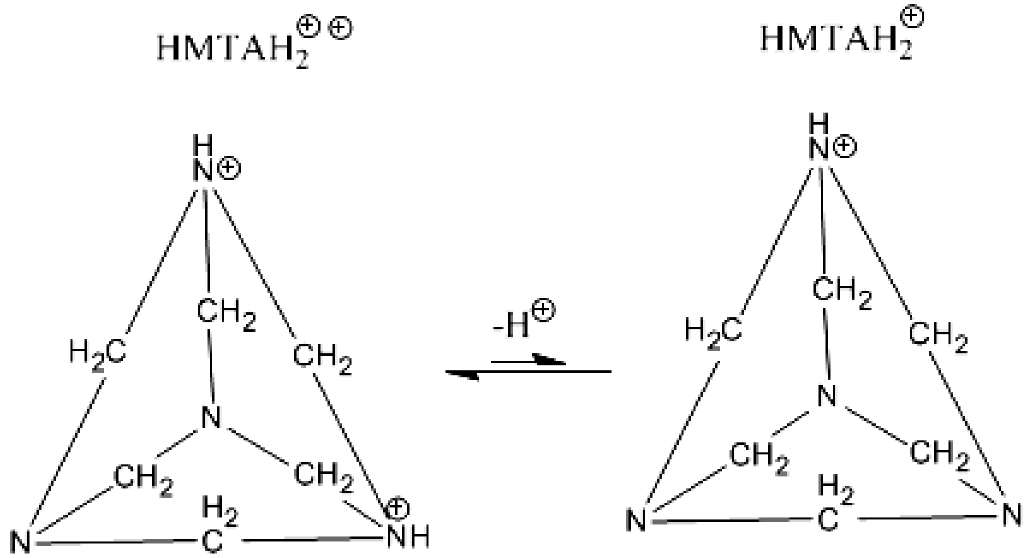

Scheme 1

Presently, this mono-cation is considered as having comparatively low concentration but playing a key role in RDX and HMX formation mechanisms. To shed some light on to these complex transformations, eventually yielding RDX and HMX, the reactions shown in **Schemes 2** and **3** are proposed and some quantum chemical calculations have been carried out. Although concentration of acetate ion in such a strong acidic medium has to be very low, it has been considered as the attacking nucleophile in the ring opening processes of HMTA skeleton. However, the acetate ion (AcO^-) could be replaced by acetic acid to play the same role. Structure **4** is a mononitrated double cation and structure **3** is the other view of it.

Depending on different protonation sites in the mono-nitrated (double cation) specie (**4** or **3**), isomeric acetoxy derivatives, **5** and **6** may form after the AcO^- (or AcOH) attack followed by ring opening reaction. Structure **5** seems to be more stable than **6** in the gas phase and aqueous phase (see Table 1). Thereafter, structures **5** and **6** produce **7** and **8**, respectively after dinitration so that the former one (**7**) is more favorable than its isomer **8** (see Table 1). The acetate attack on **7** forms **9** in which pro-RDX skeleton is discernable. The attack of acetate on different sites of **8** also forms a pro-RDX specie (**11**) and pro-HMX (**12**) and **10**.

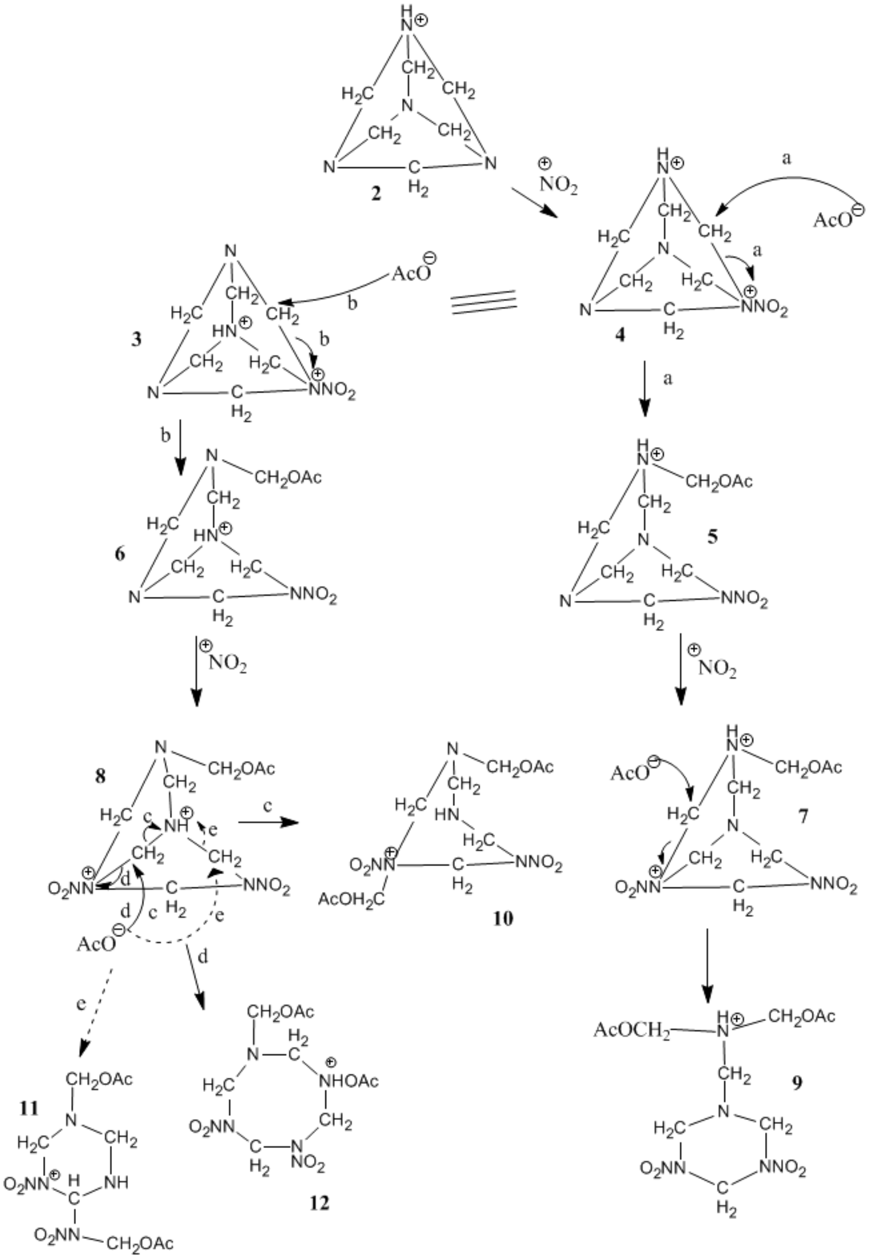

Scheme 2

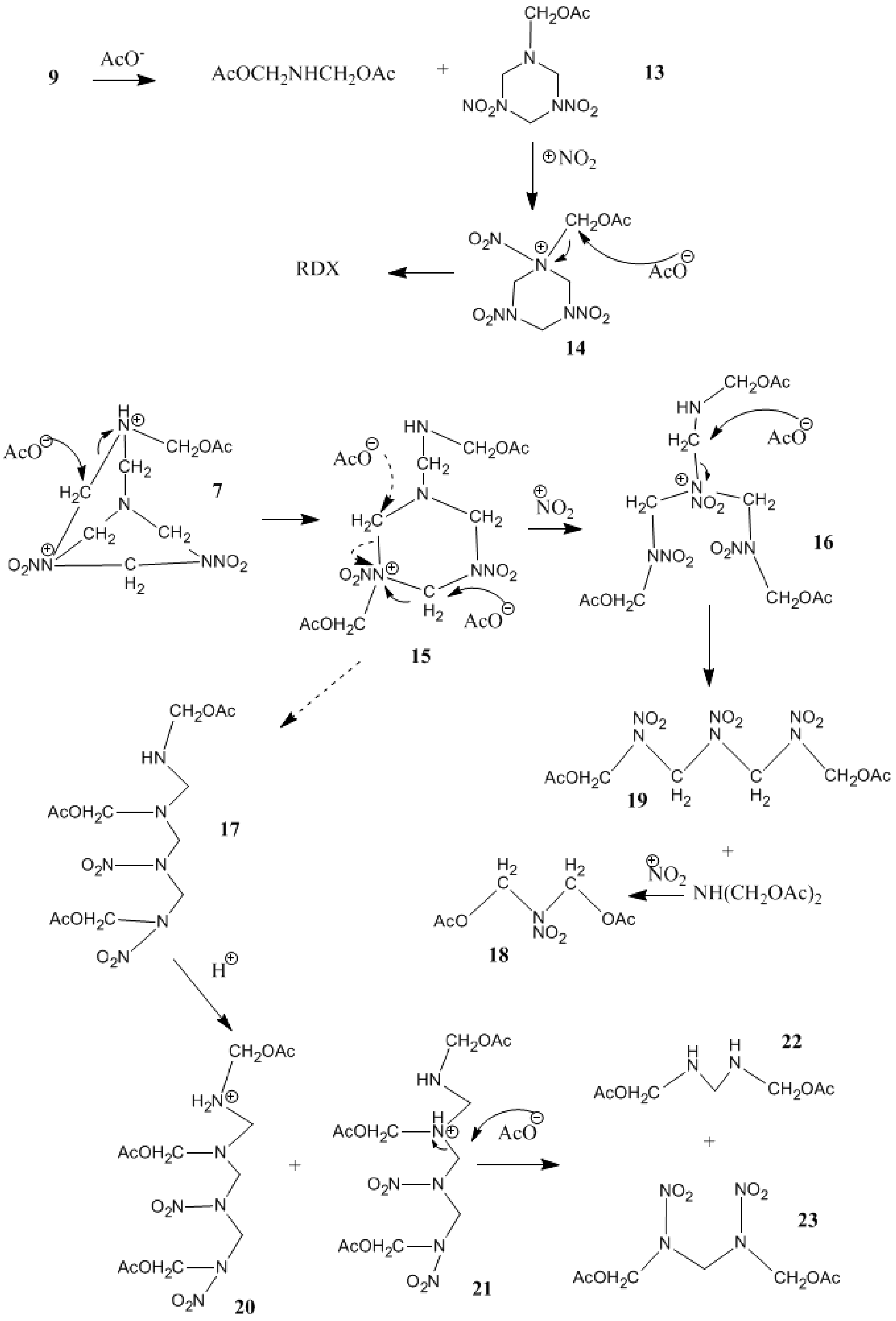
9
AcO⁻
AcOCH2NHCH2OAc
+
13
⊕NO2
14
RDX
7
15
16
17
18
19
20
21
22
23
⊕NO2
NH(CH2OAc)2
H⊕
AcO⊖
CH2OAc
AcOH2C
NO2
O2N
NNO2
O2NN
HN
H2N⊕
OAc
AcO

Scheme 3

Table 1: Various energies of the structures considered

No	Formula	E	ZPE	E_{corr}	E_{aq}	$E_{aq\ corr}$	MW
5	$C_8H_{16}N_5O_4$	-888.79	0.2774	-888.51	-888.86	-888.59	246.247
6	$C_8H_{16}N_5O_4$	-883.61	0.3010	-883.31	-883.69	-883.39	246.247
7	$C_8H_{16}N_6O_6$	-1093.44	0.2874	-1093.15	-1093.72	-1093.44	292.252
8	$C_8H_{16}N_6O_6$	-1093.44	0.2892	-1093.15	-1093.69	-1093.40	292.252
9	$C_{10}H_{19}N_6O_8$	-1322.36	0.3421	-1322.01	-1322.42	-1322.08	351.296
11	$C_{10}H_{19}N_6O_8$	-1322.31	0.3398	-1321.97	-1322.38	-1322.04	351.296
12	$C_{10}H_{19}N_6O_8$	-1322.34	0.3420	-1321.99	-1322.41	-1322.07	351.296
20	$C_{12}H_{23}N_6O_{10}$	-1551.47	0.4068	-1551.06	-1551.53	-1551.12	411.348
21	$C_{12}H_{23}N_6O_{10}$	-1551.47	0.4066	-1551.06	-1551.53	-1551.13	411.348

Energies in au.

Note that **9**, **11** and **12** are isomeric structures ($C_{10}H_{19}N_6O_8$) having the same charge (mono cation). The stability order of them has the sequence of **9**>**12**>**11** both in vacuum and aqueous phase. The dinitrated products **7** and **8** are isomeric dications ($C_8H_{16}N_6O_6$) and **7** is more stable than **8** (in vacuum and aqueous phase).

Similarly, in both media **5** is more stable than its isomeric structure **6** (both are monocations). Then, the **5-7-9** sequence of reactions produce more stable structures in each step than the **6-8-12** and **11** sequence. The calculations indicate that optimized structure of **10** is characterized with some elongated bonds. Therefore, it has been out of consideration.

On the other hand, **9** after AcO^- attack may form RDX via structures **13** and **14** (see **Scheme 3**). Similarly, the attack of AcO^- on **7** first yields **15** then eventually **20** and **21** are produced.

However, there seems another route to exist involving the AcO^- attack on **15**, accompanied by nitration to produce **16** which is an acyclic compound.

The acetate attack on **16** as shown in the **Scheme 3** produces **19** (1,7-diacetoxy-2,4,6-trinitro-2,4,6-triazaheptane) and another product which is nitrated to yield **18** (1,3-diacetoxy-2-nitro-2-azapropane). Both of these products were experimentally detected [25]. Figure 1 shows the optimized structures of the presently considered molecules.

Figure 1: Optimized structures of some of the compounds considered

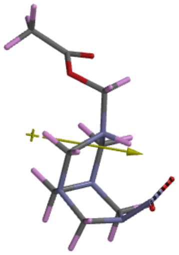

5

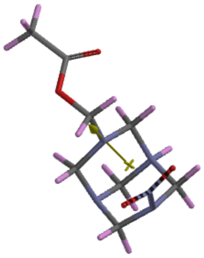

6

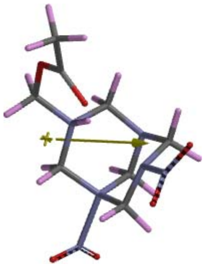

7

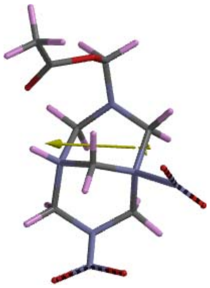

8

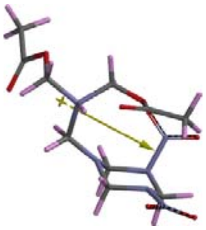

9

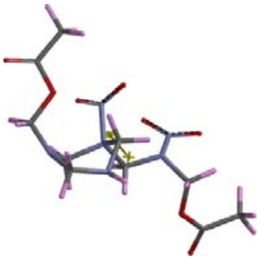

11

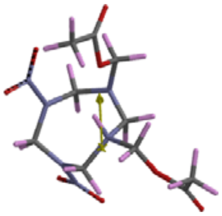

12

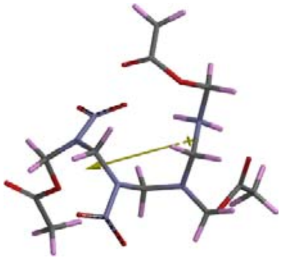

20

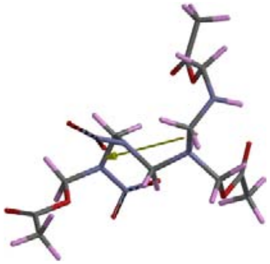

21

4. CONCLUSION

The present DFT study (B3LYP/6-31G(d,p)) puts some light on the formation mechanisms of RDX, HMX and some side products from HMTA in acidic conditions. Although the present mechanisms based on computational studies (based on the stabilities of the proposed structures) have some postulative character, however they may enlighten which of the alternative series of routes (of various branches of reactions) are to be favored etc. It should be noted that the present calculations are mainly true for gas and aqueous phases however it should be noted that in reality ionic and acid strengths of the medium etc. also play a vital role in the course of reactions.

REFERENCES

1. Agrawal, J.P. *High Energy Materials*, *Propellants, Explosives and Pyrotechnics*, Wiley-VCH, Weinheim, Germany, 2010.
2. Agrawal, J.P.; Hodgson, R.D. *Organic Chemistry of Explosives*, Wiley, Sussex, UK, 2007.
3. Fordham, S. *High Explosives and Propellants*, Pergamon , Oxford, UK, 1980.
4. Ledgard, J. *The Preparotory Manual of Explosives*, J.B.Ledgard, USA, 2007.
5. Vogel, A.I. *Practical Organic Synthesis*, 3rd ed. Longmans, London, 1967, p.326.
6. Urbansky, T. *Chemistry and Technology of Explosives*, Vol.3, Pergamon, Oxford, UK, 1967, pp.40-56.
7. Matthew, J.; Li, S.; Li, T. Reaction Mechanism of 1,3,5-Trinitro-s-triazine (RDX) Deciphered by Density Functional Theory**,** *J. Chem. Theory Comput.* **2007**, *3*, 505-513.
8. Harris, N.J.; Lammertsma**,** K. *Ab Initio* Density Functional Computations of Conformations and Bond Dissociation Energies for Hexahydro-1,3,5-trinitro-1,3,5-triazine**,** *J. Am. Chem. Soc.* **1997**, *119*, 6583-6589.
9. Rice, B.M.; Chabalowski**,** C. F. *Ab Initio* and Nonlocal Density Functional Study of 1,3,5-Trinitro-*s*-triazine (RDX**)** Conformers**,** *J. Phys. Chem. A* **1997**, *101*, 8720-8726.
10. Vladimiroff, T.; Ric**e**, B.M. Reinvestigation of the Gas-Phase Structure of RDX Using Density Functional Theory Predictions of Electron-Scattering Intensities, *J. Phys. Chem. A* **2002**, *106,* 10437-10443.
11. Fang, Z.; Wang, S.; Li, F. Study on the Nitrolysis of Hexamethylenetetramine by NMR-Spectrometry(*), Part IV: A Novel Mechanism of the Formation of RDX from HA**,** *Propellants, Explosives, Pyrotechnics* **1998**, *23*, 317-319.
12. Yang, K.; Park, Y.H.; Cho, S.G.; Lee, H.; Kim, C. K.;Koo, H-J. Theoretical Studies on the Formation Mechanism and Explosive Performance of Nitro-Substituted 1,3,5-Triazines, *J. Comput Chem*. **2010,** *31*, 2483–2492 .
13. Stewart, J.J.P. Optimization of parameters for semi empirical methods I, Method, *J. Comput. Chem.* **1989**, *10* , 209–220.
14. Stewart, J.J.P. Optimization of parameters for semi empirical methods II, Appl., *J. Comput. Chem.* **1989**, *10* , 221–264.
15. Leach, A.R. *Molecular Modeling*. Longman, Essex, UK, 1997.

16. Kohn, W.; Sham, L.J. Self-consistent equations including exchange and correlation Effects, *Phys. Rev.* **1965**, *140* , 1133–1138.
17. Parr, R.G.; Yang,W. *Density Functional Theory of Atoms and Molecules*. Oxford University Press. London, UK, 1989.
18. Becke, A.D. Density-functional exchange-energy approximation with correct asymptotic behavior, *Phys. Rev.* **1988**, *A 38* , 3098–3100.
19. Vosko, S.H.; Vilk, L.; Nusair, M. Accurate spin-dependent electron liquid correlation energies for local spin density calculations: A critical analysis. *Can. J. Phys*. **1980**, *58* ,1200–1211.
20. Lee, C.; Yang, W.; Parr, R.G. Development of the Colle–Salvetti correlation energy formula into a functional of the electron density. *Phys. Rev.* **1988**, *B 37*, 785–789.
21. SPARTAN 06. Wavefunction Inc., Irvine CA, USA, 2006.
22. Ralph, A.O.; MacHutchin, J.G.; Winkler, C.A. Studies on RDX and related compounds V. The effect of delayed addition of ammonium nitrate and the rate of disappearance of hexamine in the Bachmann reaction, *Canadian J. of Chem*. **1951**, *29,* 725-730.
23. Eptein, S.; Winkler, C.A. Studies of RDX and related compounds VII. Relation between RDX and HMX production in the Bachmann reaction, *Canadian J. of Chem.* **1952**, *30,* 734-742.
24. Marcus, R.A.; Winkler, C.A. Studies of RDX and related compounds XI. The conversion of PHX to AcAn. *Canadian J. of Chem*. **1953**, *31*, 602-614.
25. Klapötke, T.M. T.M.; Krumm, B.; Steemann, F.X. Preparation, characterization and sensitivity data of some azidomethyl nitramines, *Propellants Explos, Pyrotech*, **2009**, *34,* 13-23.

NEW FRONT. CHEM. (**2015**)
Volume 24, Number 1, pp. 47-53
ISSN 2393-2171; ISSN-L 2393-2171
© West University of Timişoara

Former: Ann. West Univ. Timisoara – Series Chem.
ISSN: 1224-9513

Article

STUDY OF A BIOACTIVE HYDROXYAPATITE/GELATIN COMPOSITE. PART I - SYNTHESIS AND CHARACTERIZATION OF THE MATERIAL

***Paul Albu*[1,2], *Gabriela Vlase*[1♣], *Titus Vlase*[1]**

[1] West University of Timisoara, Research Center for Thermal Analysis in Environmental Problems, 16 Pestalozzi St., Timisoara, RO-300115, Romania
[2] „Vasile Goldiş" West University of Arad, Faculty of Medicine, Pharmacy and Dentistry, Department of Pharmacy, 86 L. Rebreanu St., 310414 Arad, Romania

ABSTRACT

A biomimetic bioactive composite based on hydroxyapatite (HA) was prepared by using inorganic precursors for the mineral structure of the composite and a gelatin aqueous solution to provide the organic matrix as template for the HA crystal growth. The samples of the HA were characterized before and after the sinterization process by FTIR, XRD, SEM and EDAX analysis. The results indicate that the crystallization process ends only after sinterization at high temperature. This sinterization process also has an effect on the size and shape of the HA crystals.

Keywords: biomimetic hydroxyapatite, FTIR, SEM, EDAX, XRD.

1. INTRODUCTION

In the last two decades an important part of the research on bone substitute materials was focused on ceramic materials, like calcium phosphates [1] because of their biocompatible, bioactive, biodegradable and osteoconductive properties [2-6].

The mineral phase of the bone tissue consists in natural hydroxyapatite crystals with a general shape of needle or rod, that are distributed within the polymeric matrix of type I collagen. Research shows that these natural nanoparticles formed in physiological

---

♣ Correspondent author: Tel: +40256/592627, Fax:, E-mails: gabriela.vlase@e-uvt.ro

environment exhibits a more dynamic response in comparison with other synthetic materials, ofter with a larger crystal size [7]. Despite their small size, bone nanoparticles are stable and resist to dissolution because of the interactions that occur between the acidic peptide sequence in the extracellular matrix and the Ca^{2+} ions present in the mineral nanocrystals [8].

Synthetic bone regeneration materials do not present problems regarding immunological incompatibility, sterility or limited availability. This type of materials that are used as bone substitutes include inorganic materials (i.e. calcium phosphates), polymers or polymer-ceramics composite materials [9-11]. The ideal material that should be used in order to induce complete bone regeneration should be: osteoconductive, osteoinductive, osteogenic, biocompatible, bioactive and biodegradable [9].

Biomimetic preparation of synthetic bone materials [12] such as hydroxyapatite has received an increased attention of the researchers and so they have tried to prepare hydroxyapatite based composites using collagen, denatured collagen or other polymers as template for the biomimetic synthesis.

In the current study, the biomimetic HA synthesis was carried out by wet-chemical precipitation of inorganic precursor into an organic gelatin matrix. Many factors can influence the properties of HA obtained by this method, for example the precursors, pH value, stirring speed, temperature of preparation or ageing time.

2. EXPERIMENTAL METHOD

HA was prepared by wet-chemical precipitation method. In a round three-neck flask a geletine aqueous solutions is added, under magnetic stirring at 50°C. After 30 min the calcium solution was added to the biopolymer mix, under continuous stirring and then the phosphate solutions was added dropwise with an 1 $cm^3 \cdot min^{-1}$ flow. The pH value was set to 11-12 by adding NH_4OH 25%. The reflux process was employed at 50°C for 3 h under continuous stirring at 300 rpm. After 3 hours the white precipitate was washed and filtered under vacuum for 20 min. The precipitate was aged at room temperature for 24h and then dryed for another 48 h at 35°C. The sample batch was divided in two, so we could perform a comparison between the characterization of HA and sintered HA at 900°C.

The Fourier Transform Infrared spectra of the samples were recorded on a Spectrum 100 Perkin Elmer device by U-ATR technique. They were used to determine if there are some structural differences of HA samples before and after sinterization process.

The X-ray Diffraction difractograms were recorded on a X'Pert Pro MPD by Philips – FEI company PANalitical BV, The Netherlands, operating at 65kV and 55 mA. This difractograms are useful to characterize the crystallization phase of the ceramic composite before and after the sinterization process.

Scanning Electron Microscopy and EDAX investigations were performed on a Fei Quanta 250 electron microscope, at 15 and 20 kV, in order to determine the shape and crystal size of the HA sample.

3. RESULTS AND DISCUSSIONS

FTIR Spectrometry

Figures 1 and 2 show the recorded spectra of the HA, $Ca_{10}(PO_4)_6(OH)_2$, samples before and after the sinterization process. Spectrum has a peak at 3647 cm^{-1} corresponding to –OH stretching vibration and a peak at 668 cm^{-1} due to bending vibration of –OH. Between 1209 and 1138 cm^{-1} there are several peaks associated with P=O vibration. There is a clear band splitting, showing a high cristallinity of HA, between 1100-936 cm^{-1} there are eight peaks corresponding to stretching and bending vibrations of $(PO_4)^{3-}$ groups.

The main features observed in the spectrum for HA before sinterization and differing from the spectrum recorded after sinterization are the broad band in the range of 3250 cm^{-1}, attributed to absorbed water during the synthesis process, and the presence of only 2 peaks corresponding to $(PO_4)^{3-}$ group vibrations at 1060 cm^{-1} and 1042 cm^{-1}, respectively, showing that HA is not fully crystallized at this stage.

Figure 1: FTIR spectrum for biomimetic HA: before sinterization

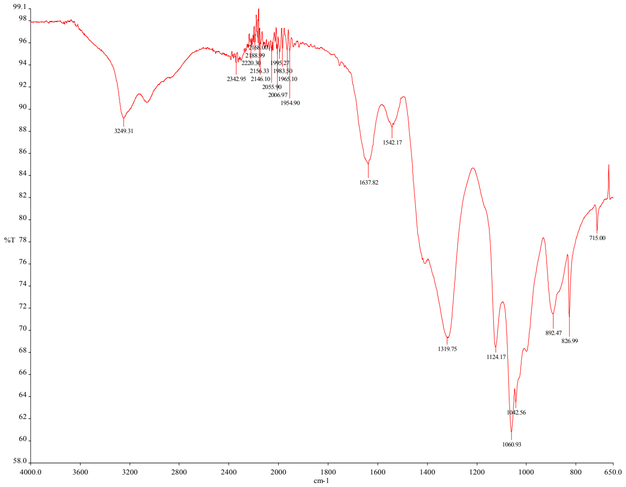

Figure 2: FTIR spectrum for biomimetic HA: after sinterization

XRD Analysis

The XRD patterns were recorded to determine if there is a higher degree of crystallinity after sinterization. The difractograms for the sintered HA (Fig.4) show the expected increase of the crystallinity for the sintered HA. Slightly broad peaks are implying small size crystallites [4], in the range of some hundred nanometers. The pattern of HA also shows that there are several directions for the growth of HA crystallites.

Figure 3: XRD patterns for biomimetic HA: before sinterization

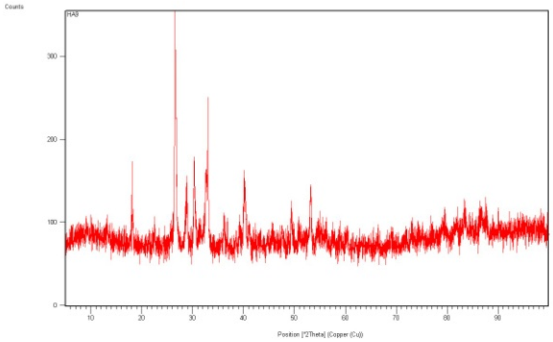

Figure 4: XRD patterns for biomimetic HA: after sinterization

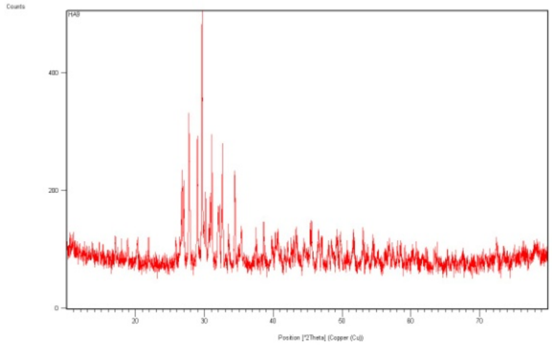

SEM and EDAX analysis

SEM micrographs of the HA before and after sinterization are shown in Fig.5 and Fig.6, respectively. In the first case, due to the biopolymer matrix the crystallites have needlelike shape and with nanodimensional size. After sinterization the nanocrystallites have needlelike and spherical shape, most likely due to interaction between the organic matrix and the Ca^{2+} ions.

EDAX spectra (Fig.7) show that nitrogen atoms are present in the sample which confirms the growing of the HA particles in the biopolymer matrix. After calcination (Fig.8) the nitrogen is not present in the spectrum, which is expected because at 900°C organic matter volatilises. Carbon cannot be measured quantitatively, because the support of the sample is also carbon based.

Figure 5: SEM image of biomimetic HA: before sinterization

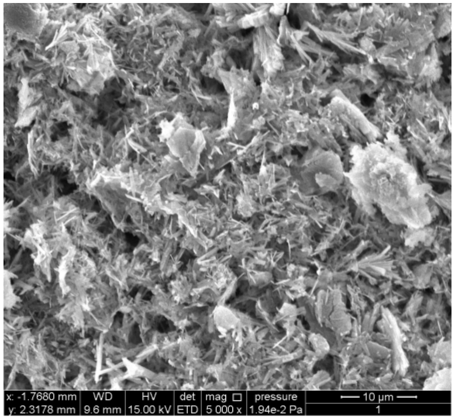

Figure 6: SEM image of biomimetic HA: after sinterization

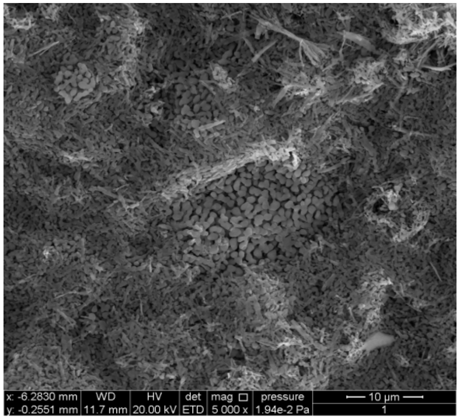

Figure 7: EDAX spectra of biomimetic HA: before sinterization

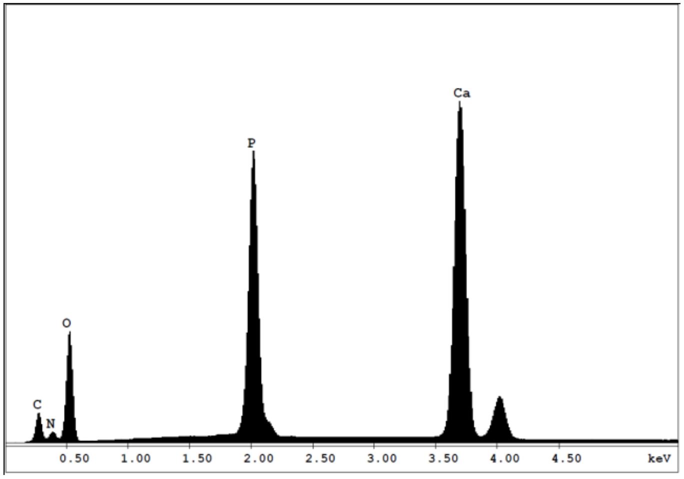

Figure 8: EDAX spectra of biomimetic HA: after sinterization

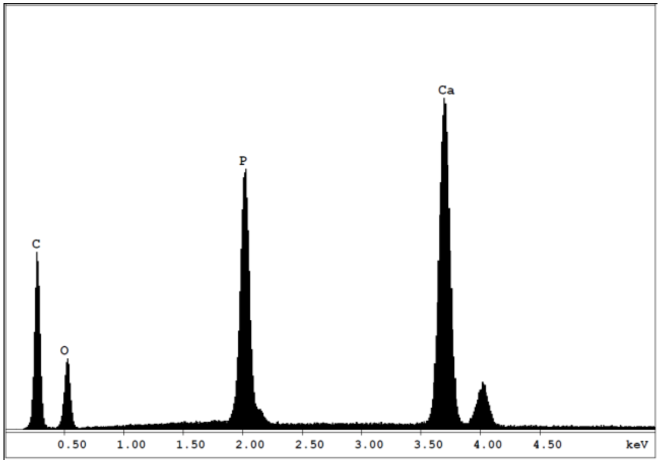

4. CONCLUSION

A biomimetic prepared hydroxyapatite was synthesized and characterized by several instrumental analytical methods: FTIR, XRD, SEM and EDAX. The results of the analyses confirmed that stoichiometric hydroxyapatite was prepared in respect with the conditions imposed by the molar ratio of calcium and phosphorous compounds (Ca:P = 1.67) used in the synthesis process, according to data collected from the literature. The crystallization process was not complete after the first step of the synthesis, only after the sinterization process at 900°C.

ACKNOWLEDGEMENT

This paper was supported by grant POSDRU/159/1.5/S/133391

REFERENCES

1. Mateus A.Y.P., Barrias C.C., Ribeiro C., Ferraz M.P., Monteiro F.J., Comparative study of nanohydroxyapatite microspheres for medical applications. *Journal of Biomedical Materials Research Part A,* **2008**, *86A(2)*, 483–493.
2. Bucholz R., Carlton A., Holmes R., Hydroxyapatite and tricalcium phosphate bone graft substitutes*, Orthop Clin N Am,* **1987***, 18,* 323-334.
3. Daculsi G., Passuti N., Martins S., Deudon C., LeGeros R., Raher S., Macroporous calcium phosphate ceramic for ling bone surgery in humans and dogs: Clinical and histological study. *Journal of Biomedical Materials Research,* **1990**, *24*, 379-396.
4. Gauthier O., Bouler J., Weiss P., Bosco J., Daculsi G., Aguado E., Kinetic study of bone in growth and ceramic resorption associated with the implantation of different

injectable calcium-phosphate bone substitutes. *Journal of Biomedical Materials Research*, **1999**, *47*, 28-35.

5. Rey C., Calcium phosphate biomaterials and bone mineral: Differences in composition, structures and properties. *Biomaterials*, **1990**, *11*, 13-15.
6. Yuan H., Kurashina K., de Bruijn J., Li Y., de Groot K., Zhang X., A preliminary study on osteoinduction of two kinds of calcium phosphate ceramics. *Biomaterials*, **1999**, *20*, 1799-1806.
7. Liou S., Chen S., Liu D., Synthesis and characterization of needlelike apatitic nanocomposite with controlled aspect ratio. *Biomaterials*, **2003**, *24*, 3981-3988.
8. Alves Cardoso D., Jansen J.A., Leeuwenburgh S.C.G., Synthesis and application of nanostructured calcium phosphate ceramics for bone regeneration. *Journal of Biomedical Materials Research B: Applied Biomaterials*, **2012**, *100B*, 2316-2326.
9. Dorozhkin S., Calcium orthophosphate-based biocomposites and hybrid biomaterials. *Journal of Material Science*, **2009**, *44*, 2343-2387.
10. Navarro M., Michiardi A., Castano O., Planell J.A., Biomaterials in orthopaedics. *Journal of The Royal Society Interface*, **2008**, *5*, 1137-1158.
11. Seal B.L., Otero T.C., Panitch A., Polymeric biomaterials for tissue and organ regeneration. *Materials Science and Engineering R*, **2001**, *34*, 147-230.
12. Chang M.C., Modification of hydroxyapatite/gelatin composite by polyvinylalcohol. Journal of Materials Science, **2005**, *40*, 505-509.

NEW FRONT. CHEM. (**2015**)
Volume 24, Number 1, pp. 55-60
ISSN 2393-2171; ISSN-L 2393-2171

Former: Ann. West Univ. Timisoara – Series Chem.
ISSN: 1224-9513

Article

THE SYNTHESIS AND STUDY OF SOME COMPLEXES OF METHYLENEDISALICYLIC ACID

***Andreea Nădăban*(1)♣, *Gabriela Vlase*(1,2)**
[1] West University of Timişoara, Faculty of Chemistry, Biology , Geography, Department of Biology and Chemistry, J. H. Pestalozzi street, no. 16, Timişoara, 300115, Romania, Tel./Fax.0256320280.
[2] Research Center for Thermal Analysis in Environmental Problems, West University of Timişoara, J. H. Pestalozzi street, no. 16, Timişoara, 300115, Romania.

ABSTRACT

The aim of this paper is the synthesis and characterization of the methylenedisalicylic acid (MDSA) and its complexes with Cu^{2+}, Pb^{2+} and Ag^{+}. In order to study these four compounds, the FT-IR spectrometry and thermal methods of analysis were used. The results of this study indicated different behaviors between these three cations, as expected according to their electronic structure and oxidation numbers.

Keywords: methylenedisalicylic acid, MDSA, complexes, study, characterization

1. INTRODUCTION

The coordination chemistry has become a field of high interest due to its wide range of possible applications. Metal complexes are used successfully in medicine, as active components of a variety of drugs [1]. Recently, researches were conducted using all the metals in the Periodic Table, with coordination numbers varying from 2 to 12. The new synthesis methods and physical methods for the study of structure have played an important role in the development of this branch of chemistry. The importance of catalysts and the role of metals in biochemistry have attracted the researchers' interest in towards the study of metal complexes [2].

♣ Correspondent author's e-mail: andreea.nadaban93@e-uvt.ro

There are several studies presented in the literature involving the synthesis of methylenedisalicylic acid but all of them describe the same method for this synthesis: treatment of salicylic acid with formaldehyde using 40% sulphuric acid [3,4,6]. In this ligand there are two active groups: hydroxyl and carboxyl and this may be expected to act as a multidentate ligand [3]. But the presence of the inactivating CH_2-group can cause steric effects. Ahmed et al. stated that the structure of the methylenedisalicylic acid (MDSA) can consist of two salicylic acid molecules joined by a methylene bridge in the ortho- position [6].

Over the years, studies were conducted on methylenedisalicylic acid, as a ligand in complexes [5-7]. The reported metals used in the literature were rare earths (M= La, Ce, Pr, Nd, Sm, Gd, Ho, Yb, or Y) [5] and transitional metals (M= Co(II), Ni(II), Cu(II), Mn(II), Zn(II), Fe(II), Fe(III)) [6]. Some of these studies revealed biological activity for some of the samples, illustrating a possible application as antimicrobial agents in medicine [6].

2. MATERIALS AND METHODS

2.1. Methods

The synthetized compounds were analyzed using the coupled techniques: TG-DTG-DTA, UATR (Universal Attenuted Transmitance Reflectance). These were assembled by a physical coupling of the two Perkin-Elmer units' software: a Diamond thermobalance and a Spectrum 100 FT-IR spectrometer.

2.2. The synthesis of the ligand

The ligand, MDSA, was prepared according to the literature [6], using the following: 13.8 g salicylic acid, 4.8 g formaldehyde (30% concentration) and 90 g sulphuric acid (50% concentration). The mixture was refluxed for 8 hours. Then the compound was cooled, filtered, washed with cold water and ethanol to remove any salicylic acid in excess. Afterwards, MDSA was recrystallized from acetone and a pale pink powder was obtained.

2.3. The synthesis of the complexes

The MDSA complexes were prepared using ethanolic solutions of MDSA (0.005 moles) with the following metal salts: Cu(II) and Pb(II) acetates and silver nitrate, $AgNO_3$ (0.01 moles). The compounds were refluxed for 1-2 hours, then they were filtered while still warm, washed with ethanol and dried in air [6].

3. RESULTS AND DISCUSSIONS

3.1. Solubility

The solubility of the synthetized complexes and ligand was determined using some common solvents. The results presented in Table 1 indicate that the MDSA is soluble in all the solvents that were used, while the complexes of MDSA with Cu^{2+}, Pb^{2+} and Ag^{+} are slightly soluble in methanol, ethanol and dimethylformamide (DMF) and insoluble in the other solvents.

Table 1: The solubility of the ligand and the complexes in different solvents

Compound	MeOH	EtOH	BuOH	Acetone	Ethyl acetate	DMF	Benzene	p-xylene
MDSA	S	S	S	S	S	S	S	S
Cu-MDSA	SS	SS	IS	IS	IS	SS	IS	IS
Pb-MDSA	SS	SS	IS	IS	IS	SS	IS	IS
Ag-MDSA	SS	SS	IS	IS	IS	SS	IS	IS

S = soluble, SS = slightly soluble, IS = insoluble

3.2. The study of MDSA

The FT-IR studies on the ligand suggested that the synthesis of MDSA was successful. Characteristic peaks are present in the spectrum: the C=O peak (in the carboxyl group) at 1655 cm^{-1} and the C=O stretch and in plane OH bending (specific for the COOH group) at 1442 cm^{-1} and 1292 cm^{-1} (Figure 1a). The results also indicate that two isomers of MDSA were obtained, due to the peaks for 1, 2, 3- and 1, 2, 4 - trisubstituted aromatic compounds at 1156 cm^{-1} and 1209 cm^{-1} respectively.

Figure 1: (a) The FT-IR spectrum for MDSA; (b) The thermogravimetric curves for MDSA

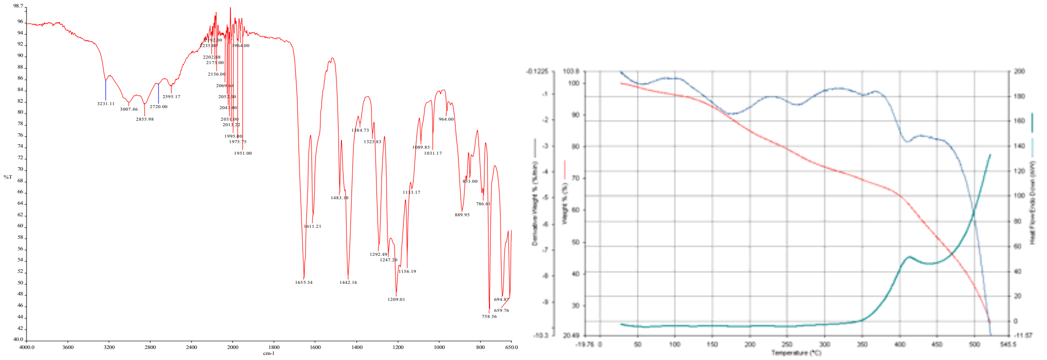

(a) (b)

The thermogravimetric studies for MDSA present the decomposition of the ligand between 25 and 530ºC in many steps, which can be hardly separated on the TG (Weight) and DTA (Heat flow) curves, but separable on the DTG (Derivative Weight). On the DTG curve, there are 6 maximums in the analyzed temperature interval (Figure 1b). The first four steps have very weak thermal effects, while the last two steps are exothermic processes. The first decomposition steps are due to the loss of the crystallization water and humidity. The last decomposition step does not end in the temperature interval that was studied.

3.3. The study of the three complexes

After the comparison of the FT-IR spectra of the MDSA and the metal complexes, specific peaks appeared for the carboxylate ion (around 1385 cm^{-1}) and for the bonded phenolic OH group (around 3150 cm^{-1}). The peak for the carboxyl group (C=O) around 1655 cm^{-1} disappeared, a first sign of the success of the reaction.

The comparative analysis of the FT-IR spectra for the three coordination compounds shows a similarity between the Cu^{2+} and Pb^{2+} complexes and a different coordination for the Ag^{+} complex.

Figure 2: The comparison of the FT-IR spectra for Ag-MDSA (blue), Cu-MDSA (red) and Pb-MDSA (black)

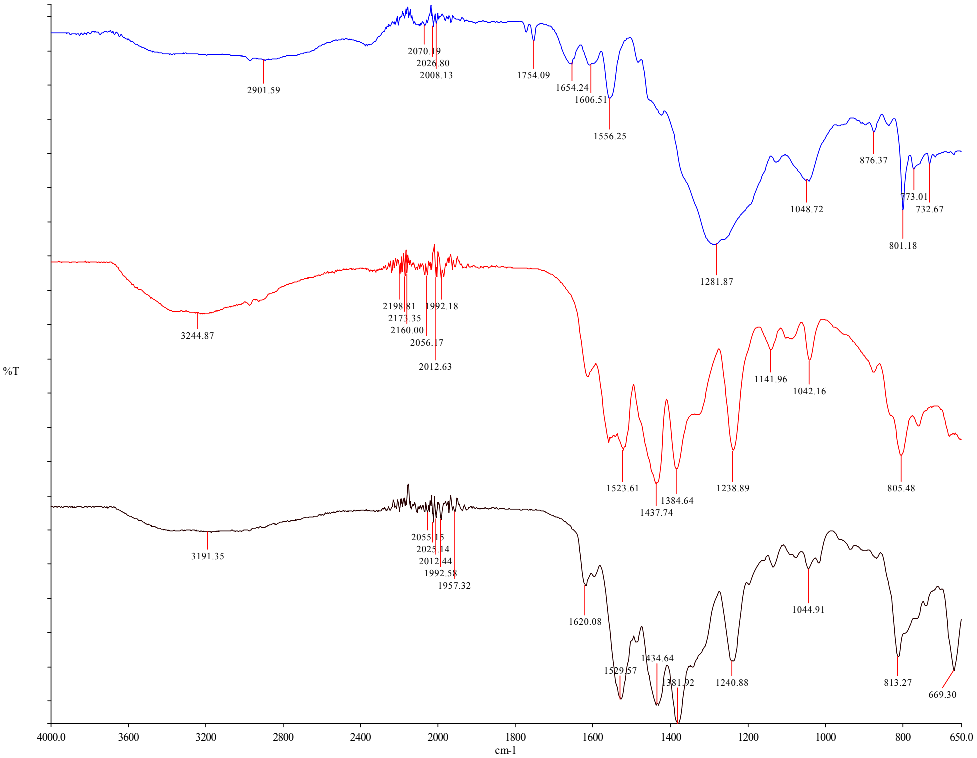

The thermogravimetric studies for the Cu^{2+} complex were conducted between 25 and 500ºC with a heating rate of 10ºC/min, in air atmosphere. The Cu-MDSA complex had two decomposition steps: the first, between 45 and 242ºC, due to the loss of two molecules of crystallization water and the second step, between 242 and 253 ºC, representing the decomposition of the complex, when the metal-complex bond was broken (Figure 3a).

The results of the TG studies for the Pb-MDSA complex were quite similar to the Cu^{2+} compound.

The results for the Ag^{+} complex were slightly different from the first two complexes. The thermogravimetric analysis was conducted between 25 and 523ºC, with a heating rate of 5ºC/min. A lower heating rate was necessary in order to separate some of the decomposition processes. This complex had four decomposition steps. The difference is the fact that Ag-MDSA has four interior coordination water molecules and the exothermic process appeared at a temperature higher with 100ºC than the others. This suggests a stronger metal-ligand bond (Figure 3b). The thermal effects of the decomposition reaction for the three complex compounds vary in the following order: Pb-MDSA < Ag-MDSA < Cu-MDSA and the thermal stability varies as following: Cu-MDSA < Pb-MDSA < Ag-MDSA.

Figure 3: The thermogravimetric curves for (a) Cu-MDSA and (b) Ag-MDSA

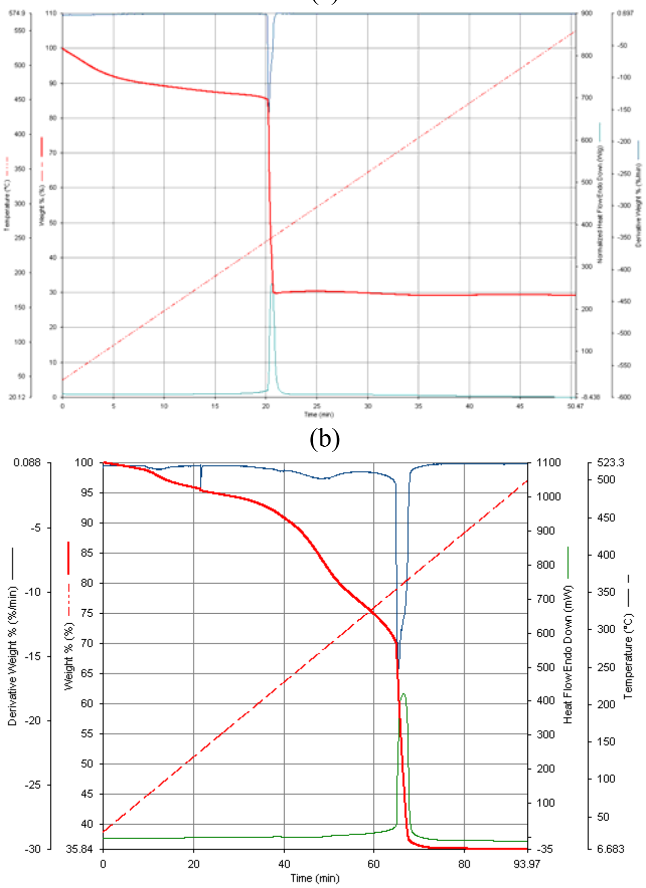
(a)

(b)

4. CONCLUSION

The purpose of this paper was the synthesis of the methylenedisalicylic acid (MDSA) and some complex compounds with Cu^{2+}, Pb^{2+}, Ag^{+}. This ligand and its complexes were analyzed using FT-IR spectrometry and thermogravmetric analysis. The results indicate that these synthesis reactions were successful.

A different behavior can easily be noticed between the Cu^{2+} and Pb^{2+} cations and Ag^{+} from the FT-IR spectra, as well as from the thermoanalytical curves for the three compounds. This was expected to happen due to the electronic structure and the oxidation numbers of the three cations. For Cu^{2+} and Pb^{2+} complexes, an octahedral geometry is expected, however Ag^{+} usually prefers a linear geometry. Therefore, it can be deducted that $[Ag_2(MDSA\text{-}4H)\cdot(H_2O)_4]\cdot 2H_2O\cdot(NO_3^-)$ has four molecules of water in the interior coordination sphere, as well as two molecules in the exterior sphere of coordination. In contrast, the other two complexes, $[Cu_2(MDSA\text{-}4H)]\cdot 2H_2O$ and $[Pb_2(MDSA\text{-}4H)]\cdot 5H_2O$ present coordinated water molecules only in the exterior coordination sphere.

These studies will be continued in the future with other investigation methods to assure the stability and the geometry of these complex compounds.

ACKNOWLEDGEMENT

The authors wish to thank the Research Center for Thermal Analysis in Environmental Problems for the assistance given to this research.

REFERENCES

1. Guo, Z., Sandler, P. J., Metals in medicine, *Angew. Chem. Int. Ed.* **1999**, *38*, 1512 – 1531.
2. Wilkinson, G., Gillard, R. D., McClleverty, J. A., *Comprehensive Coordination Chemistry – The Synthesis, Reactions, Properties & Applications of Coordination Compounds*, Publisher Elsevier Science, New York, USA, 1987, 1011-1031.
3. Kahl, L., Ueber Condensationsproducte von Aldehyden mit Phenolen und Phenolcarbonsäuren und davon derivirende Diphenylmethanfarbstoffe, *Ber. Dtsch. Chem. Ges.* **1898**, *31*, 143–151.
4. Clemmensen, E., Heitman, A. H. C., Methylenedisalicylic acid and its reaction with bromine and iodine, *J. Am. Chem.Soc.* **1911**, *33*, 733-745.
5. Sivapullaiah, P. V., Soundararajan, S., Methylene di salicylates of rare-earths, *J.I.I.Sc.* **1976**, *58*(7), 289-293.
6. Ahmed, A. H., Omran, A. A., El-Sherbiny, G. M., Synthesis, Characterization and Biological Evaluation of Some Methylenedisalicylic Acid Complexes, *J. App. Sci. Res.* **2006**, *2*(1), 44-50.
7. Aliyu, H. N., Toudou, N. A. M., Spectrophotometric Analysis of Cobalt (II), Nickel (II), Copper (II) and Zinc (II) Complexes with Methylenedisalicylic Acid, *ARPN J of Sci and Tech* **2012**, *2(*3), 142-146.

NEW FRONT. CHEM. (**2015**)
Volume 24, Number 1, pp. 61-67
ISSN 2393-2171; ISSN-L 2393-2171
© West University of Timişoara

Former: Ann. West Univ. Timisoara – Series Chem.
ISSN: 1224-9513

Article

COMPUTING OMEGA AND SADHANA POLYNOMIALS OF HEXAGONAL TRAPEZOID SYSTEM $T_{B,A}$

Mohammad Reza Farahani ♣
Department of Applied Mathematics, Iran University of Science and Technology (IUST), Narmak, Tehran, 16844, Iran

ABSTRACT

Let $G(V,E)$ be a connected graph, with the vertex set $V(G)$ and edge set $E(G)$. Omega polynomial $\Omega(G,x)$, was proposed by *M.V. Diudea.* It was defined on the ground of "opposite edge strips" *ops*. The Sadhana polynomial *Sd* can also be calculated by ops counting and was proposed by *Ashrafi* and co-authors. In this paper we compute the Omega and Sadhana polynomial s and their indices of a Hexagonal system $T_{b,a..}$

Keywords: Molecular graph, Omega polynomial, Sadhana Polynomial, qoc strip, Hexagonal trapezoid system.

1. INTRODUCTION

Mathematical calculations are absolutely necessary to explore important concepts in chemistry. Mathematical chemistry is a branch of theoretical chemistry for discussion and prediction of the molecular structure using mathematical methods without necessarily referring to quantum mechanics. In chemical graph theory and in mathematical chemistry, a molecular graph or chemical graph is a representation of the structural formula of a chemical compound in terms of graph theory.

♣ Tel:+98-919-247-8265, E-mails: Mr_Farahani@Mathdep.iust.ac.ir & MrFarahani88@gmail.com

A topological index is a numerical value associated with chemical constitution purporting for correlation of chemical structure properties, chemical reactivity or biological activity.

Let $G(V, E)$ be a connected molecular graph without multiple edges and loops, with the vertex set $V(G)$ and edge set $E(G)$, and vertices/atoms $x, y \in V(G)$. Two edges $e=uv$ and $f=xy$ of G are called co-distant, "*e* co *f*", if and only if they obey the following relation: [1, 2]

$$d(v,x)=d(v,y)+1=d(u,x)+1=d(u,y)$$

Relation *co* is reflexive, that is, *e co e* holds for any edge *e* of *G*; it is also symmetric, if *e co f* then *f co e* and in general, relation *co* is not transitive. If "*co*" is also transitive, thus an equivalence relation, then *G* is called a *co-graph* and the set of edges is $C(e):=\{f\in E(G)|e \text{ co } f\}$), called an *orthogonal cut* (denoted by *oc*) of *G*. In other words, $E(G)$ being the union of disjoint orthogonal cuts:

$$E(G)=C_1 \cup C_2 \cup C_3 \cup \ldots \cup C_{k-1} \cup C_k$$

and $C_i \cap C_j = \acute{\emptyset}$ for $i \neq j$ and $i, j=1, 2, \ldots, k$.

Klavžar [3] has shown that relation *co* is a theta *Djoković*-*Winkler* relation [4, 5].

Let $m(G,c)$ be the number of qoc strips of length c(i.e., the number of cut-off edges) in the graph *G*.

The *Omega Polynomial* $\Omega(G,x)$ [6-9] for counting *qoc* strips in *G* was defined by *Diudea* as

$$\Omega(G,x)=\sum_c m(G,c)\,\mathrm{x}^c$$

The summation runs up to the maximum length of *qoc* strips in *G*. The first derivative (in x=1) equals the number of edges in the graph

$$\Omega'(G,1)=\sum_c \mathrm{m}(\mathrm{G},c)\times c=|E(G)|$$

$$\Theta(G,x)=\sum_c m(G,c)c.\mathrm{x}^c$$

$$Sd(G,x)=\sum_c m(G,c)\mathrm{x}^{|E(G)|-c}$$

$$\Pi(G,x)=\sum_c m(G,c)c.\mathrm{x}^{|E(G)|-c}$$

$\Omega(G,x)$ and $\Theta(G,x)$ polynomials count *"equidistant edges"* in *G* while $Sd(G,x)$ and $\Pi(G,x)$, *"non-equidistant edges"*. The first derivative (computed at $x=1$) of these counting polynomials provide interesting topological indices:

The Sadhana index $Sd(G)$ was defined by *Khadikar et al*. [10,11] as

$$Sd(G)=\sum_c m(G,c)\left(|E(G)|-c\right)$$

where $m(G,c)$ is the number of strips of length c. The Sadhana polynomial $Sd(G,x)$ was defined by *Ashrafi* and co-authors in 2008, [12].

Clearly, the Sadhana polynomial can be derived from the definition of Omega polynomial by replacing the exponent c by $|E(G)|-c$.

Then the Sadhana index will be the first derivative of $Sd(x)$ evaluated at $x=1$. The aim of this study is to compute the Omega and Sadhana polynomials of a Hexagonal trapezoid system $T_{b,a}$. Here our notations are standard and mainly taken from [13-16].

2. RESULTS AND DISCUSSION

In this section we compute counting polynomials mentioned in the text of a family of benzenoid graphs (see Figure 1 and references [16-18]) that called Hexagonal trapezoid system Tb,a. A hexagonal trapezoid Tb,a ∀a,b∈ℕ & a≥b is a hexagonal system consisting a−b+1 rows of benzenoid chain in which every row has exactly one hexagon less than the immediate row. An especial case of this family is triangular benzenoid Gn, that is equivalent with a hexagonal trapezoid system T1,n. It is easy to see that the triangular benzenoid Gn ∀n∈ℕ has n2+4n+1 vertices and $\frac{3}{2}n(n+3)$ edges (see Figure 2).

Figure 1: A general representation of the hexagonal trapezoid system $T_{b,a}$ ($\forall a,b\in \mathbb{N}$)

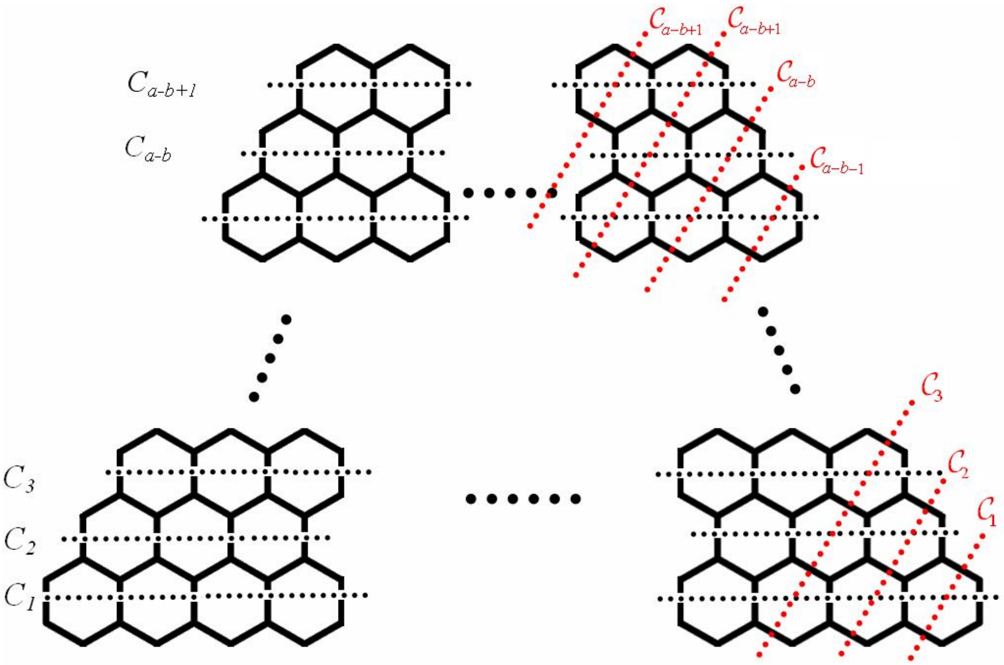

Theorem 1: The Omega polynomial of the Hexagonal Trapezoid System Tb,a ($\forall a,b\in\mathbb{N}$) is as follows:

$$\Omega(T_{b,a},x)=\sum_{i=1}^{a-b+1}\mathrm{x}^{a+2-i}+\sum_{i=1}^{a-b}2\mathrm{x}^{i+1}+2bx^{a-b+2}$$

Proof. Let $G=T_{b,a}$ be the hexagonal trapezoid system. In general case the number of vertices of hexagonal trapezoid $T_{b,a}$ is equal to $2a+1+\sum_{i=2b+1}^{2a+1}i=a^2-b^2+4a+2$ for all $a,b\in\mathbb{N}$ and the number of edges of $T_{b,a}$ is equal to $2a+\sum_{i=3b+1}^{3a+1}i=\frac{3}{2}(a^2-b^2)+\frac{9}{2}a+\frac{b}{2}+1.$

To compute the Omega polynomial of G, it is enough to calculate $C(e)$ for every e in $E(G)$. Thus, from Table 1 we have

$$\begin{aligned}\Omega(T_{b,a},x)&=\sum_{c}\mathrm{m}(T_{b,a},c)\mathrm{x}^{c}\\&=\sum_{c_i,i=1}^{a-b+1}\mathrm{m}(\mathrm{T}_{b,a},c_i)\mathrm{x}^{c_i}+\sum_{C_i,i=1}^{a-b}\mathrm{m}(\mathrm{T}_{b,a},C_i)\mathrm{x}^{C_i}+\mathrm{m}(\mathrm{T}_{b,a},C_{a-b+1})\mathrm{x}^{C_{a-b+1}}\\&=\sum_{i=1}^{a-b+1}\mathrm{x}^{a+2-i}+\sum_{i=1}^{a-b}2\mathrm{x}^{i+1}+2bx^{a-b+2}\\&=x^{a-b+2}+x^{a-b+1}+\ldots+x^{a+1}+x^{a}+2x^{2}+2x^{3}+\ldots+2x^{a-b+1}+2bx^{a-b+2}\end{aligned}$$

Hence we proved Theorem 1. ■

Table 1: The number of co-distant edges for all natural numbers a,b such that $a\geq b$

quasi-orthogonal cuts	Number of co-distant edges	No
c_i $\forall i=1,\ldots,a-b+1$	$a-i+2$	1
C_i $\forall i=1,\ldots,a-b$	$i+1$	2
C_{a-b+1}	$a-b+2$	$2b$

Theorem 2: The Sadhana polynomial of the hexagonal trapezoid system $T_{b,a}$ is

$$Sd(T_{b,a},x)=\sum_{i=1}^{a-b+1}\mathrm{x}^{|E|+i-a-2}+\sum_{i=1}^{a-b}2\mathrm{x}^{|E|-i-1}+2bx^{|E|+b-a-2}$$

And the Sadhana index of $T_{b,a}$ is equal to

$$Sd(T_{b,a})=\tfrac{1}{2}(9a^3+27a^2-3b^3-b^2)-6a^2b+6ab+3a$$

Proof. The proof is analogous to the proof of Theorem 1 and by using Table 1, we have

$$Sd(T_{b,a},x)=\sum_{c} m\left(T_{b,a},c\right)\mathrm{x}^{|E(T_{b,a})|-c}$$

$$=\sum_{c_i,i=1}^{a-b+1}\mathrm{m}(\mathrm{T}_{b,a},c_i)\mathrm{x}^{|E(T_{b,a})|-c_i}+\sum_{\mathrm{C}_i,i=1}^{a-b}\mathrm{m}(\mathrm{T}_{b,a},\mathrm{C}_i)\mathrm{x}^{|E(T_{b,a})|-\mathrm{C}_i}$$

$$+\mathrm{m}(\mathrm{T}_{b,a},\mathrm{C}_{a-b+1})\mathrm{x}^{|E(T_{b,a})|-\mathrm{C}_{a-b+1}}$$

$$=\sum_{i=1}^{a-b+1}\mathrm{x}^{|E|+i-a-2}+\sum_{i=1}^{a-b}2\mathrm{x}^{|E|-i-1}+2bx^{|E|+b-a-2}$$

where $|E(T_{b,a})|=\frac{3}{2}(a^2-b^2)+\frac{9}{2}a+\frac{\mathrm{b}}{2}+1.$

And also the Sadhana index of $T_{b,a}$ is equal to

$$Sd'\left(T_{b,a},\mathrm{x}\right)|_{x=1}=\left[\sum_{i=1}^{a-b+1}(|E|+i-a-2)\mathrm{x}^{|E|+i-a-3}+2\sum_{i=1}^{a-b}(|E|-i-1)\mathrm{x}^{|E|-i-2}+2b(|E|+b-a-2)x^{|E|+b-a-3}\right]_{x=1}$$

$$=\left(|E|-a-2\right)\left(a-b+1\right)+\sum_{i=1}^{a-b+1}i+2\left(|E|-1\right)\left(a-b\right)\text{-}2\sum_{i=1}^{a-b}i+2b(|E|+b-a-2)$$

$$=\left(\frac{a^2+b^2+-2ab+3a-3b+2}{2}\right)-2\left(\frac{a^2+b^2+-2ab+a-b}{2}\right)$$

$$+(-a^2+2b^2-ab-5a-2)+|E|(3a-b+1)$$

$$=\left(\frac{3a^2-3b^2+9a+b+2}{2}\right)\left(3a-b+1\right)-\left(\frac{3a^2-3b^2+9a+b+2}{2}\right)$$

$$=½(9a^3+27a^2-3b^3-b^2)-6a^2b+6ab+3a.■$$

Corollary 1. [16] Let G_n be the Triangular Benzenoid.

- The Omega polynomial of G_n is equal to $\Omega(G_n,x)=3x^2+3x^3+\ldots+3x^{n+1}$
- The Sadhana polynomial of G_n is equal $Sd(G_n,x)=3x^{|E|-2}+3x^{|E|-3}+\ldots+3x^{|E|-n-1}$

where $|E|=\frac{3}{2}n(n+3)$ and the Sadhana index $Sd(G_n)=\frac{9n^3}{2}+\frac{15n^2}{2}+9n-2.$

Corollary 2. Let LHn=Tn,n be the Linear Hexagonal Chain with 4n+2 vertices and 5n+1 edges ∀n∈ℕ (see Figure 3). One can see that Ω(Gn,x)=2nx2+xn+1, Sd(LHn,x)=2nx5n-1+x4n and Sd(LHn)=10n2+2n.

Figure 2: Graph of Triangular Benzenoid G_7.

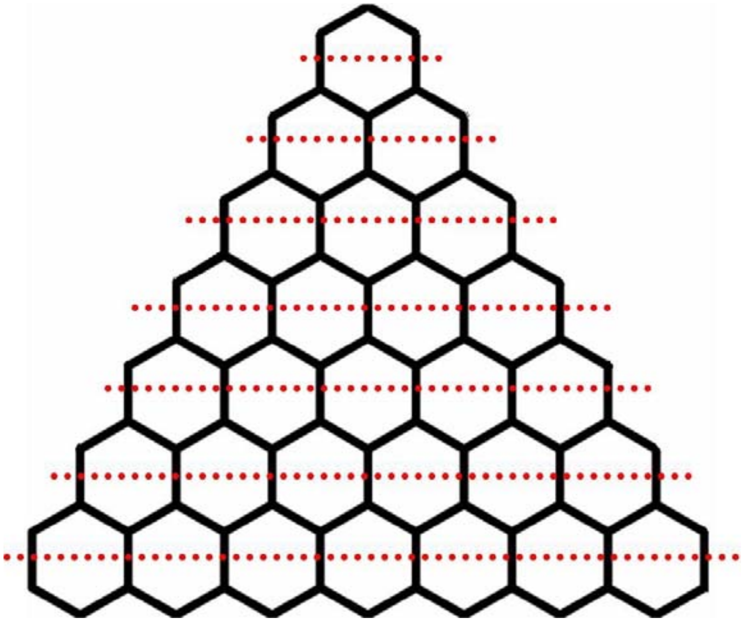

Figure 3: Graph of Linear Hexagonal Chain LH_n.

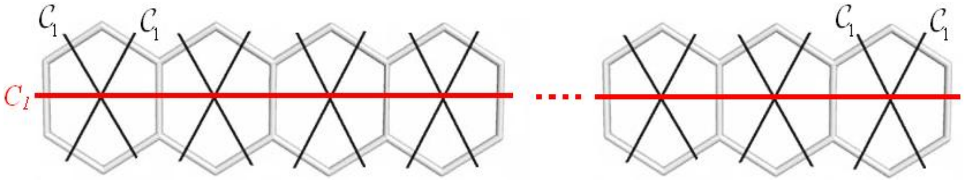

4. CONCLUSION

In this paper, I was counting a new counting topological polynomial and its index for a family of Hexagonal system "Hexagonal Trapezoid System $T_{b,a}$" and its especial cases "G_n be the Triangular Benzenoid" and "Linear Hexagonal Chain LH_n.". $\Omega(G,x)$ and $Sd(G,x)$ polynomial and their indices are useful for counting the *quasi-orthogonal cut qoc* strip in structure of connected molecular graph, Nanotubes and Nanostructures.

REFERENCES

1. M.V. Diudea, S. Cigher, A.E. Vizitiu, O. Ursu and P. E. John. Croat. Chem. Acta, 79(3), 445-448. (2006).
2. A.E. Vizitiu, S. Cigher, M.V. Diudea and M.S. Florescu, MATCH Commun. Math. Comput. Chem. 57(2), 479-484 (2007).
3. S. Klavžar, MATCH Commun. Math. Comput. Chem., 59, 217 (2008).
4. D.Ž. Djoković, J. Combin. Theory Ser. B, 14, 263 (1973).

5. P.M. Winkler, Discrete Appl. Math., 8, 209 (1984).
6. M.V. Diudea, Carpath. J. Math. 22 43–47 (2006).
7. P.E. John, A.E. Vizitiu, S. Cigher, and M.V. Diudea, MATCH Commun. Math. Comput. Chem., 57, 479 (2007).
8. A.R. Ashrafi, M. Jalali, M. Ghorbani and M.V. Diudea. MATCH, Commun. Math. Comput. Chem., 60 (2008), 905–916
9. M.V. Diudea and A. Ilić, Carpath. J. Math., 20(1) (2009), 177 – 185.
10. P.V. Khadikar, V.K. Agrawal and S. Karmarkar, Bioorg. Med. Chem., 10, 3499 (2002).
11. P.V. Khadikar, S. Joshi, A.V. Bajaj and D. Mandloi, Bioorg. Med. Chem. Lett., 14, 1187 (2004).
12. A.R. Ashrafi, M. Ghorbani and M. Jalali, Ind. J. Chem., 47A, 535 (2008).
13. M. Ghorbani, Digest. J. Nanomater. Bios. 6(2), 2011, 599-602
14. M.R. Farahani, K. Kato and M.P. Vlad. Studia Univ. Babes-Bolyai. Chemia 2012 57(3), 177-182.
15. M.R. Farahani. Acta Chim. Slov. 2012, 59, 965–968.
16. M. Ghorbani, M. Ghazi. Digest. J. Nanomater. Bios. 5(4), 2010, 843-849
17. M. Ghorbani, M. Ghazi. Digest. J. Nanomater. Bios. 5(4), 2010, 837-841.
18. Z. Bagheri, A. Mahmiani and O. Khormali. Iranian Journal of Mathematical Sciences and Informatics. 2008 3(1), 31-39.

NEW FRONT. CHEM. (**2015**)
Volume 24, Number 1, pp. 69-79
ISSN 2393-2171; ISSN-L 2393-2171

Former: Ann. West Univ. Timisoara – Series Chem.
ISSN: 1224-9513

Article

A COMPARATIVE STUDY ON THE OBTAINING OF ALPHA-Fe_2O_3 NANOPARTICLES BY TWO DIFFERENT SYNTHESIS METHODS

Oana Stefanescu[1]♣, Corneliu Davidescu[1], Cornelia Muntean[1]

[1]Politehnica University Timisoara, Applied Chemistry and Inorganic Compounds Engineering, 6 Vasile Parvan Blvd., 300223, Timisoara, Romania

ABSTRACT

This paper deals with the synthesis of α-Fe_2O_3 nanoparticles by two different synthesis methods: precipitation and thermal decomposition of carboxylate complex. The effect of temperature on the characteristics of the obtained powders was investigated by thermal analysis, XRD, FTIR spectroscopy and SEM. This study compares the results obtained by the two methods mentioned above, in which the mechanism of α-Fe_2O_3 formation is different. The iron hydroxide precipitate obtained at 90°C was annealed at 300°C with formation of α-Fe_2O_3 nanoparticles. By thermal decomposition of the Fe(III) carboxylate combination at 300°C, the cubic γ-Fe_2O_3 is obtained, which turns to hexagonal α-Fe_2O_3 nanoparticles, at 500°C.

Keywords: carboxylate combination, precipitation, α-Fe_2O_3, nanoparticles

1. INTRODUCTION

The methods used for the synthesis of iron oxides are from the most different ones assuring specific performances to the resulted oxide. Each method presents advantages regarding some applications and disadvantages regarding other applications. Thus, it is explained that the usage of different synthesis methods result in oxides with different morphologies. The particularity of iron oxides synthesis methods is to obtain well crystallized, single phases. The materials research is focused on the obtaining of iron oxides nanoparticles due to the unique dependence of the properties on the nanoparticle size [1]. The

---

♣ Correspondent author: Tel:+40737686813, E-mail: oanaelenastefanescu@yahoo.com

researchers concerns are oriented towards an efficient control on purity, homogeneity, porosity, grain size, grain size distribution, morphology and phase composition, all these factors being decisive for the characteristics of the final product. The choice of the most suitable synthesis method for the iron oxides and the identification of the optimal synthesis conditions ensure the premise for the maximization of its advantages [2]. Among iron oxides, hematite (α-Fe_2O_3) is widely studied due to its applications as pigment, sensor, electrode material and recently photocatalyst [3-6]. α-Fe_2O_3 is the most stable iron oxide with high resistance to corrosion, low cost, biocompatibility, high efficiency, non-toxic characteristics [3, 7]. In the last years, the researchers have developed some unconventional methods and precursors for the obtaining of hematite with specific properties, such as: the hydrothermal method, precipitation, the sol-gel method, combustion [8-12]. These methods present a series of advantages: homogeneous distribution of the oxide at molecular scale, high reactivity, fine granulation, high specific surface and porosity, due to low formation temperatures, control on particles sizes.

2. METHOD

The purpose of this paper is to illustrate and compare two synthesis methods, precipitation of Fe(III) hydroxide and thermal decomposition of Fe(III) carboxylate type precursors, for the obtaining of α-Fe_2O_3. This approach will provide a better insight on the influence of the starting precursor on the formation and features of α-Fe_2O_3.

2.1. Theoretical Method

The methods used show two different preparation procedures for α-Fe_2O_3, as in Fig.1 (a,b).

Figure 1: General schemes for the preparation of α-Fe2O3 nanoparticles, by: a.) precipitation, b.) thermal decomposition of Fe(III) carboxylate type precursors

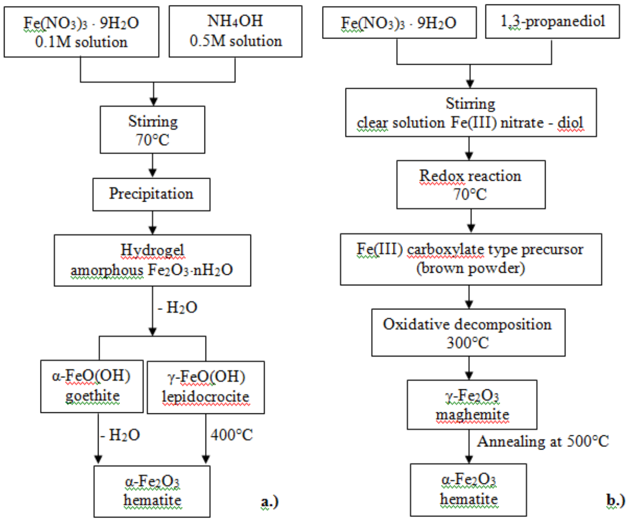

Precipitation

Iron (III) nitrate nine-hydrate as iron source and ammonium hydroxide as precipitating agent were used, both of analytical purity and purchased from Merck. These reagents were used to prepare iron oxide particles. Iron (III) nitrate was dissolved in distilled water, with stirring, to give a 0.1M solution. 0.5 M ammonium hydroxide solution was added drop wise into the 0.1M iron nitrate solution under vigorous stirring. The volume ratio of the solutions was 1:1. The resulted product was a dark brown precipitate, which was filtered, washed three times with distilled water and dried at 90°C, 20h. The sample was further annealed at 200°C, 300°C and 500°C, 3h.

Thermal decomposition of Fe(III) carboxylate type precursors

There was synthesized a precursor of Fe(III) carboxylate type starting from iron(III) nitrate nine-hydrate and 1,3-propandiol (1,3PG), both of analytical purity purchased from Merck. 0.0375 moles $Fe(NO_3)_3{\cdot}9H_2O$ were solubilised in 0.0633 moles 1,3PG until a homogenous, viscous mixture was formed. The reagent quantities were calculated according to the reaction stoechiometry [13] with a diol excess of 50% for the obtaining of 3g Fe_2O_3. The resulted mixture was heated in an oven, when the redox reaction between the NO_3^- and diol, took place at ~70°C, with formation of the Fe(III) carboxylate combination. The decomposition of the complex combination at 300°C leaded to γ-Fe_2O_3 (maghemite) [14]. By direct annealing of the complex combination at 500°C, α-Fe_2O_3 (hematite) was obtained.

2.2. Experimental Method

Thermal analysis studies were carried out using a 1500 D MOM Budapest derivatograph in air, in the temperature range 25 – 500°C, with a heating rate of 5°C/min, using a sample mass of ~ 100 mg and α-Al_2O_3 as reference material. There was also used a Diamond Perkin Elmer Thermobalance, where the experiments were achieved under identical conditions, in air, maintaining the following experimental parameters: the temperature range 20 – 500°C, heating rate of 10 °C/min and a sample mass of ~ 10 mg. FT-IR spectra of the synthesized and annealed samples were recorded on a Shimadzu-Prestige-21 spectrometer. The samples were measured as KBr pellets, in the range 400 – 4000 cm^{-1} with a spectral resolution of 4 cm^{-1}. XRD was used to examine the crystallinity and phase constitution of the samples prepared by the two methods. The phase evolution was investigated by Rigaku Ultima IV X-ray diffractometer using monochromatic CuKα radiation (λ = 1.54056 Å). The average crystallite size was calculated using the whole pattern profile fitting method (WPPF). The instrument influence has been subtracted using the diffraction pattern of a Si standard recorded in the same conditions. The crystalline phases were identified using JCPDS-ICDD files. The morphology and microstructure of the particles were observed by scanning electron microscopy (SEM) using a Inspect S FEI microscope (operating at 30 kV and 10-18 mm working distance).

3. RESULTS AND DISCUSSIONS

Precipitation

Results of thermal analysis measurements for the precipitate dried at 90°C are summarized in Fig.2. As one can see, there seems to be a mixture of iron hydroxides: α-FeO(OH) (goethite) and γ-FeO(OH) (lepidocrocite). The effects on TG and DTA up to 100°C correspond to the loss of physically bound water. The effects registered up to 380°C could be attributed to the loss of structurally bound water, as well as to the topotactic and pseudomorphic dehydration of α-FeO(OH) (goethite) and γ-FeO(OH) (lepidocrocite) [15]. In case of lepidocrocite it is known that on DTA there is an exothermic effect in the range 400 – 500°C as a result of the polymorphic transformation of γ-Fe_2O_3 to α-Fe_2O_3. The different thermal behaviour of goethite and lepidocrocite is due to the difference between their crystalline structures [16, 17].

Figure 2: Thermal analysis curves for the precipitate dried at 90°C

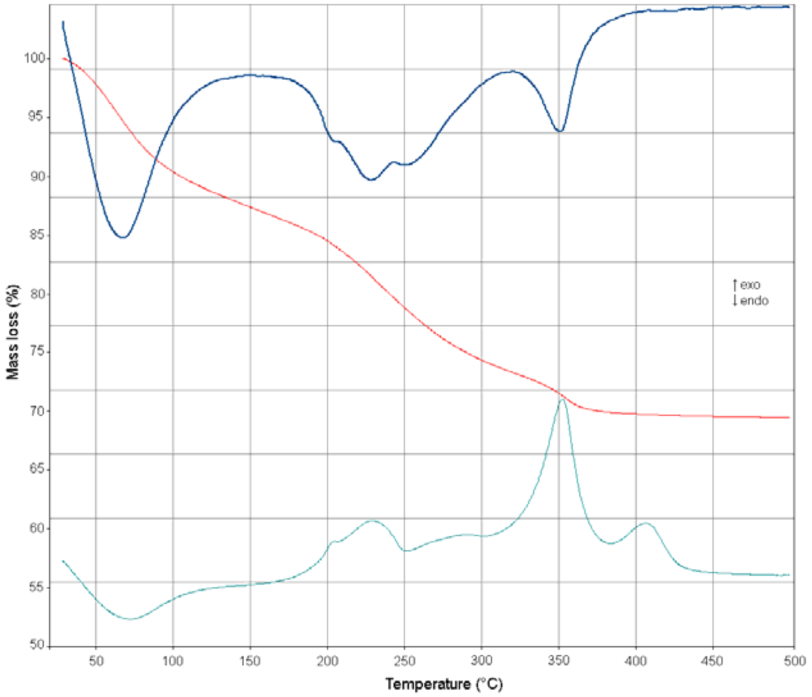

X-Ray diffraction patterns for the precipitate dried at 90°C and annealed at 200°C, 300°C and 500°C are presented in Fig.3. The samples from 90°C and 200°C are amorphous. It can be supposed that small iron oxides crystallites start forming, but the final structure is disordered. The crystallization process evolves with 300°C and it is complete at 500°C. Starting with 300°C α-Fe_2O_3 (JCPDS 01-089-2598) was the single phase identified by XRD, having a particle size of ~ 12 nm. At 500°C α-Fe_2O_3 is well crystallized with increasing particle size (~19 nm).

Figure 3: XRD patterns of the sample obtained by precipitation and annealed at different temperatures

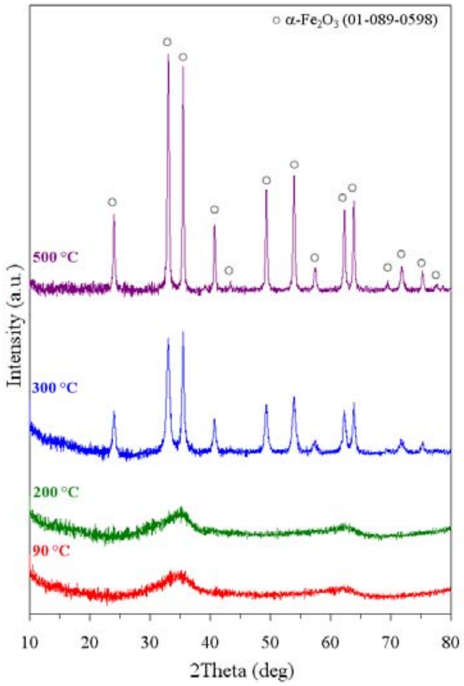

Figure 4: SEM image of α-Fe_2O_3 obtained at 300°C by precipitation

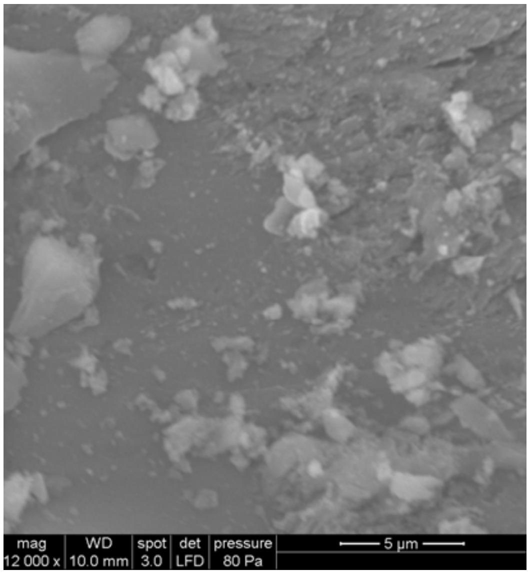

The image of the SEM micrograph (Fig.4) shows that the particles are agglomerated and have irregular shapes.

Thermal decomposition of Fe(III) carboxylate type precursors

The synthesis method of the Fe(III) carboxylate type precursor consists in the solubilisation of iron nitrate in the corresponding diol amount. The resulted solution was deposed on platinum plates and heated in static air atmosphere up to 500°C on the derivatograph, in order to establish the formation mechanism of the Fe(III) carboxylate type precursor. Figure 5 presents the TG and DTA curves of the solutions $Fe(NO_3)_3$ – 1,3PG. The DTA curve presents two exothermic effects: a weak exothermic effect at ~70 °C, which is attributed to the redox reaction between the nitrate ion and diol with formation of the Fe(III) carboxylate type precursor. The mass loss on TG corresponding to this process is due to the water evaporation, elimination of nitrogen oxides resulted during the redox reaction and the evaporation of diol excess. The second, stronger, exothermic effect in the temperature range 250-300 °C, with a mass loss on TG, corresponds to the oxidative decomposition of the formed complex combination.

According to this study, we have established at 130°C the synthesis temperature for the oxidation products. Thus, the mixture $Fe(NO_3)_3$ – 1,3PG was heated, when the redox reaction between the NO_3^- ion and diol started at ~ 70 °C with massive gas evolving (NO_2). The resulted product was heated at 130 °C, for 3h, until no nitrogen oxides were visible anymore, was grinded and washed with acetone in order to eliminate the unreacted diol excess.

Figure 5: Thermal curves for the solution Fe(NO3)3-1,3PG

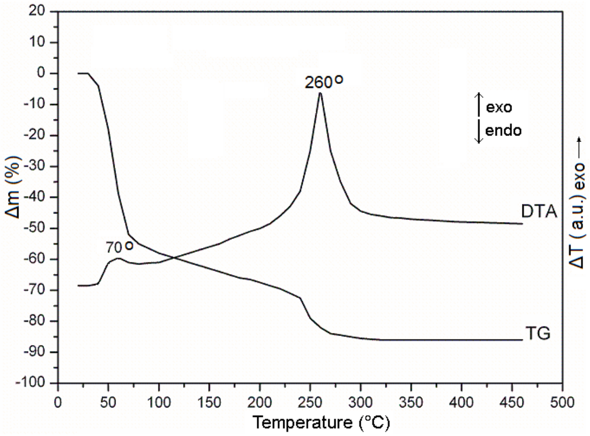

The Fe(III) carboxylate type complex combination obtained at 130°C was studied by thermal analysis and FT-IR spectrometry. The thermal behaviour from Fig. 6 indicates a mass loss up to 200°C which corresponds to the coordinated water elimination. In the temperature range 200 – 400°C takes place the oxidative decomposition with a strong exothermic effect at ~270°C leading to γ-Fe_2O_3. The weak exothermic effect at ~450°C on DTA is attributed to the polymorphic transformation of γ-Fe_2O_3 to α-Fe_2O_3. Up to 500°C, the mass loss remains constant and corresponds to the residue Fe_2O_3.

Figure 6: Thermal curves of the precursor obtained at 130°C

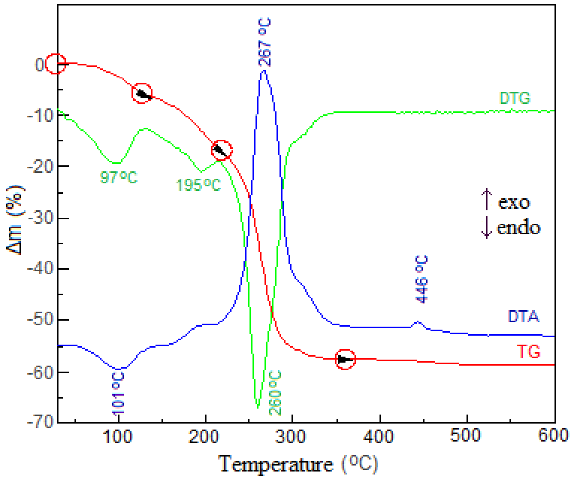

The FT-IR spectrum (Fig.7) of the precursor obtained at 130°C presents the characteristic bands for the carboxylate type complex combination $\nu_{as}(COO^-)$ in the range 1500 – 1700 cm^{-1} [18] and $\nu_s(COO^-)$ in the range 1300 – 1400 cm^{-1}[19], proving that the redox reaction was finished and the complex combination is formed. By annealing of the complex at 300°C, takes place the oxidative decomposition of the ligand (CO_2 elimination) with the obtaining of a dark brown, magnetic powder (γ-Fe_2O_3). The FT-IR spectrum changes as in Fig. 8, were the bands from 639,5, 554,7 and 441 cm^{-1} are present, corresponding to γ-Fe_2O_3 [20]. At 500 °C, the spectrum presents the intense bands of hematite (α-Fe_2O_3) at 526,6 and 443,6 cm^{-1} [21], evidencing the transformation of γ-Fe_2O_3 to α-Fe_2O_3. The powder resulted by annealing at 500°C was red and had no magnetic properties.

Figure 7: FT-IR spectrum of the precursor obtained at 130°C

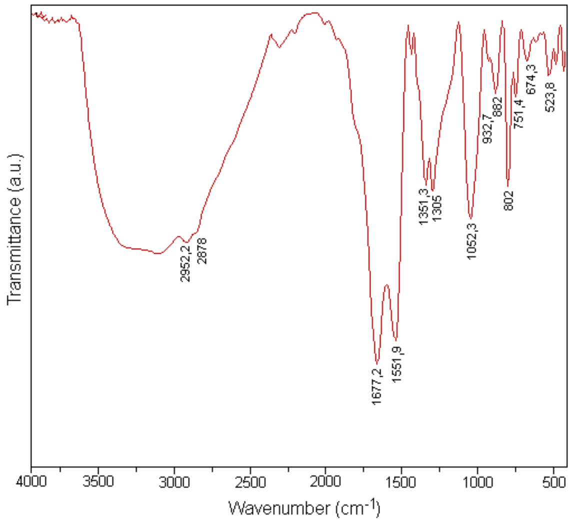

Figure 8: FT-IR spectra of the precursor annealed at 300°C and 500°C

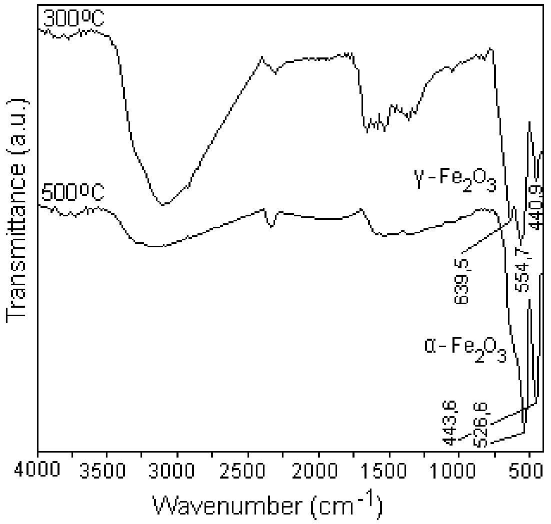

The XRD patterns from Fig.9 indicate that by annealing of the Fe(III) carboxylate precursor at 300°C, the single phase is γ-Fe_2O_3 while at 500°C γ-Fe_2O_3 is completely transformed to α-Fe_2O_3. The α-Fe_2O_3 nanoparticles obtained at 500°C have a mean diameter of ~ 40 nm. The SEM image (Fig.10) shows that the α-Fe_2O_3 particles are agglomerated.

Figure 9: XRD patterns of the samples obtained by annealing of the Fe(III) carboxylate precursor

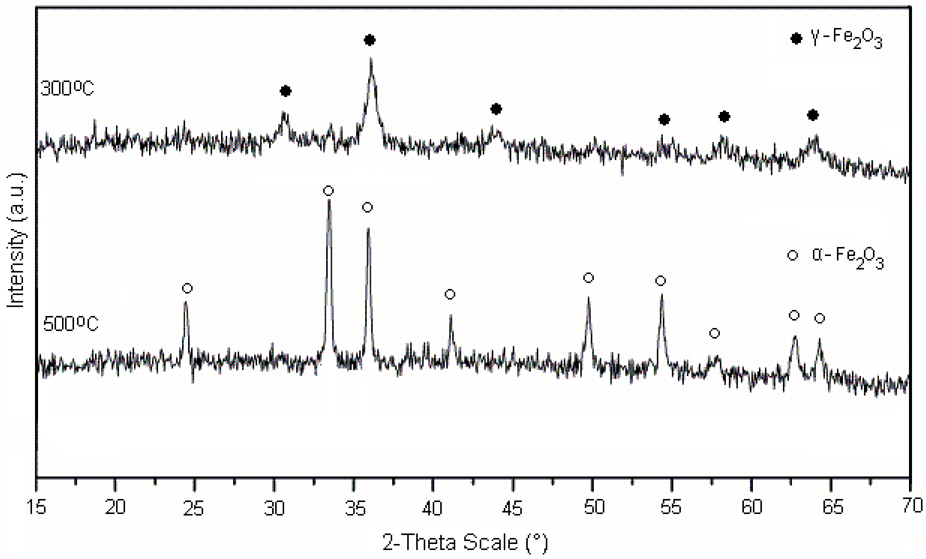

Figure 10: SEM image of the sample obtained by annealing of the Fe(III) carboxylate precursor at 500°C

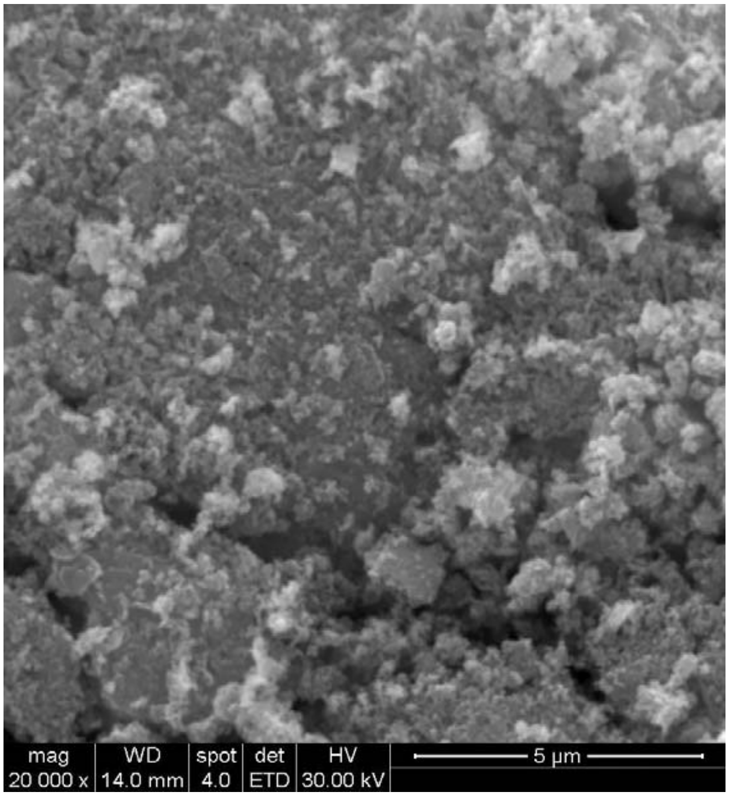

4. CONCLUSIONS

We have synthesized α-Fe_2O_3 nanoparticles using the precipitation method and the decomposition of Fe(III) carboxylate type precursors. The studies have shown that the two synthesis methods follow different mechanisms for the obtaining of the crystalline α-Fe_2O_3. The precipitation method has the transformation pathway iron hydroxides (goethite, lepidocrocite) → α-Fe_2O_3 (300°C) while the thermal decomposition of carboxylates method leads to the single phase α-Fe_2O_3 at 500°C, having as intermediate γ-Fe_2O_3 at 300°C.

The complex combinations decomposition method is a novel method for the obtaining of α-Fe_2O_3 nanoparticles. The results are comparable to those obtained by precipitation, starting from the same reagents (iron nitrate). Among the advantages of this method may be mentioned that the synthesis procedure is faster, the yield is almost 100 % and the obtained particle size (~ 20 nm) makes α-Fe_2O_3 suitable for applications as photocatalyst in water splitting.

The advantages of the precipitation method are that α-Fe_2O_3 single phase is obtained at a lower temperature in form of nanoparticles with diameters of ~ 40 nm. The method is simple and productive.

ACKNOWLEDGEMENT

This work was partially supported by the strategic grant POSDRU/159/1.5/S/137070 (2014) of the Ministry of National Education, Romania, co-financed by the European Social Fund – Investing in People, within the Sectoral Operational Programme Human Resources Development 2007-2013.

REFERENCES

1. Vestal, C.R.; Zhang, Z.J. Magnetic spinel ferrite nanoparticles from microemulsions. *International Journal of Nanotechnology* **2004**, *1*, 240–263.
2. Stefanescu, O.: New methods for the obtaining of γ-Fe_2O_3 based nanomaterials, Doctoral thesis, Politehnica University, Timisoara, 2010.
3. Satheesh, R.; Vignesh, K.; Suganthi, A.; Rajarajan, M. Visible light responsive photocatalytic applications of transition metal (M = Cu, Ni and Co) doped α-Fe_2O_3 nanoparticles. *Journal of Environemantal Chemical Engineering* **2014**, *2*, 1956–1968.
4. Teja, A.S.; Koh, P.Y. Synthesis, properties and applications of magnetic iron oxide nanoparticles. *Progress in Crystal Growth and Characterization of Materials* **2009**, *55*, 22–45.
5. Huang, M.C. The optical, structural and photoelectrochemical characteristics of porous hematite hollow spheres prepared by DC magnetron sputtering process via polystyrene spheres template. *Ceramics International* **2014**, *40*, 10537–10544.
6. Tadic, M.; Citakovic, N.; Panjan, M.; Stojanovic, Z.; Markovic, D.; Spasojevic, V. Synthesis, morphology, microstructure and magnetic properties of hematite submicron particles. *Journal of Alloys and Compounds* **2011**, *509*, 7639–7644.
7. Tadic, M.; Panjan, M.; Damnjanovic, V.; Milosevic, I. Magnetic properties of hematite (α-Fe_2O_3) nanoparticles prepared by hydrothermal synthesis method. *Applied Surface Science* **2014**, *320*, 183–187.
8. Liang, H.; Chen. W.; Yao, Y.; Wang, Z.; Yang, Y. Hydrothermal synthesis, self-assembly and electrochemical performance of α-Fe_2O_3 microspeheres for lithium ion batteries. *Ceramics International* **2014**, *40*, 10283–10290.
9. Zelenak, V.; Zelenakova, A.; Kovac, J.; Vainio, U.; Murafa, N. Influence of surface effects on magnetic behavior of hematite nanoparticles embedded in porous silica matrix. *Journal of Physical Chemistry C*, **2009**, *113*, 13045–13050.
10. Pailhe, N.; Majimel, J; Pechev, S., Gravereau, P.; Gaudon, M.; Demourgues, A. Investigation of nanocrystallized α-Fe_2O_3 prepared by a precipitation process. *Journal of Physical Chemistry C*, **2008**, *112*, 19217–19223.
11. Manukyan, V.; Chen, S.; Rouvimov, S.; Li, P.; Dong, S.; Liu, X., Furdyna, J.; Orlov, A.; Bernstein, G.; Porod, W.; Roslyakov, S.; Mukasyan, A. Ultrasmall α-Fe_2O_3 superparamagentic nanoparticles with high magnetization prepared by template-assisted combustion process. *Journal of Physical Chemistry C*, **2014**, *118*, 16264–16271.
12. Deraz, N.M.; Alarifi, A. Novel processing and magnetic properties of hematite/maghemite nano-particles. *Ceramics International*, **2012**, *38*, 4049–4055.

13. Stefanescu, O.; Stefanescu, M. New Fe(III) malonate type complex combination for development of magnetic nanosized γ-Fe_2O_3. *Journal of Organometallic Chemistry*, **2013**, *740*, 50–55.
14. Stefanescu, M.; Stefanescu, O.; Stoia, M.; Lazau, C. Thermal decomposition of some metal-oragnic precursors. Fe_2O_3 nanoparticles. *Journal of Thermal Analysis and Calorimetry*, **2007**, *88*, 27–32.
15. Nenitescu, C.D., *General Chemistry*; Editura Didactica si Pedagogica: Bucharest, Romania, 1979.
16. Popescu, M.; Piticescu, R.; Vasile, E.; Taloi, D., Petriceanu, M.; Stoiciu, M., Badilita, V. The influence of synthesis parameters on FeO(OH)/Fe_2O_3 formation by hydrothermal techniques. *Zeitschrift fur Naturforschung*, **2010**, *65b*, 1024–1032.
17. Todor, D. *Minerals thermal analysis*; Ed. Technic: Bucharest, Romania, **1972**.
18. Nakamoto, K. *Infrared spectra of inorganic and coordination compounds*, John Wiley and Sons, New York, USA, **1970**.
19. Prasad, R.; Sulaxna; Kumar, A. Kinetics of thermal decomposition of iron (III) dicarboxylate complexes. *Journal of Thermal Analysis and Calorimetry*, **2005**, *81*, 441–450.
20. Asuha, S.; Zhao, S; Wu, H.Y; Song, L.; Tegus, O. One step synthesis of maghemite nanoparticles by direct thermal decomposition of Fe-urea complex and their properties. *Journal of Alloys and Compounds*, **2009**, *472*, L23–L25.
21. Yinsheng, W; Muramatsu, A.; Sugimoto, T. FT-IR analysis of well defined α-Fe_2O_3 particles. *Colloids and Surface A*, **1998**, *134*, 281–297.